

REVIEW

## Physical principles of intracellular organization via active and passive phase transitions

To cite this article: Joel Berry *et al* 2018 *Rep. Prog. Phys.* **81** 046601

View the [article online](#) for updates and enhancements.

### Related content

- [Charge pattern matching as a ‘fuzzy’ mode of molecular recognition for the functional phase separations of intrinsically disordered proteins](#)

Yi-Hsuan Lin, Jacob P Brady, Julie D Forman-Kay et al.

- [Droplet ripening in concentration gradients](#)  
Christoph A Weber, Chiu Fan Lee and Frank Jülicher

- [Viscoelastic phase separation](#)  
Hajime Tanaka

## Review

# Physical principles of intracellular organization via active and passive phase transitions

Joel Berry<sup>1,3</sup>, Clifford P Brangwynne<sup>2</sup> and Mikko Haataja<sup>1</sup>

<sup>1</sup> Department of Mechanical and Aerospace Engineering, Princeton University, Princeton, NJ 08544, United States of America

<sup>2</sup> Department of Chemical & Biological Engineering, Princeton University, Princeton, NJ 08544, United States of America

<sup>3</sup> Department of Materials Science and Engineering, University of Pennsylvania, Philadelphia, PA 19104, United States of America

E-mail: [cbrangwy@princeton.edu](mailto:cbrangwy@princeton.edu) and [mhaataja@princeton.edu](mailto:mhaataja@princeton.edu)

Received 5 July 2017, revised 5 December 2017

Accepted for publication 9 January 2018

Published 23 February 2018



Corresponding Editor Professor Erwin Frey

## Abstract

Exciting recent developments suggest that phase transitions represent an important and ubiquitous mechanism underlying intracellular organization. We describe key experimental findings in this area of study, as well as the application of classical theoretical approaches for quantitatively understanding these data. We also discuss the way in which equilibrium thermodynamic driving forces may interface with the fundamentally out-of-equilibrium nature of living cells. In particular, time and/or space-dependent concentration profiles may modulate the phase behavior of biomolecules in living cells. We suggest future directions for both theoretical and experimental work that will shed light on the way in which biological activity modulates the assembly, properties, and function of viscoelastic states of living matter.

Keywords: phase separation, intracellular condensates, bimolecular organization, self-assembly, organelles, RNA, proteins

(Some figures may appear in colour only in the online journal)

## Contents

1. Introduction.....	2	2.2.3. Flory–Huggins model.....	9
2. Overview of theoretical passive phase separation kinetics.....	3	2.2.4. Dynamics: models A, B, C, and H.....	9
2.1. Basic theories of nucleation, growth, and coarsening .....	4	2.3. Molecular driving forces.....	11
2.1.1. Growth.....	5	2.4. Discussion.....	12
2.1.2. Coarsening.....	7	3. Experimental tests of passive and modulated passive descriptions.....	13
2.2. Classical continuum models / field theories.....	8	3.1. <i>In vitro</i> studies of phase separation in aqueous protein solutions.....	13
2.2.1. Ginzburg–Landau model.....	8	3.1.1. A brief history of globular proteins in solution: Lysozyme.....	13
2.2.2. Regular solution model.....	9	3.1.2. <i>In vitro</i> studies of proteins associated with intracellular condensates.....	15

3.2.	<i>In vivo</i> studies of passive descriptions .....	16
3.2.1.	Phase separation of Dishevelled. ....	17
3.2.2.	Steady-state size distribution of <i>Xenopus laevis</i> oocyte nucleoli.....	17
3.2.3.	Disordered nuage protein droplets: a JMAK-based analysis. ....	17
3.2.4.	Optogenetically-controlled droplet assembly: kinetic analysis of 'optoDrops'.....	17
3.3.	<i>In vivo</i> studies of modulated passive systems .....	18
3.3.1.	P granules.....	18
3.3.2.	<i>C. elegans</i> nucleoli and extranucleolar droplets. ....	18
3.4.	Studies of undriven chemically reactive systems.....	20
3.4.1.	P granules.....	22
3.4.2.	Anomalous <i>in vitro</i> mesoscopic protein clusters.....	22
3.4.3.	Complex coacervation. ....	22
3.5.	Measurements of droplet properties <i>in vitro</i> and <i>in vivo</i> .....	22
3.5.1.	Liquid-like phases.....	23
3.5.2.	Gel-like and solid-like phases.....	24
3.6.	Discussion.....	26
4.	Developing and future directions.....	27
4.1.	Models for systems with many components .....	27
4.2.	Theoretical approaches for active and driven systems away from thermal equilibrium.....	29
4.2.1.	Active droplets: centrosomes, active emulsions, and protocells. ....	30
4.2.2.	Optogenetically-controlled systems.....	31
4.2.3.	Droplet coarsening in concentration gradients.....	32
4.2.4.	Active liquid-like phases.....	32
4.2.5.	Nonequilibrium kinetic demixing.....	32
4.2.6.	Insight from other active systems. ....	33
4.3.	Phase separation-induced formation of gels, solids, and irreversible aggregates.....	34
5.	Conclusion .....	36

## 1. Introduction

Phase transitions have a rich history in the natural sciences and engineering, with our theoretical understanding dating from developments in the 19th century, largely centered in the Netherlands [1]. But the practical application of phase transitions has been ongoing for millennia, since proto-materials scientists have long exploited solid-liquid and solid-solid phase transitions in pure metals and multicomponent alloys in order to control a material's microstructure and resulting properties. In the modern era, statistical mechanics approaches and field-theoretic continuum models have enabled rapid advances, and such approaches to phase transition dynamics are now routinely employed to investigate microstructure formation processes in inanimate systems.

The concept that phase transitions could be relevant in living matter was discussed by a number of researchers during

the 20th century [2–4]. The most notable quantitative studies were those focused on the possibility of 2D phase separation within the cell membrane, which may give rise to 'lipid rafts' that organize membrane associated receptors [5]. Recently, it has been shown that transitions are ubiquitous within living cells and provide a robust means to control the 'microstructure', i.e. cellular organization, of a wide range of biological systems [6–9]. These systems include the spatiotemporal patterning of germ granules in *C. elegans* embryos [6], organization of the mitotic spindle [10], condensation of postsynaptic density in neurons [11], T cell receptor clustering and signaling [12], and the dynamics of stress granules [13].

The conventional view of intracellular organization is focused on the cell's use of membrane-bound, vesicle-like organelles to compartmentalize the cytoplasm. However, in addition to these canonical organelles, there exist many membrane-less organelles within living cells. We refer to these membrane-less structures as intracellular condensates or simply condensates [14, 15]. These include ribonucleoprotein (RNP) condensates [16] such as processing bodies and stress granules in the cytoplasm [17], and Cajal bodies [18] and nucleoli [19] in the nucleus. There are also condensates comprised of metabolic enzymes such as the purinosome [20], and protein condensates enriched in Wnt and other molecules key for intracellular signalling [21–27].

Found in the cytoplasm of *C. elegans* embryos, P granules are a type of RNP condensate implicated in specifying cell fate. Related RNP condensates are found in all animals. The exact function of P granules is poorly understood, but they are thought to impact and control cell differentiation state by recruiting key RNAs. Nucleoli are the most visible of the nuclear condensates. Nucleoli assemble around sites where ribosomal RNA (rRNA) is being actively transcribed. They are thought to impact rRNA transcription and processing, by concentrating proteins important for processing, such as the RNA methyltransferase fibrillarin.

Many intracellular condensates behave in a manner consistent with phase-separated liquids, as shown in figure 1. Such behaviors include: (1) They typically exhibit round morphologies; (2) they readily fuse with one another on contact; (3) they exhibit rapid exchange of component molecules with surrounding nucleoplasm or cytoplasm; (4) they can exhibit wetting behavior, e.g. P granules exhibit a well-defined contact angle on the nuclear envelope; (5) they can exhibit these dynamic fluid properties, and yet do not mix with one another, much like two immiscible liquid phases; and (6) they only assemble above a threshold concentration of their components.

Not only do the droplets display liquid-like behavior as far as their morphology and coalescence dynamics are concerned, they also display very interesting growth and coarsening dynamics. This is shown in figure 2 for the case of the formation and dissolution kinetics of *C. elegans* nucleoli and extranucleolar droplets (ENDs) [28]. Following the assembly of the nuclear envelope, ENDs and nucleoli condense and grow, subsequently enter a biased coarsening stage, and finally dissolve at the end of the cell cycle. In contrast to phase separation processes in inanimate systems, here phase separation takes place in a 'vessel' which is expanding and which actively consumes energy.

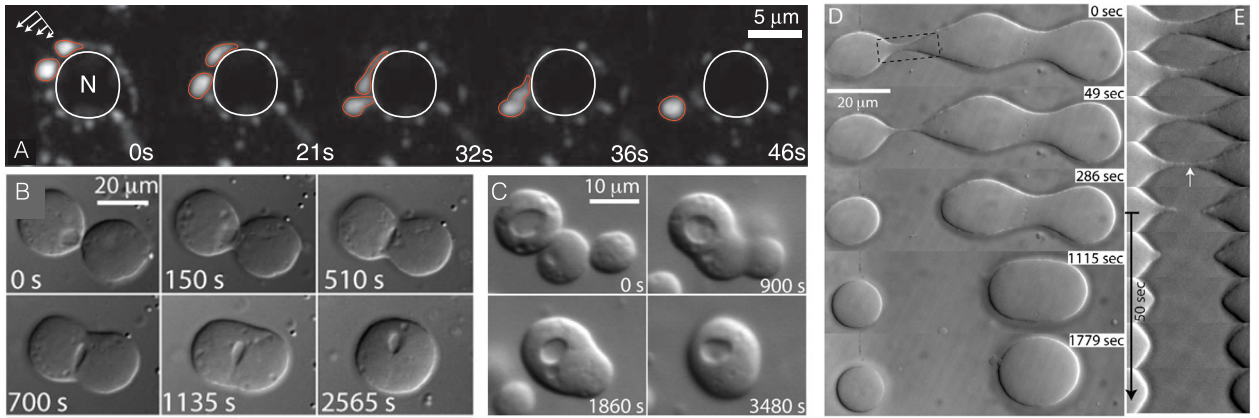


**Figure 1.** (a) From [6]. Reprinted with permission from AAAS. (b)–(e) Reproduced with permission from [7]. Copyright © Proceedings of the National Academy of Sciences of the United States of America. Examples of liquid-like behaviors exhibited by intracellular condensates. (a) *C. elegans* P granules (red outline) dripping over a nucleus (N, white line). (b)–(e) *Xenopus laevis* oocyte nucleoli. Fusion of (b) two and (c) three spherical nucleoli. (d) Three nucleoli come into contact, one connection / bridge pinches-off, the other holds and leads to fusion. (e) Close-up of the bridge pinch-off shown in (d); the resulting threads of nucleolar material are reincorporated into the rounding droplets.

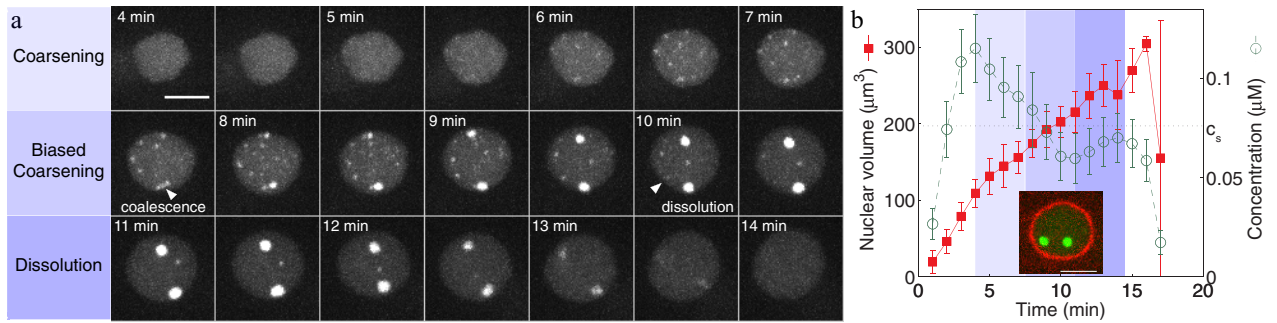


**Figure 2.** Reproduced with permission from [28]. Copyright © Proceedings of the National Academy of Sciences of the United States of America. Assembly/disassembly kinetics of *C. elegans* nucleoli and extranucleolar droplets (ENDs). (a) Temporal montage throughout the cell cycle from an embryo expressing the fluorescently tagged nucleolar protein FIB-1::GFP (FIB ≡ fibrillarin, GFP ≡ green fluorescent protein). Images are maximum-intensity projections of a 3D image stack. The nuclear envelope assembles at 0 min and breaks down at ~17 min. (b) Nuclear volume increases over time (solid red squares), resulting in a decreasing concentration of FIB-1 in the nucleoplasm (open green circles). The dotted line indicates the experimentally determined nucleolar saturation concentration,  $C_s$ .

While the existence of phase-separated droplets within living cells is now firmly established, much less is quantitatively understood about the droplet formation processes. A central challenge is that, in contrast to inanimate systems, living systems actively consume energy, and hence their behavior is not only governed by equilibrium thermodynamics, or the relaxation towards equilibrium. It is therefore prudent to ask, to what degree do classic models of nucleation, growth, and coarsening based on linear irreversible thermodynamics quantitatively describe phase separation processes within such inherently nonequilibrium systems?

In this review, we critically assess existing data on phase separation dynamics in living systems and compare them against predictions from standard theories of nucleation, growth, and coarsening. We argue that the formation of liquid droplets in many systems is indeed governed by relaxation behavior towards an effective equilibrium, but droplet formation is nonetheless strongly impacted by underlying molecular concentrations and interactions that are governed by nonequilibrium activity.

The rest of this review is organized as follows. Classic models of phase transition dynamics are reviewed in section 2, while the predictions of such models are compared against

experimental data in section 3. In section 4, we highlight several new avenues for future work in this rapidly evolving area, while concluding remarks can be found in section 5.

We note that a number of other recent review articles have been written, focusing on other aspects of intracellular phase transitions. For more details on the biology associated with intracellular phase transitions, the reader is referred to [14, 15, 29–41], while there are also several excellent reviews of the links to protein aggregation pathologies [15, 42–49], and others focused on underlying polymer physics [50, 51].

## 2. Overview of theoretical passive phase separation kinetics

In this section, we introduce and discuss classical theories of nucleation, growth and coarsening, as well as modern field-theoretic methods of studying such phase transition kinetics. Given the vast literature on phase transitions in materials science and physics, this overview is necessarily selective. We do not focus on molecular-scale modeling, coarse-grained polymer-chain simulations, or solution theories for polymers and

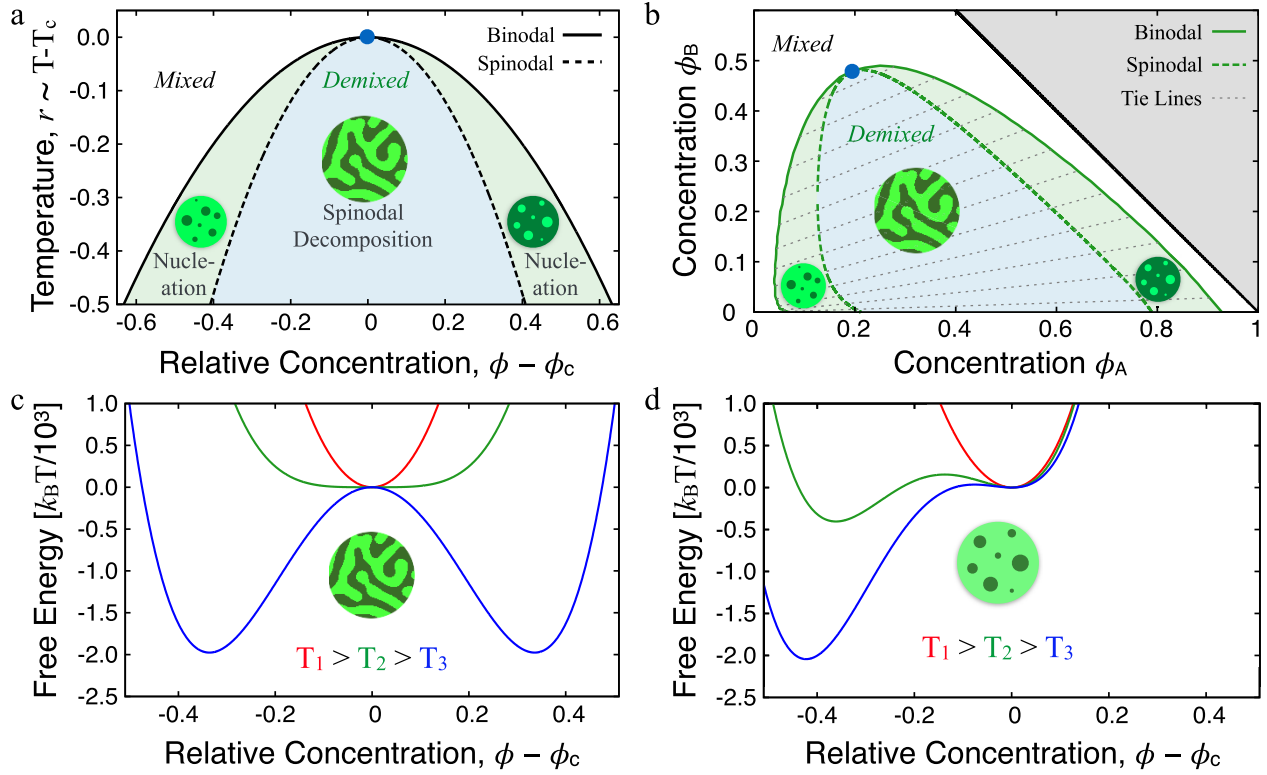


**Figure 3.** Thermodynamics of phase separation. Simple (a) binary and (b) ternary phase diagrams with regions of immiscibility and mixed phase instability delineated by binodal and spinodal boundaries, respectively, and critical points indicated by blue dots. (a) is determined from equation (1),  $\phi_c$  is the concentration at the critical point. (c) and (d) variation of free energies through 2nd order and 1st order transformations, respectively.

charged molecules such as the McMillan–Mayer, dilute electrolyte, Kirkwood–Buff, random phase approximation (RPA), Debye–Hückel, hypernetted-chain, and Derjaguin–Landau–Verwey–Overbeek (DVLO) theories (see, e.g. [52] and [42] for further information on such approaches). Applications of such theories will certainly contribute to the fundamental understanding of intracellular organization and to key molecular-scale driving forces such as specific charge patterns along protein chain sequences. While such advances are already beginning in this field [50, 53–55], the intention of this review is primarily to assess the applicability of the general physical principles of phase separation to intracellular compartmentalization. There is much to cover in this area alone.

### 2.1. Basic theories of nucleation, growth, and coarsening

In the classical thermodynamic context, phase separation is a transient, nonequilibrium process by which an initially well-mixed equilibrium state transforms to a demixed equilibrium state following an appropriate change of thermodynamic conditions. The condition-controlling parameters (temperature, molecular concentration, etc) can be any variables capable of tilting the global balance between contributions that favor molecular mixing (entropy, etc) and those that favor demixing (self-affinity, etc). For more comprehensive examinations of phase separation phenomena, we refer the reader to [56–62].

Two simple phase diagrams demonstrating the basic features of systems with mixed and demixed states are shown

in figures 3(a) and (b). The nature of the transformations depicted in figure 3 (their order) are determined by the location in phase space where the phase boundary between mixed and demixed states (the binodal) is crossed. This can have dramatic effects on how system properties change near the transition point and on the kinetics of phase separation.

A second order transition (figure 3(c)) occurs when the phase boundary is crossed at a critical point. Here the mixed phase becomes globally unstable as the critical point is approached, large-scale critical fluctuations (highly dynamic phase-separated domains) emerge with essentially no nucleation barrier, and these fluctuating domains settle below the critical point into some characteristic morphology that may coarsen with time. Nucleation processes are bypassed in this special but important case.

If the phase boundary is crossed away from a critical point but phase separation does not begin until near or below the spinodal, then critical-like behavior can still be observed. The mixed phase again becomes globally unstable at the spinodal, but the critical fluctuations are weaker and may be truncated by spinodal nucleation and growth processes just above the spinodal. Otherwise, spinodal decomposition occurs below the boundary. Finally, if the phase boundary is crossed away from a critical point and phase separation begins between the binodal and spinodal, then a first order transition occurs (figure 3(d)). Here individual droplets of the minority phase nucleate, grow, and then coarsen toward the demixed equilibrium state.

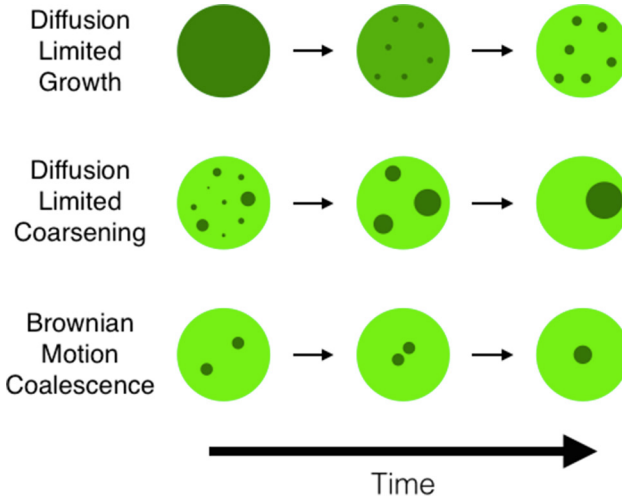


**Figure 4.** Adapted with permission from [28]. Copyright © Proceedings of the National Academy of Sciences of the United States of America. Schematic illustrations of three passive transport mechanisms. In diffusion-limited growth (DLG), molecules diffuse from the supersaturated bulk fluid into nearby droplets. In diffusion-limited coarsening (DLC) or Ostwald ripening, molecules diffuse from small droplets to large droplets, through the depleted bulk fluid. In Brownian motion coalescence (BMC), small droplets collide and fuse to form larger droplets.

These spinodal decomposition or nucleation/growth/coarsening processes may occur in sequential, well-separated regimes or may overlap. Overall phase separation kinetics may therefore vary widely in time within a given system, depending on the relative nucleation/growth/coarsening rates, and across different systems, depending on the rate-controlling physical transport mechanisms. One of the central concepts used to classify and understand phase separation kinetics is dynamic scaling. Dynamic scaling laws are formulated on the premise that domain kinetics are controlled by a single emergent length scale  $L$  within a given dynamic scaling regime [57, 61]. This implies that domain patterns exhibit self-similarity in time; features of the domain morphology increase in size with time, but their statistical properties remain invariant. In other words, the morphology within a region of size  $L$  at time  $t_1$  is statistically equivalent to the morphology within a region of size  $L(t_2/t_1)^n$  at time  $t_2$ , where  $n$  is the dynamic scaling exponent.

Dynamic scaling also implies that the evolution of physical properties associated with the droplet size distribution can be predicted based solely on the scaling of  $L$  with time. Many materials systems have been shown to exhibit dynamic scaling [61], and one relevant consequence for our purposes is that quantities associated with the droplet size distribution, such as the average domain or droplet size  $\langle R \rangle$ , commonly increase with a power law dependence on time, e.g.  $\langle R \rangle = (Kt)^n$ , during a scaling regime. Comparing measurements of quantities such as  $\langle R \rangle$  with theoretically-determined steady-state exponents  $n$  and prefactors  $K$  can therefore often help identify the specific growth or coarsening mechanisms at work.

Common passive evolution mechanisms for liquid-phase domains or droplets include those mediated by diffusive or hydrodynamic transport of droplet-forming molecules and

droplet coalescence induced by phenomena such as Brownian motion, hydrodynamic interactions, or sedimentation (see figure 4). The steady-state power law kinetic exponents and prefactors for various mechanisms are listed in table 1. These can be divided into *growth* processes, which typically dominate during the early stages of transformation following nucleation when the soluble phase is supersaturated, and *coarsening* processes, which typically dominate during the late stages of transformation when the soluble phase has been depleted.

**2.1.1. Growth.** The growth mechanisms included in table 1 are diffusion-limited growth (DLG—see figure 4), surface attachment-limited growth (SALG), and growth due to gravity sedimentation with simultaneous convection and diffusion. In all of these, a supply of excess droplet-forming molecules is available near the growing droplet. In DLG, growth is limited by the rate at which these molecules diffuse into the droplet, while in SALG growth is limited by the rate at which these molecules attach to the surface of the droplet.

The power law scaling exponents  $n$  and prefactors  $K$  for growth provided in table 1 apply to individual nucleated droplets  $R$  and, after some interval beyond the time at which overall nucleation rates become negligible, to the population average  $\langle R \rangle$ . At earlier times the observed  $n$  will be less than the predicted value due to nucleation. In cases where individual droplet morphologies or size distributions are not available, an alternative kinetic analysis can be performed by simply measuring the total volume fraction of transformed droplet phase  $\theta_d$  as a function of time. This is a common approach to analyzing early-stage growth kinetics during phase transformations. Such data can be compared with theories aimed at predicting the evolution of  $\theta_d$  according to the type of nucleation and growth kinetics in operation pre-coarsening. Two such theories, one widely known and one lesser-known, are discussed in the following subsections to identify how they may appropriately be applied to typical intracellular systems.

**Johnson–Mehl–Avrami–Kolmogorov (JMAK) Theory.** One theory that has been widely employed in the materials and physics communities to analyze the kinetics of first order phase transformations is the phenomenological JMAK theory [72–76] and its extensions [77]. Measurements of the change in volume fraction of transformed/droplet phase  $\theta_d$  with time can provide a simple though indirect way to identify nucleation and growth mechanisms consistent with observed behavior. Under the typical assumptions of random nucleation and constant, uniform supersaturation and growth rates,  $\theta_d$  is predicted by JMAK-type theories to evolve according to  $\theta_d = 1 - \exp \left[ - \int_0^t dt' J(t') V(t-t') \right] = 1 - \exp (-ct^m)$ , where  $J(t)$  is the nucleation rate,  $V(t)$  is the volume of transformed phase,  $c$  is a constant, and  $m$  is the so-called Avrami or stretch exponent. Values for  $m$  can be extracted from fits to  $\theta_d(t)$ . A commonly encountered case is that of growth at a constant rate ( $R(t) \sim t$ ,  $V(t) \sim t^3$ ), giving  $m = 3$  for heterogeneous ( $J(t) = n_s \delta(t)$ ,  $n_s \equiv$  number density of nucleation sites) and  $m = 4$  for homogeneous ( $J = \text{constant}$ ) nucleation.

**Table 1.** Compilation of selected steady-state growth and coarsening kinetic parameters  $n$  and  $K$ . See, e.g. [56, 59–61, 63, 64] for further information and/or accounts of mechanisms not cited below.

Mechanism	$n$	$K$
Diffusion-limited growth (DLG) <sup>a</sup>	1/2	$\approx 2DS_0$
Surface attachment-limited growth (SALG) <sup>b</sup>	1	$\approx k_s(T)\Delta c$
Gravity sedimentation with convective diffusion <sup>c</sup>	2	$\approx (2S_0\sqrt{EgD}/3)^{1/2}$
Diffusion-limited coarsening (DLC) <sup>d</sup> [65, 66]	1/3	$\approx \frac{8\sigma Dc_\infty V_m^2}{9N_A k_B T}$
Surface attachment-limited coarsening (SALC) [66]	1/2	$\approx \frac{64\sigma k_s c_\infty V_m^2}{81N_A k_B T}$
Brownian motion coalescence (BMC) <sup>e</sup> [67, 68]	1/3	$\approx \frac{6k_B T\theta_d}{5\pi\eta}$
Hydrodynamic coalescence (HC) <sup>f</sup> [69]	1/3	$\approx 1-10K_{\text{BMC}}$
Viscous hydrodynamic coarsening (VHC) <sup>g</sup> [68]	1	$\approx 0.1\sigma/\eta$
Inertial hydrodynamic coarsening (IHC) <sup>g</sup> [70]	2/3	$\sim (\sigma/\rho)^{1/2}$
Diffusion-limited kinetic aggregation <sup>h</sup> [71]	$1/d_f$	$\sim k_B T/\eta$
Laminar shear flow-induced coalescence <sup>i</sup>	$\langle R \rangle \sim e^{t/\tau}$	$\tau \simeq 1/(S\theta_d)$

<sup>a</sup>  $D$   $\equiv$  diffusivity of droplet-forming molecules,  $S_0 = (c_0 - c_{\text{EQ}}^\alpha)/(c_{\text{EQ}}^\beta - c_{\text{EQ}}^\alpha) \equiv$  supersaturation, where  $c_0 \equiv$  initial solute concentration upon loading,  $c_{\text{EQ}}^\alpha \equiv$  equilibrium solute concentration in the background phase  $\alpha$ ,  $c_{\text{EQ}}^\beta \equiv$  equilibrium solute concentration in the droplet phase  $\beta$ .

<sup>b</sup>  $k_s(T) = \Omega n_a \nu \Delta G \exp(-G_A/k_B T)/(N_A k_B T) \equiv$  kinetic prefactor for molecular surface attachment at a droplet, where  $\Omega \equiv$  atomic volume,  $n_a \equiv$  number of atoms per unit area at the interface in the background,  $\nu \equiv$  atomic jump frequency,  $\Delta G \equiv$  Gibbs free energy change on moving an atom from the background into the droplet,  $G_A \equiv$  activation energy for attachment,  $N_A \equiv$  Avogadro constant,  $k_B \equiv$  Boltzmann constant, and  $T \equiv$  temperature.  $\Delta c = c_0 - c_{\text{EQ}}^\alpha$ .

<sup>c</sup>  $g \equiv$  gravitational constant,  $E = 2(\eta + \eta_d)(\rho_d - \rho)/[\pi\eta(2\eta + 3\eta_d)]$  where  $\eta$ ,  $\rho$ ,  $\eta_d$ , and  $\rho_d$  are the viscosity and density, respectively, of the background and droplet phases, respectively. This result applies in the regime of large Peclet number,  $Pe = vR/D \gg 1$ , where  $v$  is a characteristic flow field velocity.

<sup>d</sup>  $\sigma \equiv$  droplet surface tension,  $c_\infty \equiv$  equilibrium molar solute concentration in the background phase with a flat interface,  $V_m \equiv$  molar volume of droplet forming molecules.

<sup>e</sup>  $\theta_d \equiv$  droplet volume fraction,  $\eta \equiv$  solvent viscosity.

<sup>f</sup> Expected to be weak in higher  $\eta$  fluids and systems with  $\theta_d \lesssim 0.2$ .

<sup>g</sup> Bicontinuous phases only,  $\rho \equiv$  solvent/fluid density.

<sup>h</sup> This is a theory for particle aggregation, not phase separation. Here  $\langle R \rangle \equiv$  average cluster/aggregate radius of gyration,  $d_f \equiv$  cluster fractal dimension. Result applies for  $R \gg$  aggregating particle size.

<sup>i</sup>  $S \equiv$  homogeneous shear rate.

It has been noted by Cahn [77] that conclusive identification of nucleation and growth mechanisms from this type of analysis is rarely valid without further independent determination of nucleation or growth rates. It is also worth emphasizing the fact that the assumptions employed by the JMAK theory are violated when diffusion controls domain growth rates, as may be the case within many intracellular systems. The theory may reasonably describe such transformations only during the very early growth stages when the diffusion zones of different droplets do not overlap. In this regime of DLG, JMAK theory predicts  $m = 3/2$  for heterogeneous nucleation and  $m = 5/2$  for a constant rate of homogeneous nucleation, but these exponents can be reasoned independently on more general grounds. The value of  $m$  when  $\theta_d \ll 1$  should be given by  $m = d + q + p$ , where  $d$  is dimension and  $q$  and  $p$  are defined from  $J(t) \sim t^q$  and  $dR(t)/dt \sim t^p$ , respectively [77]. For the steady-state growth mechanisms cited in table 1,  $p = n - 1$  such that  $m = q + d + n - 1$ .

A further issue with application of the JMAK theory in the present context stems from the fact that intracellular condensate growth does not proceed to a point where the cellular compartment is completely filled with droplet phase; these are generally low volume fraction transformations. The JMAK theory considers the case in which  $\theta_d$  plateaus at 1

as a result of eliminating all available untransformed volume. In contrast, saturation of  $\theta_d$  in intracellular transformations may be expected to generally result from the gradual depletion of available excess solute (droplet-forming molecules) at  $\theta_d^{\max} \ll 1$ . For these reasons, JMAK theory may find limited direct application to intracellular phase transitions, and caution should be taken in assessing whether the conditions required for its validity are satisfied in a given system.

*Theory of diffusion-limited precipitation.* Sufficiently early stages of condensate nucleation and growth may nonetheless be possible to analyze using JMAK-type theories or simpler physical generalizations of the type described above, but the later stages of growth (pre-coarsening, along the shoulder approaching the plateau in  $\theta_d$  versus  $t$ ) require another theory in the cases of diffusion-limited growth and/or low volume fraction transformations. We propose that the theory of diffusion-limited precipitation [78] meets this need. This theory predicts that when the diffusion zones of separated droplets overlap significantly, the approach to a steady-state  $\theta_d$  value is characterized by  $m \simeq 1$ , independent of  $d$  or nucleation type. For DLG, a crossover from  $m = 3/2$  or  $5/2$  to  $m \simeq 1$  is therefore expected as  $\theta_d \rightarrow \theta_d^{\max}$ , though the mechanism of diffusion-limitation does not change. This effective late

time exponent results from the gradual depletion of available excess solute, which causes the plateau in  $\theta_d(t)$  for diffusion-controlled transformations with  $\theta_d^{\max} \ll 1$ . Furthermore, verification of the exponent  $m \simeq 1$  requires a somewhat different data analysis procedure than that used to extract the Avrami exponent, as described below.

According to the theory of [78], the fraction of excess solute,  $\bar{\rho}/\rho_0$ , in the background phase of an initially uniformly supersaturated solution evolves at early times as  $\bar{\rho}/\rho_0 \simeq 1 - (K_1 t)^m$ . The exponent is  $m = 3/2$  for diffusion-limited growth or  $m = 3$  for surface attachment-limited growth, and  $K_1 = 2D(\rho_0/\rho_c)^{1/3}/r_s^2$  is the rate prefactor for diffusion-limitation. Here  $\bar{\rho}$  and  $\rho_0$  are the time-dependent and initial excess solute densities, respectively,  $\rho_c$  is the solute density in the droplet phase, and  $2r_s$  is the spacing between droplets, assumed to be fixed in an infinite periodic array. We can convert to droplet volume fractions using the relation  $\theta_d/\theta_d^{\max} = 1 - \bar{\rho}/\rho_0$ . The droplet volume fraction therefore grows initially as  $\theta_d/\theta_d^{\max} \simeq (K_1 t)^m$ , and the exponent  $m$  can be determined from a log–log plot of  $\theta_d/\theta_d^{\max}$  versus  $t$ . Note that this result implies  $\langle R \rangle \sim t^{1/2}$  at early times for a fixed array of droplets, consistent with DLG scaling ( $n = 1 + m - q - d = 1/2$ , table 1).

More significantly, for late times the theory predicts  $\theta_d/\theta_d^{\max} \simeq 1 - G \exp(-t/\tau_0)$ , where  $G$  is a constant and  $\tau_0 = r_s^2(\rho_c/\rho_0)^{1/3}/3D(1+Z)^{1/3}$  is the time constant for approach to equilibrium, with time exponent  $m = 1$ .  $Z$  is the fraction of excess solute already within droplets at  $t = 0$ , a factor retained to account for potential measurement resolution effects. A typical Avrami or JMAK analysis, which would involve plotting  $-\ln(1 - \theta_d)$  versus  $t$  on log–log axes to extract  $m$ , would not generate a straight line with  $m = 1$  in a system following these transformation kinetics. This is because  $\theta_d/\theta_d^{\max} \rightarrow 1$  rather than  $\theta_d \rightarrow 1$ , leading to an extra additive term in the logarithm that does not cancel out. One should therefore plot  $1 - \theta_d/\theta_d^{\max}$  versus  $t$  on log-linear axes to determine whether a straight line, corresponding to the  $m = 1$  behavior of this theory, is exhibited. We reiterate that this result applies to the shoulder approaching the plateau in  $\theta_d$  versus  $t$ ; between the initial isolated growth stage and the coarsening stage at fixed  $\theta_d$ . As discussed in section 3.2.4, we find that *in vivo* experimental data from optogenetically-controlled FUS-based droplets [79] do indeed exhibit the predicted linear  $m = 1$  behavior during this regime.

**2.1.2. Coarsening.** Kinetics during the later stages of growth, after the volume fraction of droplet phase has saturated and the soluble phase has been depleted from the background, are typically dominated by coarsening processes. Here longer-range transport between droplets or of droplets is generally required. Coarsening mechanisms considered in table 1 are diffusion-limited coarsening (DLC or Ostwald ripening—see figure 4), surface attachment-limited coarsening (SALC) Brownian motion coalescence (BMC—see figure 4), hydrodynamic coalescence (HC), viscous (VHC) and inertial (IHC) hydrodynamic coarsening, and laminar shear flow-induced coalescence. Diffusion-limited kinetic aggregation, though

**Table 2.** Sequences of kinetic regimes expected during binary fluid phase separation following a temperature quench at low ( $\theta_d \lesssim 0.1$ –0.2), intermediate ( $0.1$ –0.2  $\lesssim \theta_d \lesssim 0.3$ –0.4), and high ( $0.3$ –0.4  $\lesssim \theta_d \lesssim 0.6$ –0.7) volume fractions of transformed phase. Mechanisms likely to be most relevant to intracellular condensates are highlighted with bold text. SD  $\equiv$  spinodal decomposition.

Volume fraction	Low	Intermediate	High
Onset	<b>Droplet nucleation</b>	<b>Droplet SD</b>	Bicontinuous SD
Growth	<b>DLG, SALG</b>	<b>SD / DLG, SALG</b>	SD / DLG, SALG
Coarsening-I	<b>DLC, SALC, BMC</b>	<b>BMC, HC</b>	DLC, SALC
Coarsening-II	—	—	VHC
Coarsening-III	—	—	IHC

not strictly a phase separation process of the type focused on here, is also noted due to its potential relevance to some droplet aggregation phenomena. Derivations and discussions of the results outlined in table 1 can be found in the cited references.

The kinetic regimes expected during binary fluid phase separation and their sequences in a given temperature quenched system are outlined in table 2 as a function of the volume fraction  $\theta_d$  of transformed phase. After the onset of phase separation via either nucleation or spinodal decomposition, an initial regime of DLG with  $n = 1/2$  generally occurs in liquid–liquid systems. In low  $\theta_d$  systems (roughly,  $\theta_d \lesssim 0.1$ –0.2) a single late-time coarsening regime dominated by either DLC or BMC of droplets with  $n = 1/3$  is then expected. Inspection of table 1 reveals that DLC will be more prominent in lower  $\theta_d$  systems since  $K_{\text{DLC}}$  does not depend on  $\theta_d$ , while  $K_{\text{BMC}} \sim \theta_d$ .

For intermediate  $\theta_d$  systems (roughly,  $0.1$ –0.2  $\lesssim \theta_d \lesssim 0.3$ –0.4) a single late-time coarsening regime dominated by either BMC or HC of droplets with  $n = 1/3$  is expected. The HC mechanism, though not yet confirmed by experiments, is predicted to weaken with increasing fluid viscosity and may therefore be less prominent than BMC in typical intracellular fluids. The droplet size distribution under HC is left-skewed, similar to that of DLC, while that under BMC is right-skewed (see table 3).

In large  $\theta_d$  systems (roughly,  $0.3$ –0.4  $\lesssim \theta_d \lesssim 0.6$ –0.7) spinodal decomposition of bicontinuous structures rather than droplets occurs. If the initial fastest growing mode or characteristic domain size is sufficiently small, coarsening begins with a regime of DLC with  $n = 1/3$ . As domain sizes increase, domain interface velocities decrease and hydrodynamic effects become increasingly important. A surface tension-driven hydrodynamic coarsening mechanism then becomes dominant (VHC), leading to a second coarsening regime with  $n = 1$  [68]. At sufficiently late times, if the Reynolds number becomes  $\gg 1$ , the VHC regime may give way to a third coarsening regime (IHC) with  $n = 2/3$  [70]. These latter two mechanisms can only occur in bicontinuous phases. The domain size at which the crossover from VHC to IHC would occur is of order  $R \sim \eta^2/\sigma\rho$ , which is likely too large to be relevant to intracellular fluids where the Reynolds number is very small ( $\eta \gtrsim 0.01 \text{ Pa} \cdot \text{s}$ ,  $\sigma \lesssim 10^4 \text{ N m}^{-1}$ ,  $\rho \lesssim 2000 \text{ kg m}^{-3}$

**Table 3.** Steady-state droplet size distributions  $N(\bar{R}, t)$  obtained for selected coarsening mechanisms in the limiting regimes indicated.  $\bar{R} = R/\langle R \rangle$  is the scaled droplet radius and  $\bar{R}_{\max}$  is the largest non-zero scaled droplet radius.

Mechanism	Limit	$N(\bar{R}, t)$	$\bar{R}_{\max}$
Diffusion-limited coarsening (DLC) [65, 66]	$\theta_d \rightarrow 0$	$\frac{3^4 e \bar{R}^2 \exp[-(1-2\bar{R}/3)^{-1}]}{2^{5/3} (\bar{R}+3)^{7/3} (3/2-\bar{R})^{11/3}}$	3/2
Surface attachment-limited coarsening (SALC) [66]	$\theta_d \rightarrow 0$	$\frac{8\bar{R}}{3(2-\bar{R})^5} \exp\left(\frac{-3\bar{R}}{2-\bar{R}}\right)$	2
Brownian motion coalescence (BMC) <sup>a</sup> [63, 85, 86]	—	$\sim \frac{1}{\bar{R}} \exp\left(-\frac{(\ln \bar{R} - b)^2}{2\sigma^2}\right)$	$\sim 3/2 - \infty$

<sup>a</sup> This log-normal form is employed as an approximation to numerical solutions of analytical results and to fully numerical simulation results.  $b$  and  $\sigma$  are constants that control the mean and variance of the distribution.

gives  $R \gtrsim 0.5$  mm). It has also been argued that this  $t^{2/3}$  inertial regime cannot be a true asymptotic scaling regime because it implies that the Reynolds number of the fluid grows in time without bound [80]. This would lead to turbulence and subsequent arrest of phase separation as the domains turbulently remix. Asymptotic coarsening with saturation of the Reynolds number would instead require  $n \leq 1/2$ .

Analytic steady-state droplet size distributions for DLC, SALC, and BMC are presented in table 3 in terms of the scaled droplet radius  $\bar{R} = R/\langle R \rangle$ . DLC and SALC distributions are given for the dilute limit,  $\theta_d \rightarrow 0$ . The shape of the distributions for DLC and SALC are left-skewed, and the largest non-zero scaled droplet radii  $\bar{R}_{\max} = R_{\max}/\langle R \rangle$  are small,  $\bar{R}_{\max} = 3/2$  and 2 for DLC and SALC, respectively. In contrast, the BMC distribution is right-skewed (potentially extremely so) and generally exhibits much larger values of  $\bar{R}_{\max}$ .

In the dilute limit of idealized DLC, droplets are well-separated and interactions between droplets, generated by their diffusion fields, are mean-field-like. As  $\theta_d$  is increased above the dilute limit, droplet diffusion fields begin to significantly overlap, leading to increasingly significant spatial correlations between droplets. These interactions do not alter the DLC exponent  $n = 1/3$ , but they do lead to a monotonic increase in the coarsening rate prefactor  $K$  with  $\theta_d$ , as well as a widening of the droplet size distribution and a decrease in its left-skewed asymmetry [59, 81–84]. The ability to distinguish between DLC and BMC through the shape of the droplet size distribution may therefore be obscured when  $\theta_d \gtrsim 0.01–0.05$ . Generally though,  $\bar{R}_{\max}$  does not increase above  $\sim 2$  for DLC at large  $\theta_d$ .

We note that viscoelastic effects, which are neglected in the theories considered here, have been found to play an important role in the phase separation and gelation kinetics of some complex fluids such as protein, polymer, or micellar solutions, colloidal suspensions, and emulsions [62, 87]. In general, the theoretical frameworks for viscoelastic phase separation are not as fully developed as those for purely viscous mixtures, but their application and extension to intracellular fluids may be a worthwhile area of future study (see section 4 for further discussion).

## 2.2. Classical continuum models / field theories

In this section, classical continuum models describing the thermodynamics and kinetics of phase separation processes based on linear irreversible thermodynamics are reviewed.

The theories and kinetic scaling laws outlined in section 2.1 are derived in large part by employing thermodynamic relations, symmetries, and conservation laws under various approximations and assumptions applicable to a given set of physical conditions. The continuum models of phase separating systems described in this section provide a physically similar but more generalized thermodynamics-based framework from which the same problems and systems can be studied. Such models have been employed to derive and verify kinetic scaling laws, and efficient numerical simulation methods have enabled studies of a wide range of nucleation, growth, and coarsening phenomena in binary and multicomponent mixtures. Multiple concurrent transport mechanisms can be incorporated into these descriptions to examine emergent domain morphologies and growth/coarsening kinetics without need for many of the approximations and assumptions invoked by analytical treatments. Theories covered in this section include the Ginzburg–Landau, regular solution, and Flory–Huggins free energy functionals, and dynamics according to the Model A, B, C, and H classifications [64]. Free energies presented are Helmholtz free energies and processes described by these models are isothermal.

**2.2.1. Ginzburg–Landau model.** A useful theoretical starting point is the Ginzburg–Landau (GL) [88] free energy functional, one of the most conceptually simple approaches that can be used to understand the physics of phase separation. (This type of functional actually dates back to van der Waals [89]). Consider a mixture of A molecules and B molecules. A coarse-grained order parameter  $\phi(\vec{r})$  can be defined such that  $\phi = 0$  over regions of equal A and B mixing and  $\phi = \pm\phi_0$  in A-rich and B-rich regions, respectively, where  $\phi_0 \neq 0$  is a constant. In units of  $k_B T$ , the free energy density of this system is given by

$$f_{\text{GL}} = \frac{r}{2} \phi^2 + \frac{u}{4} \phi^4 + \frac{K}{2} |\nabla \phi|^2 \quad (1)$$

where  $r \sim T - T_c < 0$  and  $u > 0$  are constant parameters and  $K > 0$  is related to the surface tension between A-rich and B-rich domains. By varying  $r$  and/or the average (conserved) value of  $\phi = \bar{\phi}$ , the equilibrium state can be changed from a one-phase mixed state to a two-phase demixed state (see figure 3(a)). A mean-field critical point exists at  $(r = \bar{\phi} = 0)$ , a spinodal at  $r_s = -3u\bar{\phi}^2$ , and a binodal at a position that can be determined via common tangent construction (see figure 3(a)). The basic thermodynamic elements of first and second order

phase transitions in the Ising universality class are therefore present in equation (1), though quantitative application of  $\phi^4$  functionals to phase separating fluids can be a challenge, and critical behavior in  $d < 4$  is not accurately captured.

**2.2.2. Regular solution model.** Another simple description of two-component, one and two-phase systems is the regular solution (RS) model. Consider a mixture of A molecules and B molecules on a lattice consisting of N total sites. The resident of each lattice site interacts with  $z$  nearest neighbors (e.g.,  $z = 6$  on a 3D cubic lattice). There are  $n_A$  molecules of type A and  $n_B = N - n_A$  molecules of type B. The concentration is expressed as a molar or volume fraction (molar volumes of A and B molecules are equal and assumed to be constant), where the fraction of A molecules is  $\phi_A \equiv \phi = n_A/N$  and the fraction of B molecules is  $\phi_B = n_B/N = 1 - \phi$ . In units of  $k_B T$ , the free energy density of this system is given by

$$f_{\text{RS}} = \phi \ln(\phi) + (1 - \phi) \ln(1 - \phi) + \chi \phi(1 - \phi) + \frac{K}{2} |\nabla \phi|^2 \quad (2)$$

where  $\chi$  is a constant that controls the strength of intermolecular interactions.

The first two terms represent the entropy of mixing, which tend to keep the molecules well-mixed. The third term represents the interaction energy, which is governed by the interaction parameter,  $\chi \equiv \frac{z}{2k_B T} (2\epsilon_{AB} - (\epsilon_{AA} + \epsilon_{BB}))$ . The fourth term (gradient free energy) is again related to surface tension.  $\chi$  provides a simple mean-field parameter describing the balance of interactions, which can be related to the lattice nearest neighbor interaction energies  $\epsilon_{AB}$ ,  $\epsilon_{AA}$ ,  $\epsilon_{BB}$ . For  $\chi > 0$ , there is an energetic cost to having A and B molecules sitting next to one another, such that this term tends to drive the system to phase separate.

Generalization to systems with  $N$  components is straightforward. The Helmholtz free energy density can be written in terms of the local composition  $\phi_i$  of each species as

$$f_{\text{RS}} = \sum_{i=1}^N \left[ \phi_i \ln(\phi_i) + \sum_{j=1, j \neq i}^N \frac{\chi_{ij}}{2} \phi_i \phi_j + \sum_{j=1}^N \frac{K_{ij}}{2} (\nabla \phi_i) \cdot (\nabla \phi_j) \right] \quad (3)$$

where  $\chi_{ij}$  is the  $N \times N$  interspecies interaction matrix and  $K_{ij}$  is the  $N \times N$  gradient energy matrix related to the surface tension between domains with various composition differences. Incompressibility can often be invoked to reduce the number of independent order parameters from  $N$  to  $N - 1$ . Equation (2), for example, is obtained by substituting  $\phi = \phi_A(\vec{r}) = 1 - \phi_B(\vec{r})$  and defining  $K = K_{AA} + K_{BB} - 2K_{AB}$ .

**2.2.3. Flory–Huggins model.** The Flory–Huggins model can be viewed as a relatively simple extension of the regular solution model. Consider a solution of a polymer and solvent, where the polymer chain length is  $N_p$  and the volume fraction is  $\phi$ . Since the individual molecules within a polymer are attached to one another, on the lattice the configurational entropy is changed, since there are many fewer ways of configuring  $N_p$  molecules when they are required to occupy adjacent lattice sites. The free energy density is then given by

$$f_{\text{FH}} = \frac{1}{N_p} \phi \ln(\phi) + (1 - \phi) \ln(1 - \phi) + \chi \phi(1 - \phi) + \frac{K}{2} |\nabla \phi|^2. \quad (4)$$

Phase separation, also referred to as ‘coacervation’ for colloids and polymers, is favored in poor solvents, where  $\chi$  is positive, implying a net repulsion between the polymer and the solvent and/or strong self-attractions between the polymers.

**2.2.4. Dynamics: models A, B, C, and H.** Next we summarize phenomenological equations of motion that drive the concentration / order parameter fields specified in the free energies above toward thermodynamic equilibrium under various types of transport mechanisms. These dynamic equations are chosen based on their ubiquity in the materials literature or their likely relevance to intracellular systems. The standard letter-based nomenclature introduced by Hohenberg and Halperin [64] to classify the dynamic theories of critical phenomena is followed.

**Model A** or the stochastic Allen–Cahn equation, describes the dynamics of a phase transforming binary mixture with nonconserved order parameter  $\phi$  as

$$\frac{\partial \phi}{\partial t} = -\Gamma \frac{\delta F[\phi]}{\delta \phi} + \xi_A(\vec{r}, t). \quad (5)$$

Here  $\Gamma$  is a mobility constant,  $\delta F[\phi]/\delta \phi$  is local chemical potential, and  $\xi_A$  is a stochastic term introduced to account for time-averaged, weakly-correlated molecular scale fluctuation effects. The latter has mean  $\langle \xi_A \rangle = 0$  and variance  $\langle \xi_A(\vec{r}_1, t_1) \xi_A(\vec{r}_2, t_2) \rangle = 2\Gamma k_B T \delta(\vec{r}_1 - \vec{r}_2) \delta(t_1 - t_2)$ , where angled brackets denote ensemble averages.

Crystallization and gelation are examples of nonconservative transitions relevant to intracellular systems. Here the order parameter quantifies the local fraction of crystal or gel phase, and the global fraction of crystal or gel is not constrained from varying with time. Domains of the transformed phase nucleate, grow, and coarsen, but this occurs through local processes such as changes in molecular structure that typically do not require long-range mass transport. In contrast, phase separation is conservative; molecular concentrations spatially partition into domains rich or poor in particular species, and long-range molecular transport, rather than local structural rearrangements, is necessary to facilitate this (see Models B, C, and H).

In Model A, the order parameter  $\phi$  simply relaxes toward equilibrium at a rate proportional to the local chemical potential (hydrodynamic flow is neglected). During early stage ( $\theta_d \ll 1$ ) nonconserved growth, the domain wall velocity is therefore proportional to the driving force for transformation. When this driving force is constant, growth proceeds as  $R(t) \sim t$  ( $n = 1$ ), with Avrami exponent  $m = 3$  for heterogeneous and  $m = 4$  for homogeneous nucleation. When  $\theta_d \rightarrow 1$  at late times, surface tension provides the driving force for domain evolution, and domain walls move at a velocity proportional to the local curvature, consistent with classical curvature-driven kinetics. Domain size then scales during steady-state nonconserved coarsening as  $R(t) \sim t^{1/2}$ . These Model A  $n = 1$  growth and  $n = 1/2$  coarsening regimes

are not related to any of the phase separation-focused mechanisms listed in table 1, but may be relevant to the kinetics of intracellular crystallization or gelation.

**Model B** or the stochastic Cahn–Hilliard–Cook equation, is a generalized diffusion equation for systems with a conserved order parameter. We will begin with the fully generalized form for systems with  $N$  components and then outline the approximations employed in arriving at the most widely used form for incompressible binary mixtures. Consider an  $N$  component system described by  $N$  composition fields  $\phi_i$ . According to the central ansatz of linear irreversible thermodynamics [90–92], the fluxes of  $\phi_i$  are linear and homogeneous functions of the driving forces  $\nabla\delta F/\delta\phi$  and can therefore be expressed as

$$\vec{J}_i = - \sum_{j=1}^N L_{ij}(\phi_1, \phi_2, \dots, \phi_N) \nabla \frac{\delta F}{\delta \phi_j}. \quad (6)$$

$L_{ij}(\phi_1, \phi_2, \dots, \phi_N)$  is the symmetric, positive definite  $N \times N$  matrix of Onsager kinetic coefficients, which can be written in terms of the mobility matrix  $\Gamma_{ij}$  as  $L_{ij}(\phi_1, \phi_2, \dots, \phi_N) = \Gamma_{ij}\phi_j$ . Combining equation (6) with the continuity equation for conserved species, which states that  $\phi_i$  relaxes toward equilibrium at a rate proportional to the divergence of its flux,

$$\frac{\partial \phi_i}{\partial t} = -\nabla \cdot \vec{J}_i, \quad (7)$$

the complete dynamics can be written as a set of  $N$  coupled nonlinear stochastic diffusion equations,

$$\frac{\partial \phi_i}{\partial t} = \nabla \cdot \left[ \sum_{j=1}^N \left( \Gamma_{ij}\phi_j \nabla \frac{\delta F}{\delta \phi_j} \right) \right] + \xi_i(\vec{r}, t). \quad (8)$$

Here  $\xi_i(\vec{r}, t)$  satisfies  $\langle \xi_i \rangle = 0$  and  $\langle \xi_i(\vec{r}_1, t_1) \xi_i(\vec{r}_2, t_2) \rangle = -2k_B T \nabla \cdot \nabla [\Gamma_{ij}\phi_j \delta(\vec{r}_1 - \vec{r}_2) \delta(t_1 - t_2)]$ .

Various approximations are often applied to  $L_{ij}$  as appropriate for a given system, though sometimes without justification. For example, the set of dynamical equations is greatly simplified if one is able to assume a diagonal form,  $\Gamma_{ij} = 0$  for  $i \neq j$ . Further simplification results from neglecting the composition dependence, such that  $L_{ij}$  becomes a diagonal matrix of constants  $\Gamma_i$ . The standard form of Model B for a binary incompressible fluid employs these assumptions as well as  $\Gamma_1 = \Gamma_2 = \Gamma$ , giving

$$\frac{\partial \phi}{\partial t} = \Gamma \nabla^2 \frac{\delta F[\phi]}{\delta \phi} + \xi_B(\vec{r}, t), \quad (9)$$

where  $\langle \xi_B \rangle = 0$  and  $\langle \xi_B(\vec{r}_1, t_1) \xi_B(\vec{r}_2, t_2) \rangle = -2\Gamma k_B T \nabla^2 \delta(\vec{r}_1 - \vec{r}_2) \delta(t_1 - t_2)$ .

Now we examine the domain evolution kinetics produced by binary Model B. Consider an off-critical quench below the binodal, into any part the two-phase region of the phase diagram above or below the spinodal. Following nucleation or spinodal decomposition, motion of an interface delineating two phases with different concentrations of a conserved species requires long-range mass transport. Under purely diffusive transport, the dominant initial growth mechanism is diffusion of droplet-forming molecules directly from the

initially supersaturated background phase into nearby droplets. At early times when  $\theta_d \ll \theta_d^{\max}$ , Model B therefore generates DLG with  $R(t) \sim t^{1/2}$  and Avrami exponent  $m = 3/2$  for heterogeneous or  $m = 5/2$  for homogeneous nucleation. Surface attachment-limited growth ( $n = 1$ ) can also be studied by, e.g. modulating the mobility parameter such that transport at domain interfaces is the rate-limiting process. During late-stage growth (the crossover from growth to coarsening where  $\theta_d \rightarrow \theta_d^{\max}$ ), Model B kinetics is consistent with the theory of diffusion-limited precipitation ( $m \simeq 1$ , see section 2.1.1). Finally, when the supersaturation outside of droplets becomes fully depleted, Model B gives DLC (Ostwald ripening) with  $R(t) \sim t^{1/3}$ . Here the dominant growth mechanism becomes transport of droplet-forming molecules from regions of high interface curvature to regions of low curvature, via diffusion through the bulk/background phase. Surface attachment-limited coarsening ( $n = 1/2$ ) can also be studied with appropriate modification as noted above. Model B can therefore be employed to describe phase separating systems in which Brownian coalescence and hydrodynamic coarsening mechanisms have negligible effect.

**Model C** combines Models A and B to describe systems with a nonconserved order parameter  $\phi$  coupled to a conserved field  $\psi$ . The simplest form of Model C reads

$$\frac{\partial \phi}{\partial t} = -\Gamma_\phi \frac{\delta F[\phi, \psi]}{\delta \phi} + \xi_A(\vec{r}, t) \quad \frac{\partial \psi}{\partial t} = \Gamma_\psi \nabla^2 \frac{\delta F[\phi, \psi]}{\delta \psi} + \xi_B(\vec{r}, t). \quad (10)$$

In a common materials science application,  $\phi$  represents the concentration of solid phase and  $\psi$  represents temperature in a crystallizing liquid. Model C may be relevant to intracellular liquids, for example, in systems where coupled phase separation and gelation or crystallization are of interest.

**Model H** or the stochastic advective Cahn–Hilliard–Cook equation, is the most complete description of multicomponent fluids among these models, as it incorporates both diffusion and hydrodynamic flow (advection). As is apparent from table 1, strong hydrodynamic effects can qualitatively alter phase separation kinetics. Model H for an  $N$  component fluid with a constant, diagonal matrix of Onsager coefficients is

$$\frac{\partial \phi_i}{\partial t} + \vec{v} \cdot \nabla \phi_i = \Gamma_i \nabla^2 \frac{\delta F}{\delta \phi_i} + \xi_{B,i}(\vec{r}, t) \quad (11)$$

where  $\vec{v}(\vec{r}, t)$  is the fluid velocity field. When the velocity obeys the Navier–Stokes equation for an incompressible fluid, its solution is obtained from

$$\rho \left( \frac{\partial \vec{v}}{\partial t} + (\vec{v} \cdot \nabla) \vec{v} \right) = \eta \nabla^2 \vec{v} - \nabla p - \sum_{i=1}^N \phi_i \nabla \frac{\delta F}{\delta \phi_i}, \quad (12)$$

where  $p$  is pressure,  $\eta$  is viscosity, and the density  $\rho$  is constant. In the limit most relevant to intracellular fluids, that of low Reynolds number (the Stokes or creeping flow limit), the solution for  $\vec{v}$  is

$$v_j(\vec{r}, t) = \int d^2 r' T_{jk}(\vec{r} - \vec{r}') \left[ \sum_{i=1}^N \frac{\delta F}{\delta \phi_i(\vec{r}')} \nabla'_k \phi_i(\vec{r}', t) + \xi_k(\vec{r}', t) \right], \quad (13)$$

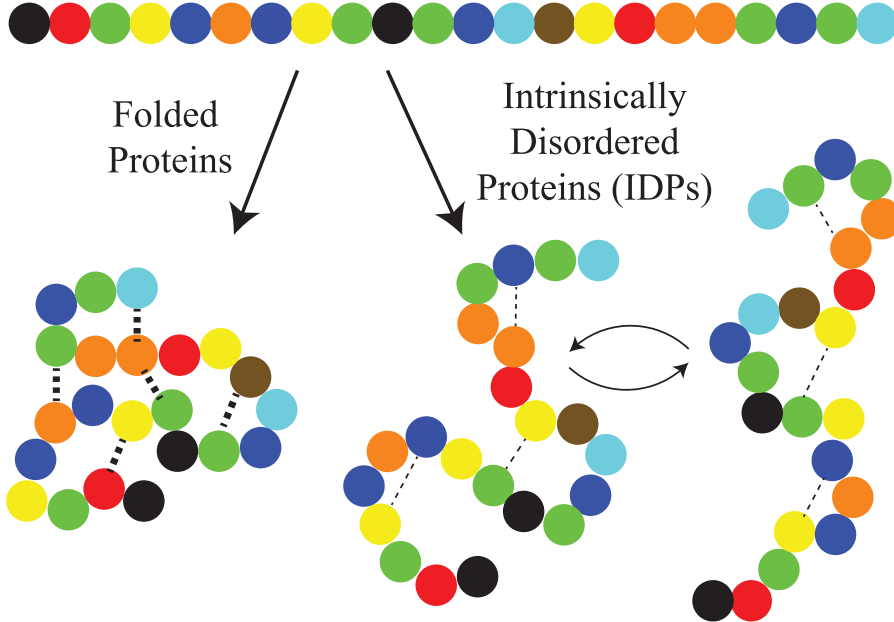


**Figure 5.** Schematic of a protein as a chain of interacting spheres. The lower three configurations highlight the difference in tertiary structure between a folded protein and an intrinsically disordered protein (IDP), or intrinsically disordered region (IDR) of a protein. Strong intrachain interactions in folded proteins (left) lead to a highly stable folded configuration. Weaker intrachain interactions in IDRs lead to multiple configurations (center, right) separated by low energy barriers; IDRs are thus said to possess conformational heterogeneity. Several proteins contain IDRs which have been identified as drivers of intracellular phase separation.

where  $j, k \in x, y, z$ ,  $T_{jk}(\vec{r})$  is the Oseen tensor which is expressed in Fourier space as  $T_{jk}(\vec{k}) = (\delta_{jk} - k_j k_k / k^2) / (\eta k^2)$ ,  $k$  is wavenumber,  $\delta_{jk}$  is the Kronecker delta,  $\langle \xi_k \rangle = 0$ , and  $\langle \xi_j(\vec{r}_1, t_1) \xi_k(\vec{r}_2, t_2) \rangle = -2k_B T \eta \nabla^2 \delta_{jk} \delta(\vec{r}_1 - \vec{r}_2) \delta(t_1 - t_2)$  [93].

In the diffusive regime, where the fluid velocity  $|\vec{v}|$  is much smaller than the interface velocity  $dR/dt$ , Model H reduces to Model B behavior. This is generally the case during growth and the early stages of coarsening, leading to initial  $n = 1/2$  DLG and  $n = 1/3$  DLC regimes. For small or intermediate  $\theta_d$ , BMC and HC also emerge from Model H dynamics under the appropriate conditions (the HC mechanism was discovered/predicted based on Model H simulation results [69]). For large  $\theta_d$  (bicontinuous phases), as  $dR/dt$  decreases with time toward  $|\vec{v}|$ , hydrodynamic effects become important and the intermediate VHC regime noted in section 2.1.2 emerges. Continued coarsening leads to an increase in Reynolds number; if  $Re \gg 1$ , the IHC regime noted in section 2.1.2 may then occur, again only for large  $\theta_d$ .

Model H therefore incorporates the physics needed to describe all of the phase separation / droplet growth and coarsening behaviors outlined in table 2. It should therefore provide a useful foundation from which to begin modeling intracellular fluids under a variety of biologically-relevant conditions. Incorporation of surface-attachment kinetics, gravitational forces, shear flow effects, and active processes such as chemical reaction kinetics (see section 3.4) are also possible.

### 2.3. Molecular driving forces

The above field-theoretic descriptions of phase separating fluids are formulated on the basis of general, broadly applicable

thermodynamic principles and mechanisms of mass transport. Details of the molecular driving forces that lead to conditions which favor phase separation are assumed to be reducible to coarse-grained, mean-field thermodynamic interaction parameters such as  $\chi$  in the regular solution and Flory–Huggins models of equations (2) and (4). It is nonetheless crucial to understand the nature of the molecular driving forces that lead to intracellular condensation, both from the perspective of biological function and to better assess the applicability of given physical descriptions and mean-field approximations.

The hypothesis that intracellular condensates represent phase separated droplets has gained strong support from the elucidation of key aspects of the underlying molecular driving forces. Many proteins within condensates exhibit repetitive protein-protein or protein-RNA binding modules and are therefore referred to as multivalent. One such set of proteins is the SH3/PRM system, whose phase separation behavior has been characterized by Rosen *et al* [8, 94]. The SH3 domain binds to proline rich motifs (PRM) and condense into liquid droplets above a saturation concentration. Moreover, higher valency constructs, e.g.  $(SH3)_n$  and  $(PRM)_n$ , where  $n > 3$ , phase separate at lower module concentrations. When these proteins are expressed in living cells, they condense into liquid-like structures, much like endogenous condensates. More recent work has utilized a multivalent SUMO/SIM system to elucidate key aspects of the compositional control of condensates [95].

A second and related driving force is proteins that exhibit conformational heterogeneity, known as intrinsically disordered proteins/regions (IDP/IDR, see figure 5). Conformational heterogeneity refers to a protein's tendency to dynamically rearrange its conformation, typically between various partially folded states. Proteins with conformational

heterogeneity are typically of low sequence complexity and are closely related to self-templating prion-like domains, although distinctions between these different types of proteins remain largely unclear. There are now many examples of IDRs that have been shown to drive phase separation *in vitro* and within living cells. This property appears to arise from a rich set of interactions associated with charged residues (poly-anionic, polycationic, or polyampholytic), as well as aromatic residues, particularly tyrosine and phenylalanine [50]. Some of the most well-known examples include RNA binding proteins found in stress granules, including FUS [96–98] and HNRNPA1 [99]. Both of these examples are also ALS-related proteins, underscoring the close links between IDPs and pathological aggregation.

One of the first IDPs to be uncovered as a driving force for intracellular phase separation is DDX4, an RNA helicase found in germ granules (Nott *et al* [9]). Nott *et al* showed that DDX4 phase separates in a salt, temperature, and protein concentration dependent manner, both *in vitro* and in cells which express a YFP-tagged DDX4 variant. LAF-1 is a closely related germ (P) granule RNA helicase, which has also been shown to undergo phase separation, and for which a disordered arginine (R) and glycine (G)-rich amino-terminal domain is both necessary and sufficient for driving phase separation. Moreover, LAF-1 droplets exhibit tunable viscosity and dynamics (Elbaum-Garfinkle *et al* [100]) as a result of the impact of salt and RNA molecules on protein-protein interaction strength (second virial coefficient) and therefore on the shape of the LAF-1 binodal [101].

Other IDPs found in P granules have recently been shown to phase separate, including PGL-3 [102], and the MEG proteins [103]. As we discuss further below, the example of P granule segregation is particularly fascinating, because the equilibrium driving forces provided by self-affinity of IDP domains appear to be modulated across the anterior–posterior (AP) axis, by nonequilibrium reaction–diffusion mechanisms. This underscores one of the central questions with which this review is concerned: How well can the formation and stability of such bodies be characterized and understood from the basic physical view of equilibrium phase transitions mediated by passive phase separation evolution mechanisms?

#### 2.4. Discussion

Above we have outlined key models that have been or may be utilized to study intracellular phase transitions. In the next part (section 3), experimental tests of some of these theoretical descriptions of phase separation in contexts relevant to intracellular phenomena will be outlined. Since these are passive descriptions, limits to their applicability in active living cells should be discernible. Our aim will therefore be to summarize current understanding of the degree to which these concepts may be reasonably applied to biological processes as well as circumstances in which they break down. Deviation from passive behavior generally occurs due to effects of active biological processes. We broadly define active systems for our purposes as those in which detailed balance (time-reversal symmetry) is broken by internal or external energy sources,

such that properties and kinetics are significantly influenced by processes other than equilibrium phase transformations mediated by thermodynamically-driven (thermally, chemically, etc) molecular transport along gradients of well-defined thermodynamic potentials. Processes that lead to violation of detailed balance can often be described as chemical reactions, though not all chemical reaction processes violate detailed balance. Active reactions may be relatively simple ones such as oligomerization or phosphorylation, or more complex processes such as metabolic activity associated with adenosine triphosphate (ATP) utilization and active transport (migration against chemical potential gradients), transcriptional activity, and so on.

To aid in distinguishing between phenomena dominated by different passive or active processes, we will divide current theoretical descriptions of inhomogeneous phase separating systems into four types;

1. Passive.
2. Modulated passive.
3. Undriven chemically reactive.
4. Driven chemically reactive.

The first type, passive systems, are those whose phase equilibria and domain kinetics exhibit no significant deviations from equilibrium thermodynamics and classical passive kinetics as overviewed in section 2.

The second type, modulated passive systems, differ from passive systems only in the addition of space and/or time-dependent (rather than fixed) equilibrium or external parameters. For example, effective molecular interaction strengths such as  $\chi$  in equation (2) may vary across the cell. The underlying causes of these variations may be biological activity, but their effect in such mixtures can be absorbed into effective equilibrium parameters and thus treated within the classical passive framework. The first two levels of description do not involve explicit treatment of chemical reactions (or any other active process), and the number of particles is a conserved quantity.

In the third category, undriven chemically reactive systems, chemical kinetics are present but no internal or external energy sources, such as biological activity associated with ATP utilization, supply work to (or drive) the system. Undriven chemically reactive mixtures satisfy detailed balance in equilibrium and therefore ultimately relax to thermal equilibrium unless, e.g. special boundary conditions are applied. Domain evolution kinetics may be altered relative to non-reactive mixtures, but thermodynamic equilibrium is not affected by the presence of reactions. In other words, undriven chemical reactions do not affect thermodynamic stability (i.e. shift phase boundaries) [104], and any nonequilibrium states should be unstable in the absence of an energy source. See below and sections 3.4 and 4.2 for further discussion of these issues.

The first three classes of models outlined here share the common fundamental feature that each is predicated on the existence of a thermodynamic free energy density and relaxation to local thermal equilibrium. Applications of passive and modulated passive descriptions to intracellular phenomena are described in sections 3.1–3.3. In section 3.4 we outline

field-theoretic descriptions of undriven chemically reactive, inhomogeneous systems and describe applications to protein/intracellular condensation phenomena.

Systems in the fourth category, driven chemically reactive, are fundamentally different from those in the other three. Here work is supplied through external forces (mechanical, electromagnetic, etc), heat transfer (conduction, radiation, etc), mass transfer (chemical reactions with reservoirs, etc), or internal energy sources (e.g. ATP, molecular motors, active swimmers, etc). Unlike undriven chemically reactive mixtures, the work done on driven mixtures can alter thermodynamic stability of phases [105]. Biological activity or driving work in general can therefore not only alter the kinetics of phase separation, it can dictate whether phase separation even occurs. This implies that active processes in cells can shift phase boundaries to, e.g. suppress or induce phase separation on the ‘wrong’ side of the spinodal or binodal, or introduce long-lived nonequilibrium steady-states such as chemically-arrested phase-separated morphologies. This distinction from undriven systems has potentially far-reaching consequences in terms of the cell’s ability to dynamically and robustly mediate condensate assembly/disassembly, as well as our understanding of how it does so.

In driven chemically reactive mixtures, reaction rates can be dictated by driving forces other than the local chemical potential and detailed balance can be violated. A well-defined thermodynamic free energy functional does not exist; rather a nonequilibrium free energy functional is sought. Deriving such functionals is a challenging fundamental problem, but one that provides interesting opportunities for new theoretical developments that combine the thermodynamics of phase transformations with highly non-equilibrium active processes in biological systems. Recent and emerging theoretical developments in this area that are of relevance to intracellular phenomena are discussed in section 4.

### 3. Experimental tests of passive and modulated passive descriptions

#### 3.1. *In vitro* studies of phase separation in aqueous protein solutions

A variety of studies concerning the *in vitro* phase separation of protein solutions into protein-rich, liquid-like droplets and a protein-poor background phase have been conducted. These have considered aspects of phase behavior as well as growth kinetics.

**3.1.1. A brief history of globular proteins in solution: Lysozyme.** Aqueous protein solutions have long been known to exhibit nontrivial phase behavior and kinetics with relationships to those of other complex fluids (polymer solutions, colloidal solutions, etc) [106–108]. Liquid–liquid phase separation in such solutions was categorized as a type of ‘coacervation’, and this term is still used in the literature, particularly among chemists. This process has historically been of interest

in regard to protein crystallization for crystallographic studies and pharmaceutical applications. The more recent linking of protein phase separation in living cells to various aging and neurodegenerative diseases [8, 42, 44–46, 98, 99, 109–112] has generated significant interest among cellular biologists, biochemists, and biophysicists. A full understanding of protein phase transitions *in vitro* may be a critical precursor to understanding and effectively treating such diseases (see section 4).

Protein solutions have also been of interest to physicists and others outside of biology since the 1970s as model systems for the study of critical phenomena and other phase transformations [62, 113–120]. Similar to polymer mixtures, their relatively large characteristic length and time scales make experimental studies easier in many regards as compared to atomic and molecular fluids. Their phase behavior generally involves clear concentration-dependent phase equilibria between mixed liquid phases, demixed liquid phases, and ordered crystals, and also often includes critical points and aggregation/gelation phenomena [62, 121–124].

The *in vitro* phase behavior of the globular protein lysozyme has been most extensively studied [122, 124–133]. Figure 6(a) shows an experimentally determined ‘state’ diagram for lysozyme. This is not a true equilibrium phase diagram because the crystal is the equilibrium state at all temperatures and concentrations below the liquid-crystal boundary; the liquid–liquid miscibility gap and gel/glass line describe metastable phases only. Metastable demixed liquid phases and gel or glass phases are common features of globular protein phase behavior, and studies of model colloidal systems have shown that this type of phase behavior occurs when intermolecular interactions are dominated by short-range attractive forces [134] (figure 6(b)). Globular proteins in solution often have short-range attractive interactions; their phase behavior is therefore consistent with this physical interpretation. In colloidal systems, as the range of attraction is increased toward and above the diameter of the colloids, the liquid–liquid binodal shifts above/outside of the crystallization boundary and the demixed liquid phases become thermodynamically stable. Similar behavior is also observed in complex fluids dominated by long-range depletion attractions (see, e.g. [135]). The distinction between thermodynamically stable and metastable liquid phases may be crucial to understanding the aging behavior of intracellular condensates and associated proteins that mature into gel-like and solid-like structures reminiscent of pathological protein aggregates implicated in human disease.

**Macroscopic phase separation kinetics.** Many studies of lysozyme phase transition kinetics have focused on crystal nucleation mechanisms [123, 128, 132, 138] and gelation/aggregation dynamics [124, 127, 131, 133], the latter often being viewed as an undesirable obstruction of the former. The macroscopic phase separation kinetics associated with lysozyme’s metastable liquid–liquid miscibility gap have also been studied. A smooth transition from nucleation behavior consistent with classical nucleation theory to behavior consistent with spinodal decomposition was reported in [123,

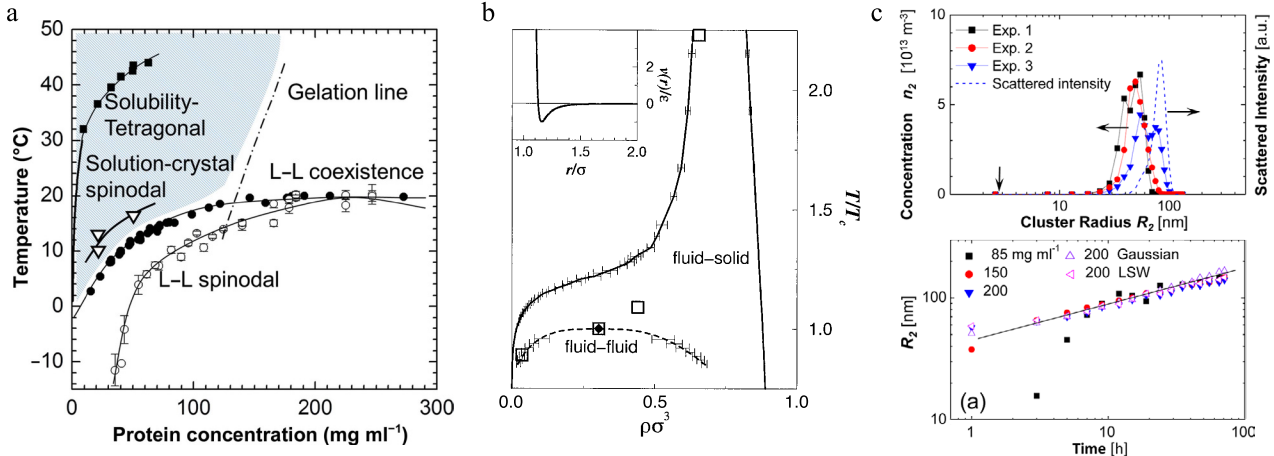


**Figure 6.** Reproduced with permission from [136]. Copyright © International Union of Crystallography. Experimentally determined phase diagram of a lysozyme solution in 0.05 M sodium acetate buffer pH 4.5 and 4.0% NaCl. The shaded area denotes compositions at which dense liquid clusters were detected. (b) From [134]. Reprinted with permission from AAAS. Typical phase diagram of colloids with short-range attraction. Diamonds, solid lines, and the dashed curve indicate fluid–fluid critical points, equilibrium coexistence curves, and the metastable fluid–fluid coexistence boundary, respectively. (c) Reprinted with permission from [137]. Copyright (2012) American Chemical Society. Measured droplet size distributions (top) and time-dependence of mean anomalous droplet radii (bottom) in lysozyme solutions. The solid line corresponds to  $n = 0.26$ .

[139], with apparent values of  $n$  between 0.15 and 0.3. Spinodal decomposition with  $n \simeq 0.30\text{--}0.34$  was reported in [140] for quenches to temperatures above those which induce crossing of the gelation boundary (see figure 16(d), Region I). Quenches to lower temperatures (Region II) were shown to lead to an arrested spinodal decomposition process in which the fastest growing fluctuation mode from the early stage spinodal structure is frozen-in by the rapid formation of a gel-like network. Increases in concentration at fixed final temperature  $T_f$  do not alter the characteristic length scale  $\xi$  of the frozen network, but quenches to lower  $T_f$  at fixed concentration decrease the length scale as  $\xi \sim (T_s - T_f)^{0.55}$ , where  $T_s$  is the spinodal temperature. This is consistent with mean-field and renormalization group predictions for the fastest early stage fluctuation growth mode, 0.5 and 0.63, respectively (see figure 16 and section 4.3 for further discussion of gelation phenomena).

**Anomalous dense liquid precursors to crystal nucleation.** An interesting and important feature of lysozyme crystal nucleation is the identification of a two-step mechanism involving a mesoscopic protein-rich liquid droplet precursor phase [132, 134, 136, 141, 142]. These dense liquid precursor droplets in lysozyme dynamically assemble and disassemble with typical radii around 100 nm and lifetimes around  $10^{-2}$  s to  $10^1$  s. They generally exist between the liquidus and liquid–liquid binodal or even above the liquidus (shaded region in figure 6(a)), and are distinct from the macroscopically phase separated droplets that appear within the metastable liquid–liquid miscibility gap. Crystal nucleation rates are many orders of magnitude higher within these protein-rich droplets than in the bulk solution [128]. Understanding the nature of their formation is an area of active study that is expected to provide important insight not only into crystallization, but also into the *in vivo* formation of disease-related aggregates such as amyloid fibrils and sickle cell polymer fibers (see section 4 for further discussion).

Though the anomalous precursor droplets are reported to have characteristic sizes around 100 nm, they have been found to exhibit (relatively slow) coarsening kinetics quite similar to those predicted by the classical theory of DLC or Ostwald ripening (see table 1) [137]. A coarsening exponent  $n = 0.26 \pm 0.03$  was measured (figure 6(c)), independent of protein concentration and droplet phase volume fraction. The droplet size distribution was found to be scale-invariant, with an extracted coarsening prefactor  $K$  within roughly an order of magnitude of the classical prediction given in table 1. A coarsening exponent  $n = 0.325$  was also measured in [143].

Different mechanisms of cluster stabilization above the metastable liquid–liquid binodal have been proposed, including equilibrium clustering as the result of a balance of short-range attractive and long-range repulsive interactions [129, 144] and transient protein oligomer (dimer) formation [145–149], but their origin is currently unclear. Arguments against the electrostatic view (short-range attraction, long-range repulsion) include its prediction of cluster sizes on the order of tens rather than  $10^4\text{--}10^6$  protein sizes with gel-like rather than liquid-like properties [145]. In the transient protein complex formation view [145], it is argued that cluster stability requires the presence of species other than protein monomers, and that these species are provided by the formation and disassembly of transient protein complexes within the dense liquid phase, i.e. chemical reactions. A reaction–diffusion model (see section 3.4) formulated from this view predicts a steady-state droplet size determined by the disassembly ( $k_2$ ) and diffusion ( $D_2$ ) rates of the complexes,  $R \simeq \sqrt{D_2/k_2}$ . This prediction is apparently in contradiction with the Ostwald-like ripening behavior observed in [137].

We mention another possible kinetic mechanism associated with stabilization of emulsions. When a third species that is immiscible or nearly immiscible in the solvent phase is added to a binary phase separating mixture, these molecules are effectively trapped within the droplet phase, implying that

a droplet can never completely disassemble [150]. The driving force for Ostwald ripening, the Laplace pressure of the droplets, which favors fewer, larger droplets, is then forced to compete with the osmotic pressure of the trapped species, which favors uniform, finite droplet sizes. The result of this competition is selection of a stable finite droplet size under certain thermodynamic conditions. When thermodynamic conditions do not favor size selection, this mechanism leads to Ostwald-like ripening with otherwise slower than expected prefactor  $K$ .

**3.1.2. In vitro studies of proteins associated with intracellular condensates.** Several studies in recent years have examined the *in vitro* phase behavior of proteins associated with particular condensates. Aqueous solutions of purified protein provide a less complex environment in which the nature of their demixing behavior and the key environmental and molecular factors that control demixing may be more readily elucidated. The degree to which *in vitro* droplets reproduce the biophysical properties of the corresponding *in vivo* condensates can be challenging to assess, but such experiments can nonetheless provide crucial information about the driving forces underlying intracellular phase transitions and the mechanisms by which they proceed.

The majority of such studies to date have focused on the mapping of phase boundaries as functions of protein, salt, and RNA concentrations, and on comparing behaviors of various mutant constructs to identify molecular players and domains necessary for phase separation. Here we summarize the results of a few such studies with relevance to the fundamental nature of the droplet formation process, and conclude with an overview of the one study (to our knowledge) that quantitatively analyzes droplet coarsening kinetics in terms of the theories of classical passive phase transition kinetics.

**Demixing and gelation of multivalent proteins.** As briefly discussed above, Li *et al* [8] studied diverse multivalent intracellular proteins in solution and found that liquid–liquid demixing transitions commonly occur at concentrations above sharply-defined phase boundaries that vary systematically with the valency of the interacting species. The resulting protein-dense droplets exhibit liquid-like behavior (spherical shapes, coalescence) and gel-like behavior, including partitioning of larger molecules into the droplet phase, a distribution of relaxation times within droplets, a three order of magnitude decrease in protein diffusion rates inside droplets, fluorescence recovery after photobleaching (FRAP) recovery rates that correlate inversely with monomer-monomer affinity and valency, and rapid diffusion of smaller molecules into and within droplets. The authors conclude that multivalent proteins exhibit liquid–liquid phase separation and that this process can be thermodynamically coupled to a sol-gel transition within the droplet phase that produces a large crosslinked network under certain conditions. It was also demonstrated that increasing the effective valency of proteins through binding of different species can dramatically alter phase behavior by shifting phase boundaries to much lower concentrations. This suggests that cells can dynamically shift phase boundaries, e.g. by employing protein kinases to control the degree of phosphorylation

of certain proteins and thus their effective valency and affinity to phase separate. A related study of protein clustering on quasi-2D artificial lipid membrane bilayers points to interesting similarities between the factors that control 3D condensate formation and those that control phase separation and clustering in 2D membranes [94].

**Disordered nuage protein droplets.** The *in vitro* and *in vivo* formation of droplets rich in the fluorescently tagged protein DDX4<sup>YFP</sup> was examined in [9]. DDX4 is a primary constituent of nuage or germ granules in mammals and contains intrinsically disordered regions (IDRs) which appear to drive phase separation. Patterned electrostatic interactions within the IDR were determined to stabilize the droplet phase, and the liquid-like environment within droplets was found to concentrate single-stranded DNA while largely excluding double-stranded DNA. The sequence characteristics that enable DDX4 droplet formation are also present in many other disordered proteins associated with intracellular condensates. These include the *C. elegans* closely related germ granule (P granule) protein LAF-1, which contains an IDR which was shown to be necessary and sufficient for driving phase separation into P granule-like droplets *in vitro* [100]. Other related germ granule proteins have also been implicated in promoting phase separation, including PGL-3 [102] and the MEG proteins [103].

**RNA, aging, composition, and signaling.** Several other *in vitro* studies have shown that RNA can dramatically alter protein phase behavior and droplet properties [28, 55, 100, 101, 151, 152], that droplet properties can be time-dependent, becoming more solid-like and potentially fibrous upon aging [46, 55, 98, 99, 111, 151, 153], and that the composition (and consequently function) of phase separated droplets can be dynamically regulated [95]. These phenomena involve aspects of phase behavior and phase separation kinetics beyond those of most simple binary fluids, highlighting the importance of employing and further developing theories and models of appropriate complexity. A recent study has also demonstrated that quite complex signaling functionalities associated with phase separated bodies, in this case a 12-component membrane-based signaling pathway that begins with T cell receptor (TCR) activation and ends with actin assembly, can be reproduced and systematically manipulated *in vitro* [12]. This emphasizes the important roles of both phase equilibria and phase separation kinetics to the proper functioning of such signaling pathways.

**Dynamic scaling analysis of FIB-1 droplets.** A quantitative study of the *in vitro* phase separation kinetics of the nucleolar protein FIB-1 was reported in [28]. At near-physiological salt concentrations, approximately spherical liquid-like FIB-1-rich droplets formed above a threshold protein concentration  $C_{\text{sat}}$  (figures 7(a)–(c)). Droplet coalescence and ripening were observed over time (figures 7(a) and (b)), and the average droplet radius  $\langle R \rangle$  was found to increase as  $\langle R \rangle \sim t^{0.32 \pm 0.11}$  (figure 7(d)). Upon addition of RNA to the solution,  $C_{\text{sat}}$  was found to decrease (figure 7(c)), and coarsening under otherwise identical conditions obeyed  $\langle R \rangle \sim t^{0.34 \pm 0.08}$  (figure 7(d)), with a larger prefactor  $K$  than that observed without RNA.

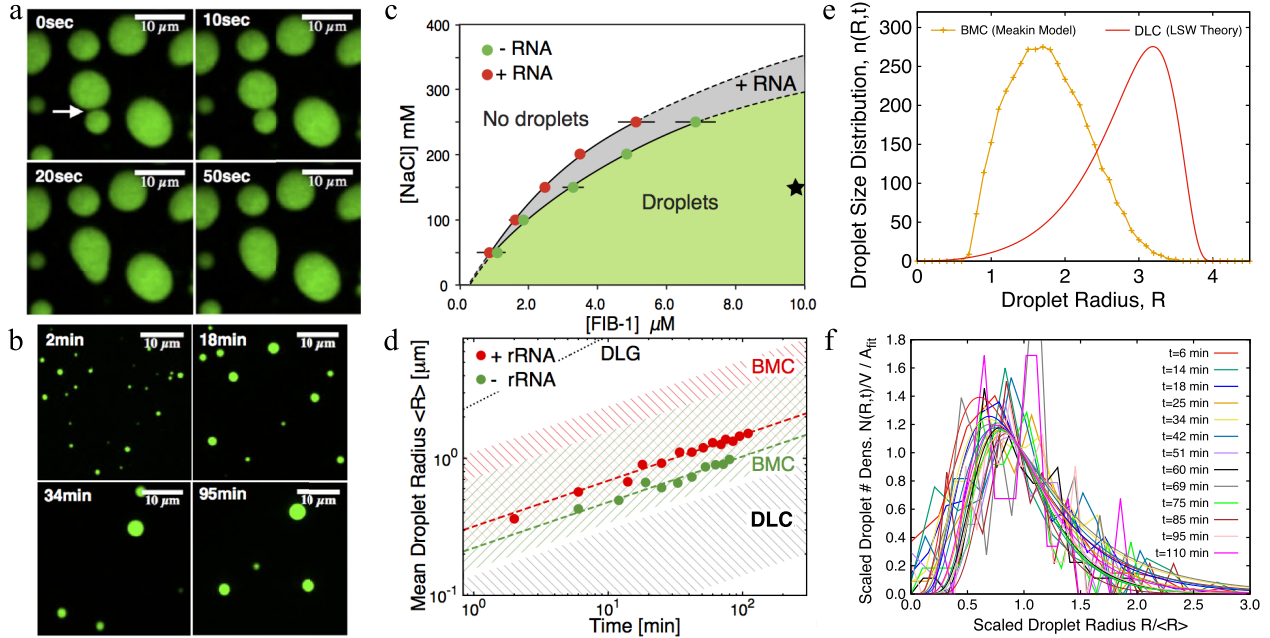


**Figure 7.** BMC and DLC-based analysis of *in vitro* FIB-1 phase separation kinetics. (a)–(d) and (f) Reproduced with permission from [28]. Copyright © Proceedings of the National Academy of Sciences of the United States of America. (a) Time-lapse images of FIB-1 droplets coalescing on a surface. (b) Maximum-intensity projections of 3D image stacks of a solution of FIB-1 droplets coarsening over time. (c) Phase diagram of FIB-1 in the presence and absence of RNA. The star indicates the protein and salt concentrations of the systems shown in (a) and (b). Data points are averages of three independent trials with the standard deviations as error bars. (d) Droplet evolution kinetics from experimental data (points) and theoretical predictions (dotted line and hatched area). DLG, black dotted line; BMC, green (−RNA) and red (+RNA); DLC, gray; power law data fits, dashed lines. (e) Comparison of theoretically-predicted droplet size distributions under BMC-dominant and DLC-dominant conditions. BMC distributions are right-skewed, while DLC distributions are left-skewed (see also table 3). BMC results were obtained using the simulation method of [86]. (f) Measured and scaled droplet size distributions, exhibiting shapes and scaling consistent with BMC.

The power law scaling exponents  $n \simeq 0.32$  and  $0.34$  are consistent with both BMC and DLC ( $n = 1/3$ ). An early-stage DLG regime with  $n = 1/2$  is not observed, consistent with the theoretical estimate that such a regime would terminate within  $\sim 1\text{--}10\text{ s}$  of nucleation (i.e. too rapidly to observe). Furthermore, the predicted scaling exponents for droplet number density  $N \sim t^\gamma$  and droplet size distribution amplitude  $N_{\max} \sim t^\delta$  are identical for BMC and DLC;  $\gamma = -1$  and  $\delta = -4/3$ . The measured values  $\gamma \simeq -1.10$  ( $-0.98$ ) with(out) RNA and  $\delta \simeq -1.23$  ( $-1.27$ ) with(out) RNA, though consistent with the predictions, therefore do not aid in distinguishing between mechanisms. Some indication is given by the measured dynamic prefactors  $K$ ; these are quantitatively consistent with those predicted for BMC ( $K \simeq 6k_B T \theta_d / 5\pi\eta$ ), whereas the predicted values of  $K$  for DLC ( $K \simeq 8\sigma D c_\infty V_m^2 / 9N_A k_B T$ ) are an order of magnitude or more smaller than those measured. This suggests that BMC may contribute to coarsening more than DLC, but is not conclusive.

A more effective way of distinguishing between mechanisms is to examine the shape and scaling of the full droplet size distribution, rather than individual moments such as  $\langle R \rangle$ . Figure 7(e) shows theoretically-predicted droplet size distributions for systems undergoing pure BMC and pure DLC. The large  $R$  tail of the approximately log-normal BMC distribution can be clearly distinguished from the opposite small  $R$  tail of the DLC distribution. Figure 7(f) shows the measured droplet size distributions, scaled by their amplitude. The large  $R$  tails provide further evidence of significant BMC contribution to

coarsening. The observed approximately linear increase of  $K$  with droplet volume fraction  $\theta_d$  upon adding RNA is also consistent with BMC only (see table 1).

Some of the deviation from the dilute limit DLC predictions could be due to the obvious fact that  $\theta_d > 0$ . As discussed in section 2.1.2, growing spatial correlations between droplets for  $\theta_d > 0$  lead to increased  $K$  and a broader, more symmetric DLC droplet size distribution [81, 82]. The estimated volume fractions in these experiments are quite small,  $\theta_d \approx 0.00025\text{--}0.0009$ , and the typical droplet spacing is quite large,  $\sim 10\text{ }\mu\text{m}$ . Extensions of the dilute limit treatment predict that  $K$  increases only by  $\lesssim 10\%$  of the dilute limit result at these  $\theta_d$  values and that the effect on the droplet size distribution is negligible [81, 82]. It was therefore concluded that *in vitro* FIB-1 droplets evolve in a manner that is most consistent with steady-state BMC, but that DLC could also play a non-negligible role. Though contributions from other mechanisms, e.g. associated with complex formation, gelation, etc, cannot be fully ruled out, these results indicate that mean-field theories of passive phase separation kinetics can quantitatively describe protein liquid–liquid phase separation in the absence of biological activity.

### 3.2. *In vivo* studies of passive descriptions

The uncertainty and limitations in extrapolating *in vitro* protein solution behaviors to the enormously complex and active intracellular environment necessitates quantitative *in vivo*

studies of condensate formation and function. Such studies are now being conducted, and evidence for similar dynamics has been observed in living cells, upon post-translational protein modifications, temperature changes, or concentration changes.

We note that the possible role of finite size effects on *in vivo* phase separation has not been carefully investigated to our knowledge. The cytosol and nucleoplasm contain roughly  $10^6$ – $10^9$  and  $10^5$ – $10^8$  protein molecules, respectively. This is a reasonably large base of ‘independent elements’ from which sound statistics should be extractable, as long as correlation lengths are not anomalously large. Intermolecular interactions and collective excitations (hydrodynamic, etc) relevant to fluid properties in the crowded but dynamic cytosol and nucleoplasm are not believed to be long-ranged relative to the size of the cell or nucleus, respectively. On the other hand, the relevant number of ‘independent elements’ in terms of droplet statistics is the number of droplets, and the relevant base length scale is the typical droplet size. For collective droplet coarsening processes in a finite system, kinetics of the droplet size distribution and associated quantities such as average droplet size must ultimately terminate when the number of droplets decreases to one. This type of finite size effect (which is more accurately a finite population effect) may impact measurements of collective droplet kinetics when the total number of droplets is small. Closer study or consideration of such issues may therefore be warranted.

**3.2.1. Phase separation of Dishevelled** An early recognition of the possibility of protein phase separation within the cell involved *in vivo* observations of the behavior of the signalling protein Dishevelled (Dvl). Key experimental observations included: (1) the appearance of internally dynamic Dvl puncta at high and sometimes endogenous concentrations, (2) a correlation between the appearance of Dvl puncta and its ability to function in Wnt signalling (a pathway in which Dvl is involved), and (3) active Wnt pathways in cells with very high Dvl concentrations, even when Wnt is not present [21–26]. In [26], Sear showed that a relatively simple model of phase separation was sufficient to explain the noted behaviors.

In [27], Sear developed theoretical descriptions of the polymerization behavior of Dvl and the FRAP recovery kinetics of Dvl-rich droplets. Since Dvl was previously shown to form equilibrium short-chain polymers [22], an interpretation of experimental results was presented in which Dvl polymer chains form and this polymerization then promotes phase separation into the observed puncta. Two possible explanations were proposed as to why a combination of polymerization and phase separation may facilitate the biological function of Dvl. First, the switch-like nature of a phase transition can be exploited to produce a switch-like response to a signal. Second, dynamic compartmentalization in droplets facilitates partitioning of other proteins. The formation of a droplet phase from polymerized molecules can lead to a network-like rather than close-packed internal structure with a relatively low Dvl concentration. This could more readily permit other proteins to rapidly shuttle in, through, and out of the droplets for enhanced functionality.

**3.2.2. Steady-state size distribution of *Xenopus laevis* oocyte nucleoli.** One model system that has been employed to study intracellular condensates is the *Xenopus laevis* oocytes, which is a large single cell ( $\geq 1$  mm) which contains a large nucleus ( $\approx 400 \mu\text{m}$ ), known as a germinal vesicle (GV). The GV contains large and numerous ( $\geq 1000$ ) nucleoli, as well as other nuclear bodies. Nucleoli in this system are not mechanically constrained by the high chromatin density typical of small somatic cell nuclei, and are highly spherical. Moreover, using microneedles and other mechanical perturbations, these nucleoli were shown to readily coalesce with one another upon contact, and undergo liquid bridge rupture upon being pulled apart [7], as shown in figure 1. They exhibit a very broad size distribution,  $P(V)$ , with a power law tail for large sizes, with exponent  $\alpha = -1.51 \pm 0.07$ . Simulations of BMC with a constant rate of new droplet nucleation were shown to produce distributions with precisely this character;  $\alpha = -1.5$ , consistent with theory [154]. Subsequent work explored the impact of gravity on the dynamics of this intracellular emulsion [155, 156]. The growth of nucleoli in this system is therefore well-described by a passive nucleation and coalescence-based coarsening process.

**3.2.3. Disordered nuage protein droplets: a JMAK-based analysis.** The *in vivo* kinetics of protein-rich droplet formation in HeLa cells expressing the fluorescently tagged protein DDX4<sup>YFP</sup> was examined in [9] (see also section 3.1.2). Droplets were observed to appear individually within the nucleus, separated in time, consistent with nucleated growth rather than a spinodal-like process. The increase in total droplet volume with time was found to be well described by the modified JMAK expression  $V_{\text{tot}}(t)/V_{\text{tot}}(t \rightarrow \infty) = 1 - \exp(-ct^m)$  with  $m = 1.01 \pm 0.01$  (figure 8(a)). This is not consistent with heterogeneously or homogeneously nucleated free growth ( $m = 3$  and  $m = 4$ , respectively) or diffusive growth ( $m = 3/2$  and  $m = 5/2$ , respectively), but the authors develop an argument that the result  $m = 1$  is consistent with growth in which the quantity of available material is limiting. This is also reminiscent of the behavior predicted by the theory of diffusion-limited precipitation (section 2.1), in which a crossover to  $m \simeq 1$  occurs in the regime where droplets compete for available material. The analysis outlined in section 2.1, plotting  $1 - \theta_d/\theta_d^{\max}$  versus  $t$  on log-linear axes to determine whether  $\theta_d/\theta_d^{\max} \simeq 1 - G \exp(-t/\tau_0)$  is obeyed, may therefore be quantitatively applicable to this type of system.

**3.2.4. Optogenetically-controlled droplet assembly: kinetic analysis of ‘optoDrops’.** Dynamic spatiotemporal control of intracellular phase transitions has recently been enabled by an optogenetic platform that uses laser light to activate phase transitions in living cells [79] (see also sections 3.5.2 and 4.2.2 for more information about this and related systems). Light-sensitive proteins that change conformation and/or multivalent interaction state upon exposure to externally applied laser light sources can be utilized as optogenetic actuators to this end. In [79], a light-sensitive protein known to self-associate upon blue light exposure was fused to the ‘sticky’ IDR from various condensate-associated proteins. Cells expressing

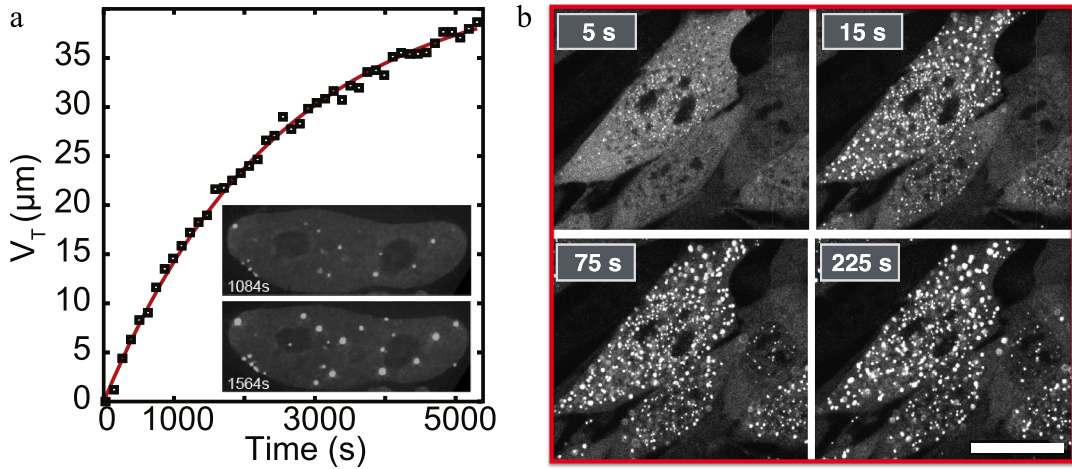


**Figure 8.** (a) Reproduced from [9]. CC BY 4.0. Variation with time of total volume of DDX4 droplet phase in HeLa cells. The red line is a fit to  $V(t) = V_{\max}[1 - \exp(-ct^m)]$ , where  $m = 1.01 \pm 0.01$  is obtained. Inset shows representative fluorescence images at two times. (b) Reprinted from [79], Copyright (2017), with permission from Elsevier. Representative fluorescence images of light-activated assembly, growth, and coarsening of optoFUS droplets in living cells at various times. Scale bar, 20  $\mu\text{m}$ .

these fusion proteins were found to exhibit highly light-tunable interactions, responding to the presence or absence of blue light exposure by condensing or dissolving optoDroplets rich in the responsive fusion proteins (figure 8(b)).

The global *in vivo* formation and growth of such optoDrops was recently examined within the classical JMAK and diffusion-limited precipitation theoretical frameworks introduced in section 2.1 [157]. As previously noted, the JMAK theory should be applicable during the early stages of growth, but since the maximum droplet volume fraction is relatively low ( $\theta_d \lesssim 10\%$ ), conditions at later stages from the passive viewpoint should be closer to those described by the theory of diffusion-limited precipitation. At even later stages, when the volume fraction of droplet phase is fully saturated, coarsening behaviors such as DLC and BMC should become dominant.

*In vivo* data for the total  $\theta_d$  of optoDrops exhibits behavior consistent with the theory of diffusion-limited precipitation. An initial  $m \simeq 2$  nucleation/growth regime consistent with mixed heterogeneous ( $m = 3/2$ ) and homogeneous ( $m = 5/2$ ) nucleation and DLG is followed by a crossover to a second  $m \simeq 1$  regime quantitatively consistent with that predicted by the theory of diffusion-limited precipitation when diffusion zones of nearby droplets begin to overlap. As the amount of free material available for growth is depleted, the volume fraction of droplet phase saturates and this semi-competitive growth regime gradually gives way to a distinct late-time coarsening regime.

The *in vivo* nucleation, growth, and coarsening kinetics of such condensates are therefore well-described by classical theories of collective passive domain evolution. The effects of biological activity do not appear to fundamentally alter the time-dependence of the droplet phase volume fraction.

### 3.3. *In vivo* studies of modulated passive systems

The second level of description that we consider maintains an equilibrium thermodynamic view with kinetics mediated by passive processes, but permits system-specific space and/

or time-dependent modulations of equilibrium or external parameters, such as molecular self-affinities or concentrations.

**3.3.1. *P* granules.** In *C. elegans* embryos, the first germ cell is established when condensates called P granules localize to the posterior of the one-cell embryo. The liquid-like P granules are initially distributed uniformly throughout the embryo, then the embryo polarizes along the anterior–posterior axis. Cortical and cytoplasmic flows develop, the polarity proteins PAR-1 and PAR-2 appear on the posterior cortex, and P granules begin to localize solely in the posterior half of the cell. The embryo then divides, creating a P granule-containing progenitor germ cell, and a non-P granule-containing somatic sister cell.

In [6], it was shown that P granule stability and morphology is controlled by time-dependent spatial protein concentration gradients that drive a spatially inhomogeneous phase separation and coarsening process (figures 9(a) and (b)). The polarity protein gradient varies the demixing point across the cell, resulting in a biased increase in droplet formation and growth at the posterior, and dissolution and negative flux at the anterior. P granules were shown to exhibit liquid-like behaviors (coalescence, dripping, and wetting), and their viscosity and surface tension were estimated as described in section 3.5. These findings led to the proposition that such demixing phase transitions may represent a fundamental physicochemical mechanism for organizing the cytoplasm.

In [158], a ternary regular solution / Flory–Huggins model (see section 2.2) was used to describe P granule phase behavior as a function of the concentration of the polarity protein MEX-5 (figure 9(c)). Spatial variations in this concentration determine whether the system is locally within the mixed or demixed region of the phase diagram. As we discuss further below, several recent studies utilizing *in vitro* reconstitution have lent further support to this model.

### 3.3.2. *C. elegans* nucleoli and extranucleolar droplets.

The nucleolus is the largest and most well-known nuclear body,

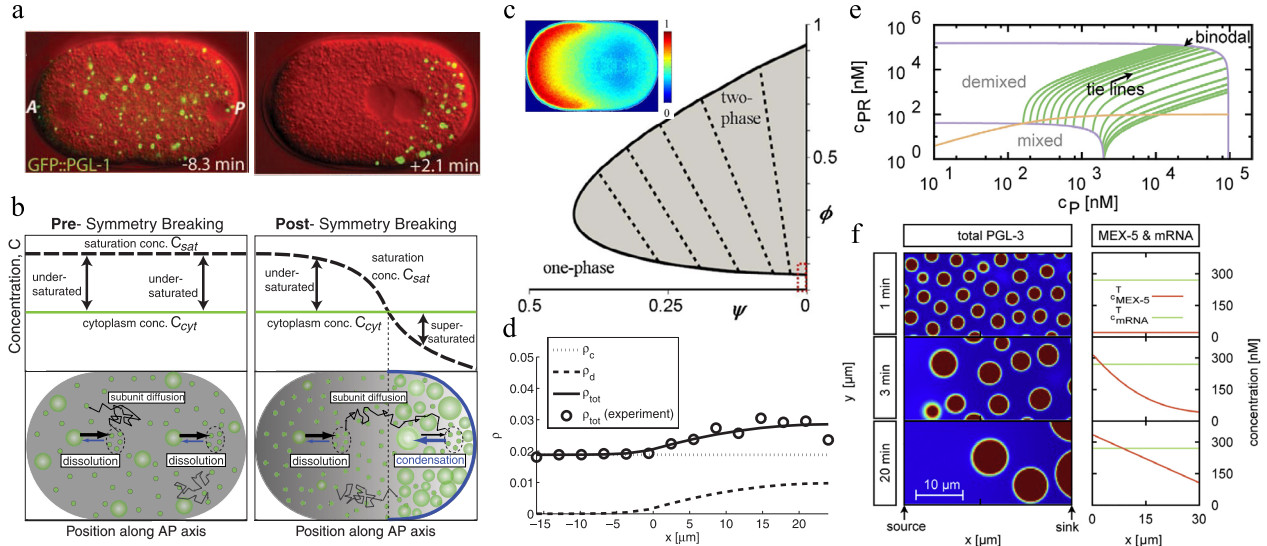


**Figure 9.** P granule assembly and anterior–posterior asymmetry can be understood as phase separation in the presence of a concentration gradient. (a) and (b) From [6]. Reprinted with permission from AAAS. (a) Fluorescent images of P granule proteins (green) superimposed on differential interference contrast (red) of a *C. elegans* embryo. Time is relative to pronuclear meeting. A = anterior, P = posterior. (b) Proposed mechanism of P granule localization. Variation in concentration of soluble components (top) and corresponding P granule dynamics (bottom). The post-symmetry breaking gradient in  $C_{\text{sat}}$  arises from gradients in polarity proteins such as MEX-5 (gray) and PAR-1 (blue). (c) and (d) Reprinted figure with permission from [158], Copyright (2013) by the American Physical Society. (c) Ternary Flory–Huggins phase diagram used to describe the cytoplasm.  $\psi$  is volume fraction of P granule constituents,  $\phi$  is volume fraction of MEX-5, dashed lines are tie lines. Inset shows the spatial MEX-5 gradient via fluorescence intensity of MEX-5::GFP averaged over four embryos. (d) Comparison of the steady-state solution (solid line) to a reaction–diffusion model for the mass density of P granule droplets  $\rho_d(x)$  and dissolved P granule constituents  $\rho_c(x)$  with experimental data for  $\rho_{\text{tot}}(x) = \rho_d(x) + \rho_c(x)$  (black circles). The computed  $\rho_d(x)$  and  $\rho_c(x)$  are also shown separately. (e) and (f) Reprinted from [102], Copyright (2016), with permission from Elsevier. Flory–Huggins reaction–diffusion model for P granule protein phase separation with messenger RNA (mRNA) binding and interactions with MEX-5. (e) Computed phase diagram for the ternary (PGL-3, PGL-3:mRNA, water) system, where  $c_p$  and  $c_{\text{PR}}$  are the concentrations of PGL-3 and PGL-3:mRNA, respectively. The orange line shows a path of increasing total PGL-3 concentration with fixed total concentration of mRNA. (f) Results from numerical calculations for the six-component (mRNA, PGL-3, PGL-3:mRNA, MEX-5, MEX-5:mRNA, water) system. Images of total PGL-3 concentration with increasing time (left) and corresponding profiles of total MEX-5 and mRNA concentrations averaged over y (right).

and is a condensate with primary functions in ribosome biogenesis and cell growth and size homeostasis. As discussed above, nucleoli are known to exhibit liquid-like properties, and in [159] it was demonstrated that their assembly and size are coupled to cell size through an intracellular phase transition in *C. elegans* embryos. These bodies did not assemble in nuclei with protein concentrations below a threshold value  $C_{\text{sat}}$ , and above this value, nucleolar size was found to scale linearly with cell size in early embryos. However, when embryo size was altered, an inverse scaling emerged in which small (large) cells exhibit large (small) nucleoli. A simple thermodynamic phase diagram-based model successfully describes these behaviors as the result of maternal loading of a fixed number  $N$  rather than a fixed concentration of nucleolar components. For fixed  $N$ , smaller cells have higher concentrations and therefore inhabit a deeper position beyond the phase boundary, leading to larger nucleoli. The stability and terminal size of these bodies can therefore be understood as the result of a concentration-dependent phase transition with  $N$  conserved between early cell cycles.

The kinetics of nucleolar assembly and disassembly, as well as those of associated extranucleolar droplets (ENDs—see figure 2(a)), were analyzed within the framework of classical phase transition kinetics in [28]. It was found that

nucleolar/END stability and morphology are controlled by a concentration-dependent phase transition, though consideration of time-varying average protein concentration and spatially heterogeneous thermodynamic interaction parameters were essential to describing the full kinetic process. Upon nuclear envelope assembly, average protein concentrations are generally high enough to place the nucleoplasm beyond the phase separation boundary. Many statistically indistinguishable droplets spontaneously nucleate and grow. Dynamic scaling behavior during the initial nucleolar/END growth/coarsening regime (figure 2(a) top panel) was observed with  $n \simeq 0.33 \pm 0.14$  (figure 10(b)), quantitatively consistent with both DLC and BMC ( $n = 1/3$ ). The measured prefactor  $K$  was  $\sim 3$  times smaller than that estimated for BMC ( $K \simeq 6k_B T \theta_d / 5\pi\eta$ ) and  $\sim 5$  times larger than that estimated for DLC ( $K \simeq 8\sigma D c_\infty V_m^2 / 9N_A k_B T$ ), both within the estimated uncertainty of the predicted values (see table 1).

The full kinetic cycle of nucleoli and ENDs, including later stages of biased coarsening and dissolution, was modeled using a binary regular solution free energy with Model H dynamics (see section 2.2) to capture the effects of hydrodynamic interactions (see figures 10(a), (c) and (d)). In the binary description, species  $A$  represents FIB-1 and other nucleolar proteins and species  $B$  represents all other nucleoplasmic

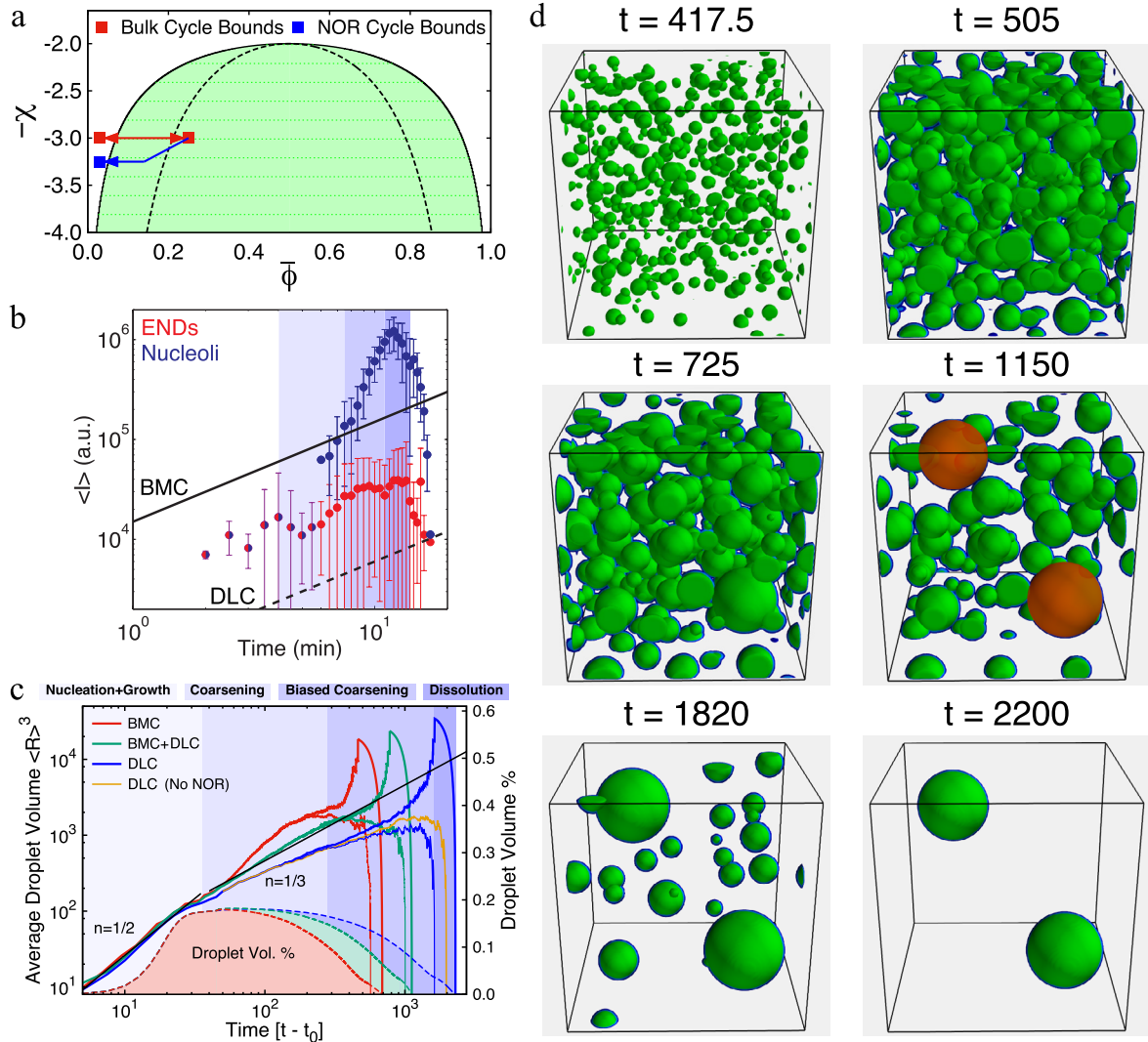


**Figure 10.** Reproduced with permission from [28]. Copyright © Proceedings of the National Academy of Sciences of the United States of America. Assembly/disassembly kinetics of *C. elegans* nucleoli and extranucleolar droplets modeled using a binary regular solution free energy with Model H dynamics (see section 2.2). (a) Phase diagram indicating time varying average concentration  $\phi$  within the nucleoplasm (red) and interaction parameter  $\chi$  within NOR domains (blue). Binodal (solid black line), spinodal (dashed black line), and tie lines (dotted green lines) are shown. (b) Mean integrated intensity of ENDs (red) and nucleoli (blue) over time. Data are pooled from 12 embryos (24 nuclei) and plotted on log–log axes. Error bars represent standard deviation. At early times ( $\lesssim 8$  min), ENDs and nucleoli are indistinguishable. Lines indicate the theoretical predictions for diffusion-limited coarsening (DLC) (dashed) and Brownian motion coalescence (BMC) (solid) mechanisms described in section 2.1. (c) Time dependence of average droplet volume and droplet volume fraction during simulations with BMC-dominant, DLC-dominant, and BMC + DLC-dominant conditions. Upper solid lines include all droplets, lower solid lines include only ENDs. (d) Time sequence of droplet configurations obtained from a DLC-dominant simulation with two NOR domains (highlighted at  $t = 1150$ ).

molecules. After the initial coarsening phase, the two larger nucleoli become distinct in correlation with local increases in rRNA concentration within the two transcriptionally active nucleolar organizing regions (NORs). The previously discussed effect of RNA in shifting *in vitro* FIB-1 phase boundaries to lower concentrations (section 3.1.2) is consistent with a change in thermodynamic Flory–Huggins interaction parameter  $\chi$ . Spatially-varying  $\chi$  values, enhanced within NORs, were employed to account for this effect. The observation that nuclear volume increases, leading to a decrease in average protein concentrations with time (figure 2(b)), indicated that the nucleus gradually exits the miscibility gap, driving droplet dissolution without explicit need for active processes.

Simulations conducted according to this sequence reproduced the central features of nucleolar/END kinetics (see figures 10(c) and (d)), and further tests of predictions afforded by the model were experimentally confirmed. It was concluded that rRNA transcription and other nonequilibrium biological activity can modulate the effective thermodynamic parameters governing nucleolar and END assembly, but do not appear to fundamentally alter the passive phase separation mechanisms.

### 3.4. Studies of undriven chemically reactive systems

The third type of theoretical approach considered in this review extends passive and modulated passive descriptions

of inhomogeneous mixtures by incorporating the effects of undriven chemical reaction kinetics within a self-consistent nonequilibrium thermodynamic framework. As discussed in section 2.4, this is appropriate when no internal or external energy sources supply work to the system. Detailed balance is satisfied, and chemical reactions do not alter thermodynamic stability or phase boundaries. This formulation is therefore most applicable to systems such as *in vitro* complex-forming protein mixtures or *in vivo* systems in which energy sources do not significantly alter thermodynamics.

The standard thermodynamic view of undriven reactions is one of added constraints on equilibrium states. In addition to phase equilibria (equality of chemical potentials between coexisting phases), a reactive system must also satisfy chemical equilibria (zero affinity of reaction) [160]. The domain of phase space in which equilibrium states can exist is therefore constrained by the addition of reactions. However, even though undriven reactions do not alter thermodynamic stability or phase boundaries, the introduction of reactions to a previously unreactive system can induce a phase transition. This is because evolution to the new stable state of simultaneous phase and chemical equilibria may require crossing a phase boundary (see, e.g. [160]). Therefore, by removing the constraint of fixed species concentrations in a closed system, reactions can be utilized in some cases to explore a wider range of phase space than would otherwise be accessible. Driven, externally-controlled reactions of the type discussed in section 4.2 (esp. section 4.2.2) can be used to dictate the concentrations of particular species, thereby providing even greater flexibility in controlled exploration of phase space.

The task of formulating a thermodynamically consistent reaction–diffusion field theory for inhomogeneous mixtures amounts to determining an appropriate functional form for the reaction rates. In classical theories of chemical kinetics for undriven *homogeneous* systems, reaction rates are determined by mean rather than local reactant concentrations. This is justified for a dilute solution of reactants undergoing spatially independent reactions, but it is a less valid approximation for inhomogeneous condensed matter. Here stronger interactions can lead to dramatic spatial heterogeneities in composition and structure (e.g. phase separation), which in turn can lead to dramatic spatial variations in reaction rates [104].

Cahn–Hilliard-type descriptions of inhomogeneous reactive mixtures have been formulated to study a variety of phenomena. Huberman [161] formulated a reaction–diffusion model for spinodal decomposition and pattern formation in reactive mixtures by adding reaction kinetics to the Cahn–Hilliard equation. Reaction rates were specified with the space-dependent analogue of those classically used for *homogeneous* mixtures, e.g.  $R = -k\phi_A(\vec{r}) + k\phi_B(\vec{r})$  for the reaction  $A \rightarrow B$  with rate constant  $k$ . (Reactions with rates of this form have been referred to as ‘ideal’ or ‘state-independent’ [149]). This study and subsequent studies of models of the same type in the 1990s [162–164] indicated that chemical reactions in general shift the phase separation spinodal and can often lead to chemically-induced arrest of phase separating morphologies at some reaction rate-dependent average domain size. This chemical freezing effect was proposed to be the origin of

similar arrested morphologies observed in spinodally decomposing polymer mixtures subject to photocrosslinking (light-induced chemical reactions) [165]. However, Lefever *et al* [166] commented that the form of the reaction rates used in these models is not consistent with thermodynamics. Carati and Lefever [167] then formulated a thermodynamically consistent form of the model and found that kinetic arrest of demixing systems only occurs under fairly restrictive conditions involving particular types of reactions (including those considered by Huberman).

More recently, Bazant [104] has presented a related, thermodynamically consistent field theory for undriven chemically reactive, inhomogeneous systems. The primary motivation for this theory was to study coupled phase transformations and chemical reactions in electrochemical phenomena, but the framework itself is general and can be applied to intracellular organization as well. This formulation extends the multicomponent Cahn–Hilliard model, equations (8) and (1), by means of a master equation for nonequilibrium chemical thermodynamics. Reaction rates are derived as (nonlinear) functions of the local thermodynamic driving force for reaction, and are expressed in terms of the local chemical potentials as

$$R = k_0 e^{-\mu^{\text{ex}}/k_B T} \left( e^{\mu_1/k_B T} - e^{\mu_2/k_B T} \right). \quad (14)$$

Here  $k_0$  is the rate constant,  $\mu^{\text{ex}}$  is the activation barrier for transitions between reactant and product states (‘ex’ is short for excess),  $\mu_1 = \sum_r s_r \mu_r$ ,  $\mu_2 = \sum_p s_p \mu_p$ ,  $s_i$  are stoichiometry coefficients, and  $\mu_r$ ,  $\mu_p$  are the chemical potentials of individual reactant and product species, respectively. The thermodynamic driving force for reaction is  $\Delta\mu = \sum_p s_p \mu_p - \sum_r s_r \mu_r$ . The activation barrier  $\mu^{\text{ex}}$  is determined by the nature of the nonequilibrium transition state for a given reaction in a given system. (Reactions with rates of this or similar form have been referred to as ‘non-ideal’ or ‘state-dependent’ [149]).

The advective Cahn–Hilliard equation, equation (11), generalized to mixtures undergoing bulk chemical reactions is then

$$\frac{\partial \phi_i}{\partial t} + \vec{v} \cdot \nabla \phi_i = \Gamma_i \nabla^2 \mu_i \mp \frac{c_s}{s_i} R(\mu_i), \quad (15)$$

where  $c_s$  is the reaction site density and  $R(\mu_i)$  denotes all terms in  $R$  that act as sources or sinks of species  $i$ . Reactions of arbitrary order and type can be accounted for within  $R$ . A simple example system is the case of a conserved binary mixture in which species  $A$  and  $B$  can be interconverted through an isomerization process. Neglecting hydrodynamics ( $\vec{v} \rightarrow 0$ ), one would typically write

$$\frac{\partial \phi}{\partial t} = \Gamma \nabla^2 \mu - k_{AB}\phi + k_{BA}(1 - \phi), \quad (16)$$

where  $k_{AB}$  and  $k_{BA}$  are reaction rates in the first-order process  $A \xrightleftharpoons{k_{BA}} B$ .

Now we must specify the forms of  $k_{AB}$  and  $k_{BA}$ . For the symmetric binary regular solution free energy density of equation (2), the equilibrium condition  $\delta F/\delta\phi_A = \delta F/\delta\phi_B$  reduces to  $\phi/(1 - \phi) = e^{X(2\phi - 1) + K\nabla^2\phi}$ . Employing equation (14),

the reaction terms in equation (16) can be shown to be thermodynamically consistent when  $k_{AB} = \tilde{k}_0 e^{-\mu_R/2}$  and  $k_{BA} = \tilde{k}_0 e^{+\mu_R/2}$ , where  $\tilde{k}_0$  is the reduced rate constant and  $\mu_R = \chi(2\phi - 1) + K\nabla^2\phi$ . The contribution from reactions,  $\tilde{k}_0[-\phi e^{-\mu_R/2} + (1 - \phi)e^{+\mu_R/2}]$ , sums to zero when the equilibrium condition for the chemical potentials is satisfied. Interested readers are referred to [104] for further details of such calculations. Applications of this approach to reactive protein and intracellular systems are discussed in the following paragraphs. Extensions to driven chemically reactive systems are discussed in section 4.2.

**3.4.1. P granules.** The origin and effects of the gradient in MEX-5 concentration associated with asymmetric P granule formation (section 3.3.1, figure 9) has been examined in some detail using a variety of reaction–diffusion models. A coarse-grained reaction–diffusion model for the evolution of the P granule droplet density was used in [158] to demonstrate that a weak spatial gradient in MEX-5 can generate dramatic morphological changes consistent with observed P granule anterior–posterior asymmetries when coupled to an underlying switch-like phase transition (figure 9(d)). In this model condensed and dissolved P granule constituents were taken to exchange via first-order forward and backward reactions. In [168] the origin of the MEX-5 concentration gradient was proposed to be an underlying gradient in MEX-5 diffusivity, caused by an interplay of phosphorylation reactions that convert MEX-5 between fast-diffusing and slow-diffusing complexes. This proposal was supported by a coarse-grained binary reaction–diffusion model for the two MEX-5 complexes and their interconversion rates.

In a more recent study, P granule-like droplets were reconstituted *in vitro* to gain insight into the mechanism by which a MEX-5/6 gradient influences the asymmetric phase separation behavior [102]. It was found that a competition for messenger RNA (mRNA) binding between the P granule protein PGL-3 and MEX-5 can regulate the formation of PGL-3-rich droplets. A six component Flory–Huggins model (see section 2.2) was constructed to describe the phase behavior and dynamics of this system, based on the interactions, binding affinities, and phase separation behavior of all components (PGL-3, MEX-5, mRNA, PGL-3:mRNA, MEX-5:mRNA, and water). Model B dynamics (see section 2.2) were employed, along with additional chemical reaction source/sink terms to describe PGL-3 and MEX-5 binding with mRNA. For the reconstituted *in vitro* system, reactions were treated within the undriven reaction–diffusion framework described above. This reaction–diffusion model therefore describes coupled diffusion, phase separation, and local competition for mRNA between MEX-5 and PGL-3, and was made quantitative by employing experimentally determined input parameters. Results of 2D simulations demonstrated that a MEX-5 gradient is indeed capable of generating P granule assembly/disassembly kinetics similar to *in vivo* observations (figures 9(e) and (f)).

**3.4.2. Anomalous *in vitro* mesoscopic protein clusters.** An unresolved problem in the field of protein phase behavior and kinetics is the formation of anomalously stable mesoscopic clusters in protein solutions, as described in section 3.1.1. An investigation based on an ideal or state-independent

field-theoretic reaction–diffusion model (section 3.4) indicated that stable clusters can indeed form, essentially by a mechanism of chemically-suppressed Ostwald ripening [148]. This apparently supported the stability mechanism proposed in [145] based on transient complex formation.

A subsequent study of the same model with thermodynamically consistent, non-ideal or state-dependent reaction rates (section 3.4), which is a more appropriate choice for inactive *in vitro* systems, revealed that the stability mechanism is disrupted and stable clusters do not form in the absence of an external energy source [149]. Restoration of detailed balance leads to destabilization of nonequilibrium steady states. The mystery of mesoscopic cluster stability therefore remains unsolved, but these studies provide an instructive example of the qualitative differences that can result from different treatments of reaction kinetics in inhomogeneous mixtures.

**3.4.3. Complex coacervation.** Some recent studies of proteins associated with intracellular condensates have provided evidence that droplet formation can be the result of charge-mediated phase separation, or complex coacervation [169, 170]. In this process, electrostatic attraction between oppositely charged macromolecules leads to phase separation into polyelectrolyte-rich droplets. The individual species, which may not tend to phase separate as monomers, react to form a new species or complex that more readily phase separates; this is often envisioned as polycations complexing with polyanions, although polyampholytic sequences (those containing both positive and negative charges) can also undergo complex coacervation. This interplay of chemical reactions and thermodynamically-driven phase separation can lead to observable behaviors that are not consistent with phase separation alone. For example, as shown in [170], the equilibrium protein concentration in the background phase may become an increasing function of total protein concentration, rather than a constant as expected for simple phase separation.

In [169], enzymatic phosphorylation/dephosphorylation (changing of charge state) of short peptides was shown to reversibly control droplet formation in model RNA/peptide systems. Electrostatic interactions between the cationic peptides and the polyanionic RNAs were concluded to drive phase separation. Various other macromolecules were observed to partition strongly into the droplets. These results suggest that cells can employ phosphoregulation of complex coacervation to reversibly form condensates and mediate dynamic intracellular compartmentalization. Similarly, in [170], intracellular phase separation in systems driven by Nephrin intracellular domain (NICD) protein was determined to be a complex coacervation process involving NICD co-assemblies with negatively and positively charged partner molecules. Since many disordered proteins have similar sequence characteristics to those of NICD, these findings indicate that complex coacervation may promote phase separation in a variety of intracellular systems.

### 3.5. Measurements of droplet properties *in vitro* and *in vivo*

The well-established liquid-like properties of many intracellular condensates (coalescence, dripping, wetting, dynamic

molecular exchange on timescales of seconds to minutes, etc) suggest that they are often purely viscous droplets. However, other bodies exhibit more solid, gel-like properties. Their material states have also been found to vary widely with internal and external conditions and to exhibit time-dependence in some systems, evolving/aging from liquid-like to solid-like bodies with time [46, 55, 98, 99, 111, 151, 153]. The range of accessible material states in these systems is suggestive of considerable structural and dynamic complexity, which would likely imply that developing a comprehensive molecular-scale understanding of their behavior is best considered a broad, long-term challenge. Quantitative measurements of their ‘macroscopic’ properties nonetheless provide valuable information about internal states, potential mechanisms of formation, and the effects of both passive and active processes on organelle properties.

### 3.5.1. Liquid-like phases.

**P granule viscosity and surface tension.** The surface tension and viscosity of *in vivo* P granules were quantified in [6] by analyzing their diffusion and fusion dynamics within the framework of classical liquid behavior. The viscosity of the droplet phase  $\eta$  was estimated using the Stokes-Einstein relation,  $D = k_B T / (6\pi\eta R)$ , under the assumption that the droplet phase behaves as an equilibrium Newtonian fluid. Using the internal diffusion coefficient  $D$  obtained from FRAP experiments, a value  $\eta \sim 0.1\text{--}1 \text{ Pa} \cdot \text{s}$  is obtained, similar to that of olive oil or glycerol. It should be noted that these values were appropriately characterized as rough estimates, since the applicability of the Stokes-Einstein relation for nanoscopic probes is questionable, as discussed below. Droplet surface tension  $\sigma$  was then estimated by quantifying the time scale  $\tau$  for fusion of two droplets as a function of droplet size  $R$ . Liquids should exhibit a linear trend with slope corresponding to the inverse capillary velocity  $\eta/\sigma$ . The surface tension estimated this way is  $\sigma \sim 10^{-6}\text{--}10^{-7} \text{ N m}^{-1}$ , which is comparable to that of other macromolecular systems, and generally speaking quite small.

**Microrheology of reconstituted LAF-1 droplets and the effect of RNA.** Microrheology has been used to determine the viscosity of phase separated P granule-like LAF-1 droplets *in vitro* and to demonstrate that fluid properties can be RNA-tunable [100, 152]. Microrheological bead-particle tracking measurements provide a bead diffusion coefficient  $D$ , which in combination with the relation between  $D$  and  $\eta$  given by the Stokes-Einstein relation, permits independent determination of droplet phase viscosity. A viscosity  $\eta = 34 \pm 5 \text{ Pa} \cdot \text{s}$ , similar to that of honey, was reported at physiological salt conditions, and the additional presence of  $5 \mu\text{M}$  RNA was found to decrease viscosity to  $\eta = 12.8 \pm 0.8 \text{ Pa} \cdot \text{s}$ . Decreased viscosity was found to correlate with faster molecular dynamics. Independent determination of the inverse capillarity velocity  $\eta/\sigma$  using the method described in the previous paragraph permitted direct estimation of the generally difficult to measure droplet surface tension. A value  $\sigma \simeq 10^{-4} \text{ N m}^{-1}$  was obtained.

Interestingly, RNA did not shift the saturation concentration (left arm of binodal) in this system, as was observed in other studies [28, 151]; this was surprising, in that the molecular interactions that govern phase properties are expected to be closely related to the interactions that govern phase stability. However, more recent work has utilized a fluorescence correlation spectroscopy-based technique to measure the full binodal for LAF-1, which revealed that the high concentration arm of the binodal is strongly affected by RNA [101]. Specifically, the high concentration arm of the binodal is shifted to lower concentration, consistent with RNA causing a decrease in the droplet viscosity. However, even in the absence of RNA, the ‘high concentration’ arm of the binodal is at remarkably low protein concentrations, corresponding to the semidilute polymer regime where individual LAF-1 molecules only just begin to overlap. Indeed, the droplets exhibit an apparent mesh size of  $\approx 3\text{--}5 \text{ nm}$ , such that small molecular probes can freely partition and are not subject to the ‘bulk’ viscous drag within the droplet. These findings may help explain why intracellular condensates are generally found to be highly permeable [171, 172].

**Microrheology of reconstituted Whi3 droplets and a different effect from RNA.** In [151] the RNA binding protein Whi3, which is associated with asynchronous nuclear division and other functions in large cells of multinucleated organisms, was shown to exhibit *in vitro* phase diagrams and droplet properties that vary depending on the specific mRNA present. A combination of dynamic fusion, FRAP, and microrheology measurements revealed that the inverse capillarity velocity increases linearly with the molar ratio of RNA to protein, molecular diffusion coefficients within droplets decrease with RNA concentration, and droplet viscosity increases with RNA concentration. These trends are the opposite of those reported in [100], but in line with observations of increased viscosity of LAF-1 droplets upon addition of long RNA [101], highlighting the still poorly understood importance of RNA length and composition in modulating condensate properties. Binding RNA was found to promote liquid-like Whi3 droplets *in vivo*, as opposed to droplets that become gel-like or fiber-like over time. These results suggest that mRNA may encode biophysical properties of phase separated bodies and as a consequence may play a role in preventing the formation of persistent aggregates in living cells.

**Multiple coexisting liquid phases with core-shell droplet structure.** A recent study concerning *X. laevis* nucleoli demonstrated that the coexistence of multiple types of droplet phases, each type rich in distinct immiscible proteins, is also possible [55] (see figure 11). Moreover, the organization of the immiscible liquid phases is dictated by their surface tensions, with respect to each other, as well as the low concentration (solvent) phase. This is consistent with classical understanding of phase morphology in multi-phase systems; total surface energy can be reduced when domains that have high surface tension with the solvent phase embed themselves within another immiscible phase that has lower surface tension with the solvent. These results provide an explanation for

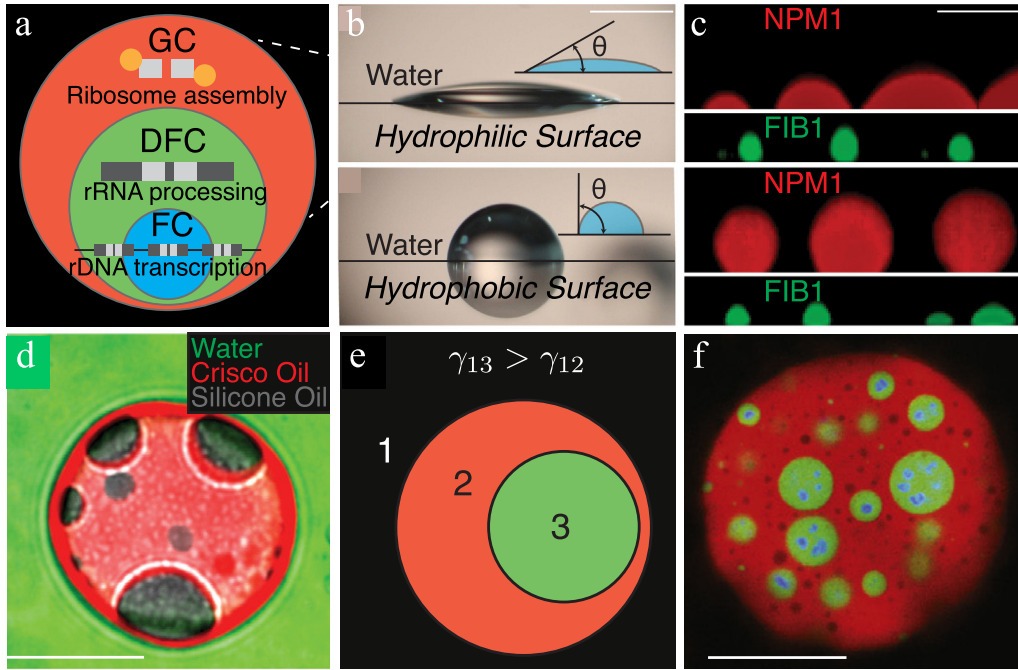


**Figure 11.** Reprinted from [55], Copyright (2016), with permission from Elsevier. Multiphase droplets in *X. laevis* nucleoli and the role of surface tension. (a) Schematic diagram of compartmentalization associated with ribosome biogenesis in the nucleolus. The outer, intermediate, and inner compartments of the nucleolus are enriched with the protein NPM1 (red), the protein FIB1 (green), and the RNA polymerase I (POL1) machinery (blue), respectively. (b) Water droplets on hydrophilic and hydrophobic surfaces. Scale bars, 1 mm. (c) *In vitro* NPM1 and FIB1 droplets on hydrophilic (upper) and hydrophobic (lower) surfaces. The greater hydrophobicity exhibited by FIB1 indicates that  $\gamma_{\text{FIB1/water}} > \gamma_{\text{NPM1/water}}$ . Scale bar, 5  $\mu\text{m}$ . (d) Non-biological multiphase droplets organized by surface tension differences ( $\gamma_{\text{silicone/water}} > \gamma_{\text{Crisco/water}}$ ): green, water; red, Crisco oil; gray, silicone oil. Scale bar, 20  $\mu\text{m}$ . (e) Schematic organization of immiscible multiphase droplets that exhibit different surface tensions with water. (f) Multiphase nucleoli after actin disruption in *X. laevis*. Scale bar, 20  $\mu\text{m}$ .

the origin of the layered core-shell structure of nucleoli and other condensates, as well as those condensates that appear to reflect multi-phase immiscibility that does not result in complete engulfment of one droplet within another.

**3.5.2. Gel-like and solid-like phases.** Mixtures that undergo liquid–liquid phase separation upon crossing a phase boundary may also be subject to other phase transitions involving non-liquid states. Classical liquid-to-gel, liquid-to-glass, and liquid-to-crystal transitions are examples commonly encountered in passive materials. Biological mixtures are in principle subject to the same types of phase changes under appropriate conditions. Many globular proteins such as lysozyme are well-known to form gel-like structures *in vitro* at sufficiently high concentrations and/or low temperatures [124, 126, 140] (see section 3.1.1). Such gels have also been reported to transform into fibers and/or crystals over time [109, 126], with resemblance to the proteinaceous pathological aggregates—amyloid fibrils or plaques—believed to be the fundamental cause of aging-associated and neurodegenerative diseases such as Alzheimer’s disease and ALS [42, 44–46, 109, 173].

**Cytotoxicity of aggregates.** Similar phenomena have recently been observed for key proteins associated with both condensate assembly and human disease. Following up on early *in vitro* observations that many proteins not connected with

neurological diseases can form fibrillar aggregates resembling clinical amyloid fibrils, it was demonstrated in [109] that early aggregates formed by many such proteins can be cytotoxic rather than simply non-functional. Such aggregates may therefore impair cellular function in ways that facilitate disease progression. It was hypothesized that aggregate toxicity arises as a general rather than highly protein-specific phenomenon because the surface of the disordered aggregates is likely to expose inappropriate amino acid combinations that lead to detrimental interactions with a variety of cellular components. Therefore the different morphologies of aggregates may lead to different clinical manifestations of amyloid formation.

**Gelation and amyloid-like fibers in FUS systems.** In [96] and [97], *in vitro* studies of the RNA binding protein FUS revealed a reversible, concentration-dependent transformation into a solid-like hydrogel state. The hydrogel state was found to be composed of morphologically uniform amyloid-like fibers with characteristic lengths on the order of hundreds of nanometers (figure 12(c)), suggesting that the mechanism of gelation may be a droplet-scale polymer-formation process (see also [8] and [50]). Low complexity (LC) polypeptide sequences were found to be necessary and sufficient for the maintenance of this reversible transformation, consistent with previously established links between LC sequences and pathological aggregates. Interestingly, while these *in vitro* fibers are reversible, true pathogenic prion-like amyloids are not.

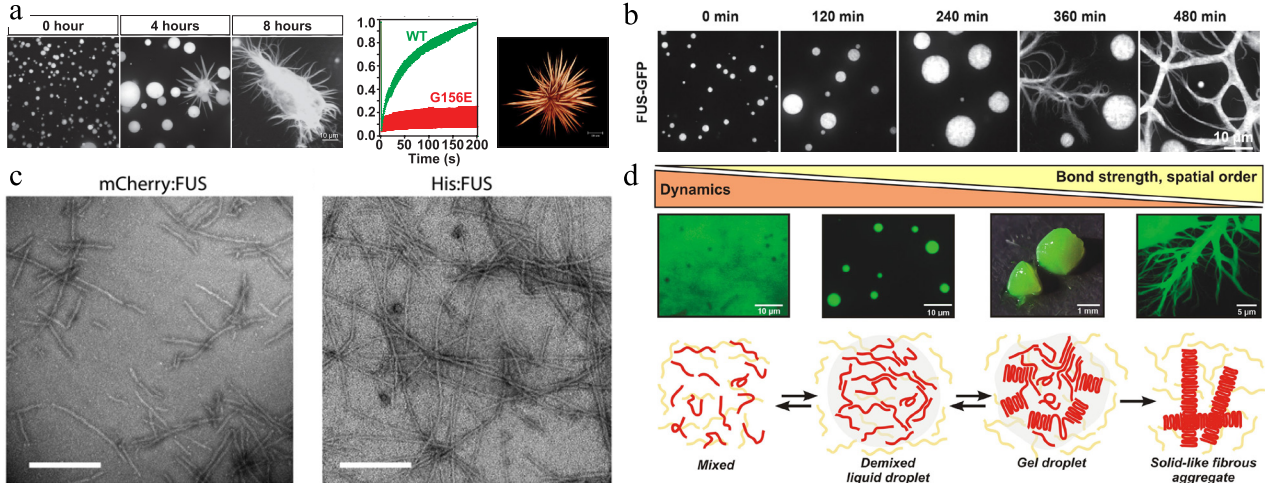


**Figure 12.** Aging of *in vitro* liquid droplets into gel-like fibrous aggregates. (a) Reprinted from [98], Copyright (2015), with permission from Elsevier. (3 leftmost panels) *In vitro* formation of fibrous mutant-FUS aggregates. (middle) FRAP data from the system represented to the left (red, G156E) and a non-fibrous WT system. (right) 3D rendering of a ‘starburst’ mutant FUS morphology. Scale bars: 10  $\mu\text{m}$ . (b) Reproduced from [46]. CC BY 4.0. *In vitro* formation of fibrous aggregates from liquid droplets. (c) Reprinted from [96], Copyright (2012), with permission from Elsevier. Transmission electron microscope images of two FUS-based hydrogel droplets, revealing polymeric amyloid-like fibers on the scale of hundreds of nanometers. Scale bars: (left) 500 nm, (right) 320 nm. (d) Reproduced from [46]. CC BY 4.0. View of phase separation by intrinsically disordered proteins leading to material phases with different structures and properties. Intrinsically disordered proteins (red) can undergo liquid–liquid demixing transitions, subsequent aging into reversible gels, and transformation into solid-like fibrous aggregates. Purified FUS protein in each state is shown along the top.

**Pathogenic mutations accelerate fibril formation.** In [110], proteins associated with inherited neurodegenerative disease were shown to have an intrinsic tendency to assemble into autocatalytically-nucleating fibrils, and pathogenic mutations in prion-like domains (PrLDs) of these proteins were shown to accelerate fibril formation. Since PrLDs in RNA-binding proteins are essential elements of condensate assembly, this provides evidence of a PrLD-based link between condensate formation and disease initiation. Other mutant motifs in other PrLDs or condensate assembly in the presence of environmental stress may similarly lead to dysregulated gelation/fibrillization within condensates and consequently disease onset and propagation.

**Stress granules in yeast cells are solid-like bodies.** In [153], yeast cells were found to exhibit both liquid-like P bodies and solid-like stress granules reminiscent of solid protein aggregates. Stress granule formation was observed to coincide with aggregate formation due to protein misfolding, suggesting that stress granules may be a type of aggregate. Rather than forming prion-like fibers, prion-like proteins were found in effect to become very ‘sticky’, leading to the nucleation and growth of solid-like stress granules. Stress granules in mammalian cells exhibited liquid-like behavior. These findings highlight the fact that condensate properties can vary widely within and across cell types.

**Aging of phase separated liquid droplets into fibrillized structures.** At least four studies then published in close succession provided evidence in support of the proposal [43] that cells, upon using liquid–liquid demixing to rapidly assemble concentrated functional membrane-less compartments, run increased risk of excessive fibrillization and eventually

disease due to a greater probability of persistent fibril formation within the dense liquid phase. In [98], *in vitro* FUS liquid droplets were found to mature into fibrous ‘sea urchin’ and ‘starburst’ structures over time, and this maturation was accelerated in amyotrophic lateral sclerosis (ALS) patient-derived mutations of FUS (figure 12(a)). Higher protein concentrations were found to correlate with more rapid fibrillization. A similar study focusing on proteins examined in [96, 97, 110] also demonstrated that upon undergoing *in vitro* liquid–liquid phase separation, enhanced fibrillization is observed within the protein-rich droplets [99]. In [111], it was shown that several RNA-binding proteins containing IDRs, which tend to phase separate *in vitro*, also age over time into amyloid-like fibers whose appearance correlates with slower FRAP recovery. The high protein concentrations within the droplets were hypothesized to accelerate the formation of the more stable amyloid-like fibers. Finally, in [151], fibers were detected and slower FRAP recovery observed in aged *in vitro* Whi-3 droplets, and suppression of RNA binding *in vivo* was found to promote formation of filamentous structures.

These studies demonstrate that liquid–liquid phase separation and fibrillization can be tightly coupled in the sense that the effective fibril nucleation barrier (if one exists, strictly speaking) appears to be much lower and/or the fibril growth rate much higher within the dense liquid phase (figure 12(d)). This is reminiscent of the two-step nucleation process by which many proteins crystallize *in vitro* (see section 3.1.1). The observation that the presence of RNA shifts the liquid–liquid phase boundaries further suggests that the cell can regulate condensate assembly, material state, and properties through variations in RNA concentration. The probability of forming pathological aggregates within condensate crucibles is hypothesized to increase significantly

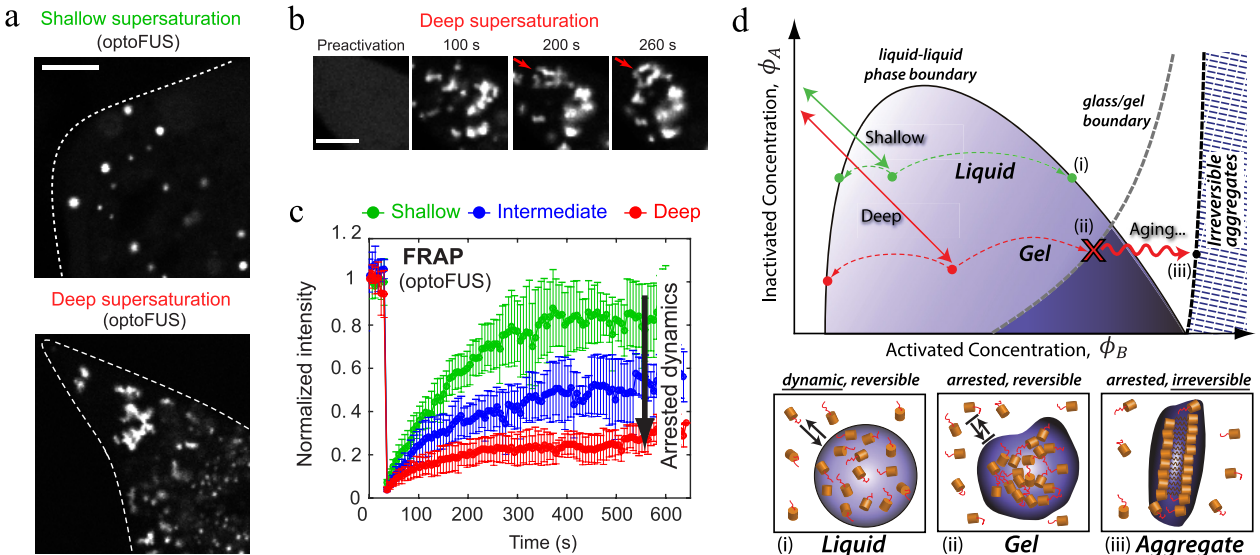


**Figure 13.** Reprinted from [79], Copyright (2017), with permission from Elsevier. (a) Change in *in vivo* optoFUS droplet morphology from spherical and liquid-like to irregular, aggregated, and gel-like with increasing supersaturation or quench depth. Dashed lines are cell outlines. Scale bar: 5  $\mu\text{m}$ . (b) Time-sequence of optoFUS droplet evolution at deep supersaturation. Scale bar: 3  $\mu\text{m}$ . (c) FRAP recovery curves of optoFUS droplets at various supersaturations. Error bars represent standard deviation across multiple samples. (d) A model for intracellular phase space. Increases in a molecular species' self-association via, e.g. conversion of molecular states through post-translational modification or exposure of RNA in RNP complexes, can lead to liquid–liquid phase separation. When the quench depth is shallow (green path (i)), liquid droplets are formed. Deep supersaturation (red path (ii)) results in formation of solid-like gel droplets and aggregates with markedly slowed molecular dynamics. Over time, the slow dynamics within initially reversible gels promote the formation of irreversible aggregates (iii).

when the associated proteins contain fibril-promoting mutations or when granule disassembly machinery is disturbed. Though it now seems clear that fibrillization is facilitated by high protein concentrations within demixed droplets, the precise nature of the fibril and/or amyloid formation process is not clear. For recent reviews of this and related topics see, e.g. [42, 44–46].

**Gel-facilitated formation of irreversible aggregates in deeply quenched optogenetic systems.** Additional insight into aggregate formation *in vivo* has recently been enabled by development of an optogenetic platform that uses laser light to activate IDR-mediated phase transitions in living cells [79] (see also sections 3.2.4 and 4.2.2). Application of this ‘opto-Droplet’ system revealed that liquid-like FUS-rich droplets can reversibly form and disassemble over many activation cycles, but that when cells are quenched deeply beyond the phase boundary (high light intensity and/or high initial FUS concentrations), semi-solid gels form (figures 13(a)–(c)). After several such activation cycles, the gels begin to transform into irreversible solid-like assemblies reminiscent of pathological disease-related aggregates. This behavior may be related to *in vitro* observations of protein crystallization kinetics in which the low molecular mobility within the dense intermediate precursor phase leads to slow crystal growth until the precursor phase is consumed and crystal growth becomes rapid [174]. This finding suggests that gel-like structures may be essential precursors for irreversible aggregate formation in some systems, and that the deep-quench or long-aging-time conditions required to generate gels (figure 13(d)) may therefore be crucial steps in disease onset and progression.

Such a scenario could present a fine-edged optimization problem for living cells; dynamic liquid-like compartments may be effective microreactors, while gel-like compartments may be effective on-the-fly storage vessels. However, the deep quenches associated with gel-like structures introduce increased risk of triggering irreversible aggregation and fibrillization, and subsequent toxic effects (figure 13(d)). Cells must maintain internal conditions that permit maximum functionality without overexposure to the danger of pathological aggregation.

**Critical fluctuations and solid-phase nucleation barriers.** Simulations of model globular protein solutions have shown that homogeneous crystal nucleation rates can be dramatically enhanced near a metastable liquid–liquid critical point [134, 141, 175]. Critical fluctuations significantly lower the crystal nucleation energy barrier, increasing nucleation rates by over 10 orders of magnitude. If irreversible aggregates are crystalline or partly crystalline, and if the rate-limiting step in their formation is the overcoming of an analogous crystallization energy barrier, then it becomes interesting to speculate on the potential role of critical or quasi-critical fluctuations that may be associated with intracellular phase separation and/or gelation/percolation transitions. The pathways for irreversible aggregate formation are likely to be quite complex, but insight from model systems such as that of [134] may prove useful in identifying key steps in such processes.

### 3.6. Discussion

The primary aim of this section has been to outline studies to date that have tested passive, modulated passive, and undriven

chemically reactive descriptions of phase separation within the contexts of protein condensation and intracellular condensate formation. These studies compose a portion of the mounting evidence in support of the concept of intracellular phase transitions and of the view that existing theoretical frameworks for describing phase separation kinetics can provide a meaningful basis for understanding condensate formation. It is also becoming increasingly clear that organelle properties and material states can vary widely and that cells can use a variety of regulation strategies to dynamically control these properties and, as a result, organelle functionality. Such strategies and their roles in biological functioning are just beginning to be understood. This survey also demonstrates that additional quantitative studies involving comparison of theory with experiment will continue to reveal where existing theories are sufficient and where opportunities for new theoretical development can be found. Three such areas that we have identified as key emerging directions of focus are examined in more detail in section 4.

#### 4. Developing and future directions

The studies outlined in the preceding sections (and others omitted due to space constraints or unintentional oversight) demonstrate that a variety of complex phenomena within living cells can be understood and in some cases quantitatively described in terms of passive or modulated passive phase separation processes. Nonetheless, many intracellular organization / condensate assembly processes cannot be adequately described or understood without explicit consideration of biological activity. We contend that the passive view provides a well-established, physically-based foundation to build upon, and into which biological activity and other highly nonequilibrium processes can be systematically incorporated when reasoning and evidence indicate that such mechanisms are central. Nonequilibrium dynamics due to ATP-dependent activity, for example, may qualitatively alter droplet fluid properties (see section 4.2.4). Activity also appears to be more formative in centrosome assembly (see section 4.2.1). Nonequilibrium phenomena can also potentially lead to droplet formation in the absence of an underlying equilibrium phase transition. More quantitative experimental work is needed to elucidate the role of highly nonequilibrium behavior in specific systems. Further development of theories for phase transitions mediated by active transport and/or modulated by chemical activity is also needed.

In this section we outline three important and emerging areas of study involving intracellular organization that require development of theories and modeling approaches beyond those typically employed for passive, few-component fluids.

1. Statistical descriptions of demixing and condensation transitions in fluids with many ( $\gg 3$ ) components are needed to better understand the interaction parameter distributions that lead to functional demixing transitions in complex biological mixtures. We will give an overview of developments in this area.

2. The roles of driven chemical reactions and other manifestations of highly nonequilibrium biological activity in intracellular organization need to be more fully understood and, ideally, unified by new theoretical developments. We will discuss some recent efforts along these lines and speculate on a few directions in which progress may be possible in the relatively short-term, citing parallel developments in related areas of study.
3. Links between phase transition-mediated condensate assembly / functionality / gelation / crystallization and pathological aggregation associated with human disease are currently of great interest. We will outline recent developments concerning this topic and describe one means of incorporating gelation kinetics into mean-field models of phase separation.

##### 4.1. Models for systems with many components

Field theoretic descriptions of multicomponent mixtures such as the regular solution and Flory–Huggins models typically remain tractable and computationally practical for systems with perhaps three to six types of components. Complex intracellular fluids such as the cytoplasm may contain thousands of different components. Eukaryotic cells typically contain  $N \sim 10^4$  types of proteins and RNA molecules, and intracellular condensates typically contain  $\sim 10^2$  types of macromolecules. Standard thermodynamic and field-theoretic approaches are rendered impractical if all or many of these components must be explicitly considered. In such cases, statistical theories that treat inter-component interactions using approximate stochastic methods become the best and perhaps only viable approach [176]. A key question for such models concerns why relatively few types of condensates are observed even though the Gibbs phase rule permits up to  $N + 2$  distinct coexisting phases. Can this type of behavior be predicted and understood from thermodynamics?

In [176], Sear and Cuesta identified parallels between the difficulties in describing many component mixtures and those encountered decades earlier by nuclear physicists in describing the complex energy spectra of large nuclei such as  $^{235}\text{U}$ . Adopting the approach developed for the nuclear physics problem, they replaced the matrix of unknown second-virial coefficients in the Helmholtz free energy of the mixture with a random matrix. Specifically, the free energy density of an  $N$  component mixture truncated after the second-virial coefficient is written

$$f = \sum_{i=1}^N \rho_i (\ln \rho_i - 1) + \frac{1}{2} \sum_{i=1}^N \sum_{j=1}^N \rho_i B_{ij} \rho_j, \quad (17)$$

where  $\rho_i$  is the number density of component  $i$ . The matrix of second-virial coefficients  $B_{ij}$  may be approximated, for example, by a random symmetric matrix filled from a distribution with mean  $b$  and standard deviation  $\sigma$  (figure 14(a)). Sear and Cuesta examined phase stability in this model and identified a crossover from a condensation transformation to a demixing transformation above  $N^{1/2}b/\sigma \simeq -1$ . Both transformations

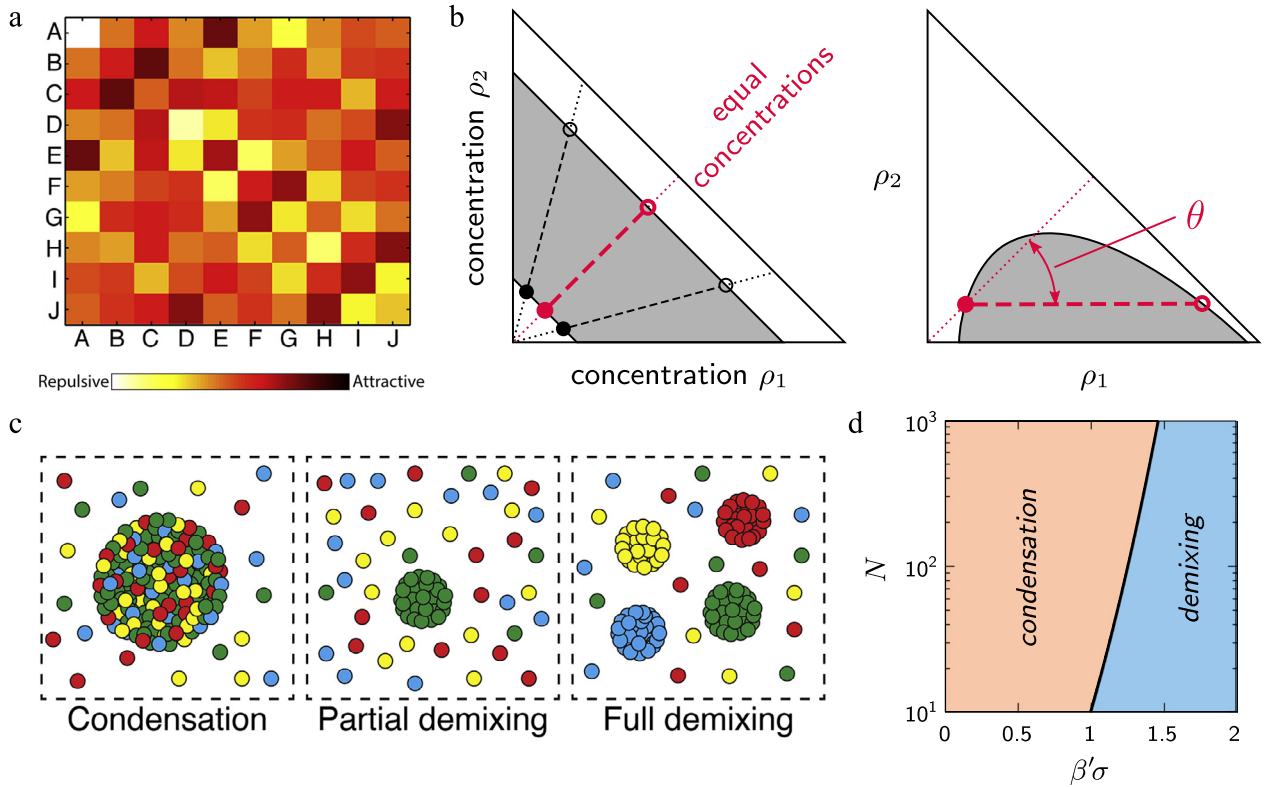


**Figure 14.** Modeling mixtures with many components. (a) Reprinted from [177], Copyright (2017), with permission from Elsevier. Example of a random interaction matrix with variance  $\sigma = 5$  for a ten component system. (b) Reprinted from [178], Copyright (2017), with permission from Elsevier. Representative phase diagrams of two-component mixtures with species concentrations  $\rho_1$  and  $\rho_2$  at constant temperature and pressure. Two-phase coexistence regions are shown in light gray, dotted and dashed lines indicate constant compositions and tie lines (circles), respectively. Red dotted and dashed lines correspond to an equimolar composition and tie lines from the boundary of the equimolar mixed phase, respectively. The angle of phase separation,  $\theta$ , is defined as the angle between the assumed initial equimolar mixed phase composition and the tie line at the transition point (solid circles).  $\theta = 0$  corresponds to condensation, while the maximum value of  $\theta$  corresponds to demixing of a single component. (c) Reprinted from [177], Copyright (2017), with permission from Elsevier. Schematics of limiting phase separated states in a four component system. Condensation is defined in the main text. Partial demixing refers to droplet formation involving only a subset of the components. Full demixing refers to droplet formation involving all components, with as many distinct droplets as there are components. (d) Reprinted from [178], Copyright (2017), with permission from Elsevier. Mean-field phase diagram for the random stochastic interaction model as a function of control parameters  $N$  and  $\beta'\sigma$  ( $\beta' = \beta z\phi/2$ ,  $\beta = 1/k_B T$ ,  $z$  is the lattice coordination number, and  $\phi$  is the assumed concentration of all high-concentration phases). The condensation/demixing boundary scales approximately as  $\sqrt{\ln N} \sim \beta'\sigma$ , which is much steeper than the central limit theorem scaling  $\sqrt{N} \sim \sigma/b$ .

involve the formation of two coexisting phases; in condensation one is enriched in all  $N$  and one is depleted in all  $N$ , while in demixing each is enriched in some components and depleted in others (figures 14(b) and (c)). Such analyses rely on the existence of self-averaging thermodynamic properties in the systems of interest. This requires in the present context that important measurables do not depend on the specific choice of  $B_{ij}$  in the limit of large  $N$ .

Jacobs and Frenkel have further explored and developed this type of approach. In [179], numerical Monte Carlo simulations were devised and employed to test the assumptions and predictions of [176], to compute coexistence bounds, and to examine improved theories for such mixtures. Their results demonstrate that the demixing contribution to phase separation in such systems is indeed self-averaging, as assumed in the analysis of Sear and Cuesta. This implies that a mixture's tendency to demix at the lowest density instability is predictable from knowledge of the mean and variance of the distribution of protein-protein interactions. Upper and lower bounds

on the maximum solute volume fraction of a stable, homogeneous phase were determined, and the composition difference between the condensed and dilute phases at the boundary between homogeneous and phase separated mixtures was predicted. It was found that nonlinear fluctuation effects must be considered to reliably predict this ‘direction’,  $\theta$ , of phase separation (figure 14(b)).

Analysis and simulation results from a more recent, related study by Jacobs and Frenkel [178] have provided an answer to the question posed at the beginning of this subsection. If condensates result from phase separation within a  $N \sim 10^4$  component fluid, why is a relatively small number of organelle types observed? Jacobs and Frenkel find that demixing is generally preferred over condensation as long as the variance of the interaction distribution exceeds a well-defined threshold (figure 14(d)). Furthermore, the extreme values of the interaction distribution tend to drive selection of a few predictable demixing components (partial demixing), meaning that demixing into phases with random compositions is

unlikely (figure 14(c)). Only a small number of interactions or concentrations need to be tuned to produce specific functional demixing transitions, as well as multiphase coexistence between demixed phases. These findings confirm that spatial organization within the cell can be robustly controlled by phase separation and indicate that intracellular mixtures are naturally poised near a small number of specific demixing phase transitions. There is ample reason to expect that further development and study of models of this type will provide answers to related questions and additional insights into the principles of intracellular organization.

#### 4.2. Theoretical approaches for active and driven systems away from thermal equilibrium

The thermodynamically consistent theory of undriven chemically reactive inhomogeneous mixtures outlined in section 3.4 applies to systems in which no work is supplied by internal or external energy sources. Its applications to protein / intracellular condensation therefore focused primarily on *in vitro* protein solutions [149] and/or inactive model intracellular systems [102]. Well-founded theories are also needed to describe highly nonequilibrium intracellular organization processes in which biological activity plays a central role. One possibility is to describe these processes using theories of driven non-equilibrium systems [90]. As discussed in section 2.4, work is supplied to driven systems through external forces (mechanical, electromagnetic, etc), heat transfer (conduction, radiation, etc), mass transfer (chemical reactions with reservoirs, etc), or internal energy sources (e.g. ATP, molecular motors, active swimmers, etc). This work breaks detailed balance and can alter the thermodynamic stability of phases [105], implying that active processes in cells can dynamically shift phase boundaries to, e.g. suppress or induce phase separation on the ‘wrong’ side of the spinodal or binodal, or readily introduce long-lived nonequilibrium steady-states such as chemically-arrested phase-separated morphologies. This possibility may have far-reaching consequences in terms of the cell’s ability to dynamically and robustly mediate condensate assembly/disassembly, as well as our understanding of how it does so.

In driven chemically reactive mixtures, the presence of driving work implies that reaction rates can be dictated by driving forces other than the local chemical potential. A well-defined thermodynamic free energy functional does not exist; rather a nonequilibrium free energy functional is sought. Bazant [105] has very recently presented a theory of thermodynamic stability for driven open systems, and based on this analysis has outlined a formal prescription of the nonequilibrium Gibbs free energy  $\mathcal{G}$  for a certain class of *homogeneous* reactive mixtures. The kinetics of such a mixture evolving in accordance with linear irreversible thermodynamics and with nonlinear reactions (as required to alter stability) is described by the general set of reaction–diffusion equations

$$\frac{\partial c_i}{\partial t} = \nabla \cdot \sum_j L_{ij} \nabla \frac{\delta G}{\delta c_j} + \sum_m s_{i,m} R_m \left( \{c_i\}, \left\{ \frac{\delta G}{\delta c_i} \right\} \right). \quad (18)$$

Here  $c_i$  are the concentrations,  $L_{ij}$  are the Onsager coefficients,  $G$  is the equilibrium Gibbs free energy,  $s_{i,m}$  are the stoichiometry

coefficients, and  $R_m$  are the reaction rates. The mixture is stable when the  $L^2$ -norm ( $\mathcal{L}_c = 1/2 \sum_i \int_V (\delta c_i)^2 dV$ ) of a concentration fluctuation  $\delta c_i$  about a homogeneous initial state decreases with time,

$$\frac{d\mathcal{L}_c}{dt} = \sum_{i,j} \int_V \left[ \delta c_i \mathcal{A}_{ij} \delta c_j - (\nabla \delta c_i) \cdot \mathcal{D}_{ij} (\nabla \delta c_j) \right] dV < 0. \quad (19)$$

The ‘autocatalytic rate tensor’  $\mathcal{A}_{ij} = \sum_n s_{i,n} \delta R_n / \delta c_j$  describes how reaction rates vary with the amount of reactants and products in the system, and the ‘chemical diffusion tensor’  $\mathcal{D}_{ij} = \sum_l L_{il} \delta \mu_l / \delta c_j$  describes whether and to what degree the mixture is stable or unstable with respect to diffusion.  $\mu_l$  are the chemical potentials.

For linear stability of the homogeneous initial state with slow diffusion relative to reactions,  $\mathcal{A}_{ij}$  must be negative definite. For linear stability of the homogeneous initial state with slow reactions relative to diffusion,  $\mathcal{D}_{ij}$  must be positive definite. This analysis shows that homogeneous mixtures can be controllably stabilized or destabilized (phase separation induced) by altering the balance of autocatalytic and chemical diffusion contributions. Introduction of sufficiently autocatalytic reactions ( $\mathcal{A} > 0$  with large enough positive eigenvalue) to a stable homogeneous system ( $\mathcal{D} > 0$ , outside the spinodal) can induce phase separation. Introduction of sufficiently auto-inhibitory reactions ( $\mathcal{A} > 0$  with large enough negative eigenvalue) to an unstable mixture ( $\mathcal{D} < 0$ , inside the spinodal) can suppress phase separation.

Further decomposing  $\mathcal{A} = S - \mathcal{R}_{ij}^{-1} G''$ , where  $S_{ij} = \sum_n s_{i,n} \partial R_n / \partial c_j$  is the ‘solo-autocatalytic rate tensor’ and  $\mathcal{R}_{ij}^{-1} = -\sum_n s_{i,n} \partial R_n / \partial \mu_j$  is the ‘differential reaction resistance tensor’, Bazant writes the nonequilibrium Gibbs free energy  $\mathcal{G}$  (in terms of its second variation) for the considered class of homogeneous reactive mixtures as

$$\begin{aligned} \mathcal{G}'' &= G'' - \mathcal{R}S \\ \sum_{l,n} s_{i,n} \frac{\partial R_n}{\partial \mu_l} \frac{\delta^2 (\mathcal{G} - G)}{\delta c_l \delta c_j} &= \sum_n s_{i,n} \frac{\partial R_n}{\partial c_j}. \end{aligned} \quad (20)$$

$\mathcal{G}$  incorporates the equilibrium Gibbs free energy  $G$  associated with reversible chemical work involving thermodynamic reservoirs and a state-dependent excess energy associated with irreversible work done by nonequilibrium driving forces. This nonequilibrium free energy is necessarily a function of the reaction rates  $R_n$ , specifically of their variations with concentration ( $S_{ij}$ ) and chemical potential ( $\mathcal{R}_{ij}^{-1}$ ). The reaction rates themselves are influenced by both the local equilibrium chemical potential and whichever forces enter the nonequilibrium chemical potential.

Formally, integration of equation (20) gives the nonequilibrium chemical potential  $\mu_i^{\text{noneq}} = \delta \mathcal{G} / \delta c_i$ , and double integration gives the nonequilibrium free energy  $\mathcal{G}$ . These integrations can only be performed in some special cases. Thermodynamic stability can nonetheless be determined from the sign of the time derivative of the second variation of  $\mathcal{G}$ ;  $d\delta^2 \mathcal{G} / dt < 0$  implies stability,  $d\delta^2 \mathcal{G} / dt > 0$  implies instability. A nonequilibrium steady state corresponds to  $\delta \mathcal{G} = 0$ .

The stability analysis in terms of  $\mathcal{R}_{ij}^{-1}$  and  $S_{ij}$  demonstrates that phase separation is suppressed (the spinodal region shrunken) by driven auto-inhibitory reactions. This corresponds to negative eigenvalues of  $S$ , such that the reaction rate decreases as it generates increasing product concentrations. Conversely, phase separation is enhanced (the spinodal region expanded) by solo-autocatalytic reactions or by negative differential resistance. These conditions correspond to positive eigenvalues of  $S$ , (the reaction rate increases as it generates increasing product concentrations) and negative eigenvalues of  $\mathcal{R}_{ij}^{-1}$ , respectively.

As noted by Bazant [105], a description based on equation (20) could be useful in understanding how driven reactions provide the cell with a means of controlling intracellular organization. The stability arguments above indicate that active intracellular reactions can potentially suppress (induce) phase separation below (above) the equilibrium spinodal, according to the nature of the reactions themselves. In this subsection we outline other approaches and studies that have examined the effects of activity, driving forces, or highly nonequilibrium conditions in various ways.

Before doing so, we note that evidence of reaction-induced phase separation and reaction-induced-arrest of phase separating patterns in *undriven* systems can be found in studies of various materials such as curing polymer blends [180] and polymerizing monomer solutions [181]. Here polymerization proceeds with time until the mixture crosses a phase boundary and begins to demix. Demixing is subsequently arrested at a characteristic domain size that is set by the competition between reaction kinetics and domain growth/coarsening kinetics. These systems therefore appear to contradict expectations from thermodynamics (above) that nonequilibrium states cannot be stabilized in the absence of supplied energy. Such an apparent contradiction is perhaps surprising in the context of simple fluids, but in complex fluids, glasses, polymers, polycrystals, etc, long-lived nonequilibrium states are more often the rule than the exception. Further study of *undriven* complex mixtures in which, e.g. polymerization induces phase separation, may therefore be informative in understanding the nature of intracellular condensates. It seems possible that polymerization could both drive the onset of phase separation and regulate condensate size. (See also section 3.2.1 and, e.g. [27, 50]).

#### 4.2.1. Active droplets: centrosomes, active emulsions, and protocells.

Centrosomes are condensates that play a key role in organizing the intracellular microtubule network, in particular the mitotic spindle. Structurally, they generally consist of a pair of centrioles surrounded by a pool of pericentriolar material (PCM, see figure 15(a)). As the cell prepares to divide, these centrioles are duplicated, and two centrosomes subsequently grow by accumulating PCM at the centriole pairs. The increase in centrosome size during this stage follows a sigmoidal growth curve (figure 15(c)). The rate of growth and terminal size are functions of the size of the cell, and the two centrosomes within a given cell are of approximately the same size.

In [182], a description based on phase separation, diffusion, and chemical reactions was used to model centrosome assembly as an autocatalytic nucleation/growth/coarsening process. A simplified ternary Flory–Huggins model was used to derive equilibrium conditions, growth rates, and critical radii for single or paired phase separating droplets in the presence of first order and autocatalytic chemical reactions. The three species involved are cytosol-soluble PCM components  $A$ , cytosol-insoluble PCM components  $B$ , and all other cytosol components  $C$  (figure 15(a)). The two types of PCM material are postulated to correspond to two phosphorylation states with different assembly properties. Chemical reactions interconvert between these two states and also drive an autocatalytic process in which  $A + B \rightarrow 2B$ .

The model was shown to be capable of reproducing the key features of centrosome assembly kinetics: (1) Catalytic activity at centrioles can lead to guaranteed nucleation of centrosomes only at centrioles (in the case where species  $B$  is not created via phosphorylation reactions in the bulk cytosol). (2) The sigmoidal growth curve is reproduced when the autocatalytic reaction is active and is localized within the centrosome, while non-sigmoidal growth occurs in the absence of this autocatalytic reaction (figure 15(b)). Quantitative agreement with experimental growth data was obtained upon estimating and fitting model parameter values (figure 15(c)). (3) The two coexisting centrosomes are stable, spherical, and of similar size, with competitive DLC suppressed by the nonequilibrium effects of the chemical reactions, which instead favor droplets of equal size for sufficiently large activities. We note that other mechanisms, e.g. associated with spatially-varying equilibrium interaction parameters, can also suppress DLC in this manner. (4) Centrosome size was found to scale with cell volume, in agreement with experimental findings. The authors therefore concluded that centrosomes are autocatalytically-nucleated, phase separated droplets of PCM organized by localized activity at centrioles.

This model was further applied in [183] to predict centrosome/PCM growth rates in various mutant conditions. A generalized and more detailed exposition of this modeling framework and its broader applicability to suppression of Ostwald ripening in active emulsions, including living cells, is given in [184].

Finally, in an interesting recent extension of this work, Zwicker *et al* propose that the mechanism of size selection in nonequilibrium chemically-active droplets provides a possible explanation for prebiotic protocell formation during the early stages of the development of life on earth [185]. They show that phase separated active droplets in the presence of an energy source are subject to a spontaneous shape instability that leads to droplet division above some critical size that depends on supersaturation, reaction rates, and droplet properties. They hypothesize that phase separated prebiotic droplets, possibly containing RNA and simple peptides, could have spontaneously nucleated, grown, and by their chemical nature become concentrated reaction centers. They would then become subject to the aforementioned shape instability, would divide, and then continue propagating in this manner, forming an early metabolism composed of active membrane-less

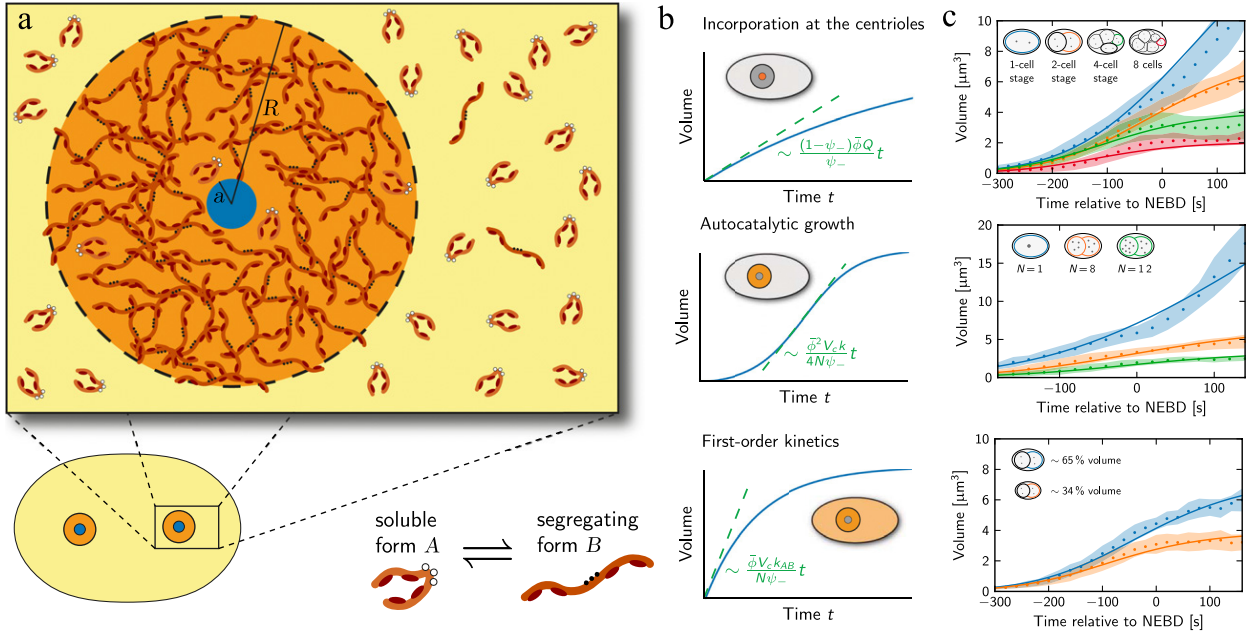


**Figure 15.** Reproduced with permission from [182]. Copyright © Proceedings of the National Academy of Sciences of the United States of America. Model of centrosome assembly as an autocatalytic nucleation/growth/coarsening process. (a) Schematic representation of a cell with two centrosomes (lower left). A single centrosome (upper panel) contains centrioles (blue) and a dense PCM phase (orange). Two PCM component conformations, cytosol-soluble A (globular) and cytosol-insoluble (elongated), exchangeable via phosphorylation/dephosphorylation reactions (lower right). (b) Theoretically-derived forms for the increase in droplet volume with time for three types of reaction-limited growth, wherein droplet material is created only at the centrioles (upper, centriole activity-driven), only inside the droplet (middle, autocatalytically-driven), and throughout the cell (lower, first-order  $A \rightarrow B$  reaction-driven). Dashed lines show the largest volume growth rates and their functional forms. (c) Comparison of theoretically-determined *C. elegans* centrosome growth behaviors (lines) to experimental data (mean = dots, standard deviation = shaded area). Time  $t = 0$  is set to that of nuclear envelop breakdown (NEBD). Results are shown for wild-type cells of several sizes from the one- to the eight-cell stage (upper), cells with an aberrant number  $N$  of centrosomes (middle), and cells with altered volumes (lower, quantified fraction of wild-type volume is noted).

droplets. Cell membranes may have formed much later by mechanisms deriving from amphiphilic molecule accumulation at the droplet interfaces.

**4.2.2. Optogenetically-controlled systems.** Optogenetic approaches to externally controlling protein interactions in living cells have recently begun to be applied to studies of intracellular phases [79, 186–188]. Such approaches involve the use of light-sensitive proteins as optogenetic actuators that change conformation and/or multivalent interaction state upon exposure to externally applied laser light sources. This allows localized, real-time control of intermolecular interactions in living cells. In [79], a light-sensitive protein known to self-associate upon blue light exposure, the photolyase homology region (PHR) of *Arabidopsis thaliana* Cry2 [186], was fused to the ‘sticky’ IDR from various condensate-associated proteins, including FUS, DDX4, and HNRNPA1. These IDR-Cry2 fusion proteins were found to exhibit highly light-tunable interactions, allowing dynamic spatiotemporal control of light-induced intracellular phase transitions (optoDrop formation). Droplet assembly localized into targeted subcellular regions was achieved under conditions of sufficiently deep supersaturation and fast inactivation (light-activated molecules convert back to their native state, or inactivate, at some characteristic rate  $k_2$ ). Cells driven to deep supersaturation were found to form solid-like gels, and these gels were initially reversible but

underwent aging into irreversible aggregates upon cyclic activation.

A simple kinetic binary reaction–diffusion model was shown to accurately describe the steady-state average concentrations in the droplet and background phases under various light-activation conditions. This allowed the saturation concentration  $C_{\text{sat}}$  and the activation/inactivation rate constants,  $k_1$  and  $k_2$ , respectively, to be quantified for each system. A ternary regular solution reaction–diffusion model with Model B dynamics (see section 2.2) was then formulated to provide a thermodynamics-based description of both phase behavior and kinetics. Light-induced chemical reactions were treated using the ideal or state-independent reaction–diffusion framework (section 3.4) with driven, time-dependent reaction rates. This choice is appropriate since the laser supplies external work that drives the concentrations to nonequilibrium steady-state values. The three essential species are inactivated fusion proteins  $A$ , activated fusion proteins  $B$ , and all other (soluble) proteins  $C$ . In this description, a system’s position within phase space can be controlled in two ways; by varying the total droplet-forming protein concentration in the cell (expression level,  $\bar{\phi}_A + \bar{\phi}_B$ ) or by varying the light intensity to modify the steady-state ratio of activated to inactivated molecules  $\phi_B^{\text{ss}}/\phi_A^{\text{ss}}$ .

Key features of localized activation behavior, in which the laser source is focused onto a finite subcellular region, were quantitatively described using a phase transition-based reaction–diffusion model constructed in the spirit of the JMAK

approach. The model quantifies how, upon localized activation, droplet localization is opposed by diffusive spreading and promoted by deactivation and condensation within the nucleating and growing droplet phase. The simulated evolution of the droplet volume fraction field  $\theta_d(\vec{r}, t)$  was shown to agree well with experimental data, supporting the view that the essential behaviors of these systems can be reasonably well-understood in terms of the classical physics of coupled diffusive spreading, activation/deactivation kinetics, and phase transition-driven droplet nucleation/growth.

**4.2.3. Droplet coarsening in concentration gradients.** As discussed in sections 3.3.1 and 3.4.1, chemical activity within the cell can create spatial gradients in the concentrations of molecular species implicated in phase separation. The most prominent example of this type of behavior is the MEX-5 protein associated with asymmetric P granule formation in *C. elegans* embryos (see figure 9(c)). The gradient in MEX-5 concentration across the cell strongly influences the phase separation-mediated formation of P granules, leading to non-classical segregation and ripening of droplets toward the posterior side of the cell and droplet dissolution on the anterior side.

In [189], an extension of the classical Lifshitz–Slyozov–Wagner theory of DLC (see table 1) was presented to describe droplet ripening kinetics in such systems. The derived growth law (given below for the case of well-separated droplets) demonstrates that there is a broken symmetry generating position-dependent droplet growth rates and drift velocities;

$$\frac{dR_i}{dt} = \frac{D}{c_{\text{EQ}}^{\beta} R_i} \left[ \bar{c}(x_i) - c_{\text{EQ}}^{\alpha}(x_i) \left( 1 + \frac{\ell_c}{R_i} \right) \right] \quad (21)$$

and

$$\frac{dx_i}{dt} = \frac{D}{c_{\text{EQ}}^{\beta}} \left[ \frac{\partial \bar{c}(x)}{\partial x} \Big|_{x_i} - \frac{\partial c_{\text{EQ}}^{\alpha}(x)}{\partial x} \Big|_{x_i} \left( 1 + \frac{\ell_c}{R_i} \right) \right]. \quad (22)$$

Here  $R_i$  is the radius of droplet  $i$  located at position  $x_i$ ,  $D$  is the diffusion constant of droplet-forming molecules,  $\ell_c$  is the capillary length,  $\bar{c}(x_i)$  is the average concentration of droplet-forming molecules far away from droplet  $i$ , and  $c_{\text{EQ}}^{\beta}$  and  $c_{\text{EQ}}^{\alpha}(x_i)$  are the equilibrium concentrations of droplet-forming molecules within the droplet and background phases, respectively, at  $x_i$ .

The results presented in [189] describe a spatially biased coarsening process in which droplet positions are not homogeneously distributed in space and the droplet size distribution does not necessarily broaden continuously with time as in classical Ostwald ripening. A dissolution boundary moves through the system with time, segregating droplets toward the side where the supersaturation is highest. Apparent coarsening exponents  $n$  vary with position and time, but the mean droplet radius increases with  $n > 1/3$  during the early stages of coarsening when droplets and material are segregating toward one end of the system. A transient period of arrest then occurs due to narrowing of the droplet size distribution, which temporarily minimizes the driving force for ripening, abruptly decreasing  $n$  toward zero. Eventually a late-stage

$n = 1/3$  regime emerges, though the droplets are highly segregated to one side of the system. Sufficiently steep concentration gradients, rather than simply accelerating coarsening, therefore also lead to a transient regime of arrest.

**4.2.4. Active liquid-like phases.** Evidence has also emerged that condensed droplets in living cells can behave as ‘active liquids’ whose fluid properties are influenced by energy-consuming biological processes. In [7], the apparent viscosity of Xenopus nucleoli (see section 3.2.2) was found to increase by approximately an order of magnitude when cells were depleted of the key metabolic molecule ATP. These nucleoli exhibited more non-spherical shapes and tended to aggregate into irregular clusters. In a later study, FIB-1 FRAP recovery rates and fractions were also found to drop significantly upon ATP-depletion in *X. laevis* and mammalian cells [55]. These results indicate that active processes can play a large role in mediating internal dynamics, in this case with ATP promoting liquidity and preventing aggregation.

Theoretical insight as to physical mechanisms by which activity modifies droplet properties in this manner is currently lacking. However, a recent study has shown that ATP behaves as a biological hydrotope at physiological concentrations; it acts to prevent the formation of aggregates of hydrophobic proteins as well as to dissolve already formed aggregates [190]. This property suggests that ATP may shift condensate phase boundaries and consequently modulate droplet compositions and viscoelastic properties.

**4.2.5. Nonequilibrium kinetic demixing.** Complex fluids may demix due to an equilibrium phase transition, but demixing driven by nonequilibrium kinetic effects, in the absence of a phase transformation, can also occur.

**Large differences in diffusivity.** In [191] it was demonstrated that a simple model system of identical spherical particles with short-range repulsive interactions can demix if the diffusivity of some particles is sufficiently smaller than that of the other particles. Evidence of an effective attractive interaction between the slower particles, caused by cage-creating collisions with the faster particles, is cited as the cause.

Fortunately, true equilibrium phase transitions are accompanied by a number of often measurable thermodynamic and kinetic signatures; discontinuities or kinks in the variation of thermodynamic quantities, kinetics-independent phase boundaries, dynamic scaling behaviors, etc. Nonetheless, when these are weak, unmeasurable, or happen to resemble those of purely nonequilibrium behavior, confusion can arise. In the example noted above, the clusters are composed purely of the slower particles, and the system evolves eventually to a fully demixed state. Measurements of the concentration of slow particles in the non-clustered phase would therefore reveal a continuous decrease in the apparent value of  $C_{\text{sat}}$ , which is not consistent with equilibrium phase behavior. Further development of ways to identify and distinguish thermodynamic versus nonequilibrium signatures in complex intracellular systems should prove worthwhile.

**Density-dependent mobilities.** In [192], two out-of-equilibrium intracellular systems were modeled using lattice descriptions in which molecules are assumed to have local density-dependent mobilities. The first is molecular motor-driven translation of mRNA molecules along microtubules in a cell. The apparent liquid–liquid phase separation of mRNA molecules in the cytoplasm has been shown to be affected when the molecular motors dynein or kinesin are knocked down [193]. Since these motors consume energy and actively move mRNA molecules, this behavior suggests that active transport plays a role in the formation of the droplet phase. The droplets would not be in thermodynamic equilibrium if this were the case. An out-of-equilibrium lattice model in which mRNA hopping rates are decreased when more nearest neighbors are present was found to drive the formation of a condensed liquid phase. Such behavior was found to be a generic result of molecular hopping rates that decrease strongly when the local particle density is high. This is similar to the phenomenon of motility-induced phase separation (MIPS) discussed in the following subsection; the primary difference is that particle velocities rather than hopping rates vary with local particle density in MIPS.

The second out-of-equilibrium system studied in [192] was the apparent phase separation of chromatin that is being transcribed in the nucleus from chromatin that is not active. A simple out-of-equilibrium block copolymer lattice model with density dependent hopping rates was also found to exhibit microphase separation behavior. Another model for chromosome positioning involving inhomogeneous activity-based segregation can be found in [194].

Both models employed in [192] satisfy detailed balance, but since they describe out-of-equilibrium systems, the energy driving the dynamics does not have to be  $k_B T$ . The energy may be supplied, e.g. by molecular motors. Therefore, whether these models do or do not faithfully describe the systems that inspired them, they do describe potentially realizable systems in which the basic behaviors are qualitatively those of equilibrium liquids, but the system is nonetheless out-of-equilibrium. Consequences of this nonequilibrium behavior include the expectation that the effective surface tension of the liquid phase, instead of  $\sim k_B T/a^2$ , presumably  $\sim w_M/a^2$ , where  $w_M$  is the work done by the motors on one of the molecules of the liquid and  $a$  is a molecular diameter.

**4.2.6. Insight from other active systems.** There is a long and well-known history of applying thermodynamics-based physical theories to biological systems, and attempting to extend the original passive formulations to active phenomena. Current efforts to do so in the field in intracellular organization can therefore likely benefit from approaches taken and lessons learned in other contexts. Here we note two interesting areas of study that may prove instructive in this respect.

**Motility-induced phase separation.** The study of motility-induced phase separation (MIPS) [195–198] has advanced rapidly in recent years. The challenge is to describe a system of self-propelled particles; driven, active swimmers such as certain microorganisms, bird flocks, or autophoretic synthetic

colloids (see also [199, 200] for models specific to active colloids). Systems of motile particles with purely repulsive interactions, unlike their passive counterparts, can undergo an intrinsically nonequilibrium phase separation process—MIPS. The general requirement for this to occur is that the speed of the motile particles must decrease sufficiently rapidly as their local density increases. This creates a positive feedback loop that drives a demixing instability and evolution toward a coexistence of a dilute gas-like phase and a dense, much less mobile liquid-like phase.

Efforts to formulate a generic theoretical description of MIPS have attempted to connect equilibrium and nonequilibrium thermodynamics, and to identify the conditions under which the equilibrium view breaks down and new, inherently nonequilibrium effects emerge [195]. The activity of motility enters within a drift velocity term in the kinetic equations, as opposed to, e.g. the chemical reaction terms of interest in this review. Interestingly, this drift velocity term can be viewed in a thermodynamic sense as an effective potential, similar to the way in which chemical reaction terms can be reformulated as static, long-range interactions (see, e.g. [201]).

In the case of MIPS, a generic thermodynamic description of self-propelled particles with density-dependent speeds can be directly mapped to a system of passive particles with attractive interactions, to lowest order in a gradient expansion. This mapping breaks down at higher orders in gradients and fundamentally new nonequilibrium phenomena emerge in systems with sufficient activity [195]. When detailed balance is broken, as in MIPS and in ATP/fuel-rich intracellular environments, a thermodynamic mapping to an effective passive system cannot fully account for all behaviors; the system is irreducible and corrections will be required. Nonetheless, taking a similar approach to systematically mapping links between chemically active phase separating systems and passive phase separation may be a worthwhile effort.

An Active Model B that introduces motility via a nonintegrable gradient term has been formulated and studied in this context [202]. This gradient term leads to a minimal violation of detailed balance, making Active Model B likely the simplest description that goes beyond the thermodynamic mapping to purely passive systems. For a Ginzburg–Landau free energy (section 2.2), the chemical potential takes the form

$$\mu = \frac{\delta F}{\delta \phi} = -\phi + \phi^3 - \nabla^2 \phi + \lambda(\nabla \phi)^2, \quad (23)$$

where the last term is the nonintegrable motility term. Study of this model revealed that motility has little effect on its coarsening exponents, perhaps generating a small decrease from  $n = 1/3$ . On the other hand, motility was found to modify the phase boundaries, a macroscopic equilibrium property. Chemical reactions can have an analogous effect on Model B phase behavior. Further examination and relation of approaches along these lines may therefore be warranted.

**Active gel physics.** Finally we note one other line of study in which activity is merged with foundational thermodynamic and hydrodynamic principles; active gel physics [203]. The primary motivation for the theory of active gels is to describe

the mechanical behavior of cells in terms of their crosslinked network of filaments, which are acted upon by energy-transducing molecular motors that locally break detailed balance. These systems, being gel-like, behave elastically over sufficiently short times and are liquid-like over sufficiently long times, and among their interesting features is the ability to spontaneously move.

The formalisms developed for active gels follow a similar line of distinguishing between low order perturbative expansions around thermodynamic equilibrium states (with controlled validity but limited applicability) and simpler but less controlled low order expansions of long wavelength perturbations (weak gradients) guided by allowed symmetries. The new ingredient in this case is an ‘active stress’ rather than an active drift velocity or chemical activity. The weak gradient approach ultimately employs only conservation laws and symmetries, as do several of the field theoretic approaches emphasized in this review, but it has successfully described a wide variety of phenomena, both biological and non-biological. These include the actin-myosin filament network, active chirals and smectics, defect instabilities, low-Reynolds-number chaos, Turning pattern formation, novel topological singularities, anomalous particle-size-independent diffusivity, cell motility, cell division, cytoplasmic and nucleus spinning, meiotic spindle fluctuations, stress fibers, and plasma membrane rafts [203].

Active gel phenomena may or may not be directly relevant to intracellular condensates. Recent developments concerning aging and gelation, as discussed further in the following subsection, may provide a link, but the emergence of its unified field-theoretic framework as a powerful tool to describe a wide range of active systems could hint at paths forward in the present field. As emphasized in [203], even though the vast complexity of the cellular environment is reduced to a small number of variables within such descriptions, the microscopic details are expressed in the values of these (generally measurable or computable) variables and in the phase space that they create. Limits of validity are inevitably reached and these must be investigated, but the goal of a coherent and unified theoretical framework for intracellular condensation may not be as naive as the apparent complexity of the problem may suggest.

#### 4.3. Phase separation-induced formation of gels, solids, and irreversible aggregates

The study of links between phase transition-induced condensate formation and subsequent gelation, crystallization, and pathological aggregate formation appears to currently pose several important and challenging open questions. Understanding the physics of gelation in intracellular mixtures is one first step toward unravelling the nature of these links. Gelation describes the formation of an infinite network with elastic solid-like properties, within an initially fluid system. If the bonds that form the network (cross-links) are covalent, then a chemical or irreversible gel is formed. If the cross-linking bonds are physical or non-covalent, e.g. hydrogen or van der Waals interactions, then a physical or thermoreversible gel is formed.

Current understanding of gelation in passive materials does not stem from a single unified theory; several competing and more-or-less related theories are employed. These include the classical statistical approach of Flory-Stockmayer theory [204, 205] and percolation theories [206], both of which describe gelation as a continuous transition and provide predictions for critical exponents, analogous to those associated with classical thermodynamic phase transitions. Kinetic theories such as Smoluchowski’s aggregation formalism [207], diffusion-limited aggregation [208], and cluster-cluster aggregation [209], describe gelation as a kinetic critical phenomenon resulting from aggregation, and have successfully reproduced morphological features of many systems. Statistically-based field theoretic approaches are also employed to describe, for example, the formation of inhomogeneous physical gels in complex fluids [210]. The broad similarities between physical gelation and glass formation [211, 212] have also led to merging of concepts and theories originally developed to describe the glass transition. The theory of active gels discussed in the previous section has also emerged recently [203].

As noted in section 2.1, application of the concepts and theories of viscoelastic phase separation [62, 87] to intracellular fluids may be a worthwhile area of future study in this regard. These approaches have been developed to account for viscoelasticity in the phase separation and gelation kinetics of complex fluids such as protein solutions, polymer solutions, colloidal suspensions, emulsions, and micellar solutions. They can be viewed as generalizations of the standard Model B and Model H theories introduced in section 2.1, constructed to describe dynamically asymmetric mixtures containing both fast and slow components. With sufficiently strong attractive interactions between the slow-component molecules, phase separation in such mixtures generally results in a long-lived, transient gel structure rich in slow-component molecules. This gel network can bear stress, leading to an asymmetric division of stress between the components and consequently deformation of the gel phase as phase separation proceeds.

A simple example of the application of this type of view is found in polymer solution theory. It has been observed that some dilute long-chain polymer solutions form a low volume fraction of polymer-rich droplet phase that exhibits anomalously slow coarsening ( $n \ll 1/3$ ) when deeply quenched [62]. Droplets are seen to undergo vigorous Brownian motion and to collide, but rarely to coalesce. It has been theorized that this weakly coarsening ‘moving droplet phase’ is the result of the droplets behaving like elastic bodies over the time scale of collisions. If the characteristic rheological time of the droplets becomes comparable to or smaller than the characteristic time of a Brownian collision (contact time), then viscoelastic effects should become important and may lead to suppression of coalescence [62]. Theoretical estimates of these two time scales indicate that this condition can be realized in practice, and therefore that the observed strong deviation from BMC scaling may be a consequence of droplet phase viscoelasticity.

*A minimal kinetic model for coupled binary phase separation and gelation.* In the spirit of the field theoretic modeling

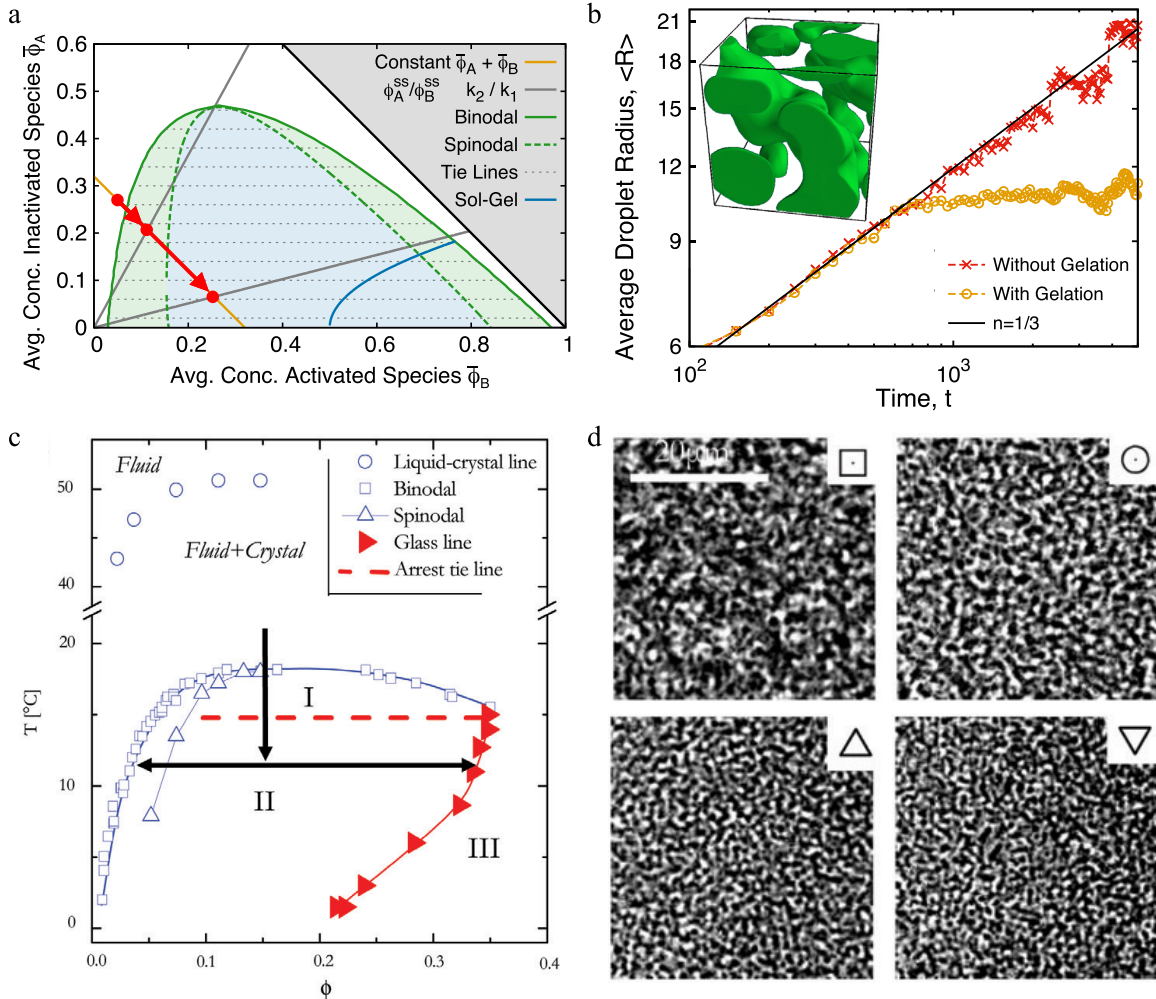


**Figure 16.** Field theoretic model for ternary fluid phase separation and gelation with chemical reaction kinetics. (a) Phase diagram for  $\chi_{AB} = \chi_{AC} = -3$ ,  $\chi_{BC} = 3.75$ ,  $\phi_B^* = 0.5$ ,  $p_0 = 8$ ,  $m = 2$ . The gold line corresponds to a path of fixed  $\bar{\phi}_A + \bar{\phi}_B$ , along which a given system is driven according to the reaction rates  $k_1$  and  $k_2$ . Gray lines correspond to reaction-driven steady-state  $\bar{\phi}_A/\bar{\phi}_B$  ratios at two different  $k_2/k_1$  ratios. Red points and arrows denote two corresponding reaction/activation-driven paths, one which induces a shallow quench into the two-phase region (no crossing of blue sol-gel boundary) and one which induces a deep quench (and crossing of blue sol-gel boundary upon phase separation). (b) A comparison of droplet growth/coarsening kinetics with and without gelation. Inset: Example simulation morphology of an arrested gel structure resulting from a deep quench and subsequent arrest of phase separation ( $\lambda_i = 0.7$ ,  $c_0 = 0.01$ ,  $M_c = 0.02$ ). (c)–(d) Reproduced from [140]. © IOP Publishing Ltd. All rights reserved. (c) Lysozyme solution state diagram showing quenches that lead to classical spinodal decomposition (Region I) and quenches that lead to gelation-arrested spinodal decomposition (Region II). (d) Late-time gel network morphologies from quenches to increasingly lower  $T_f$ .

approaches outlined in section 2.2, we expand here on one relatively simple Cahn–Hilliard-type field theoretic approach as a starting point for describing simultaneous liquid–liquid demixing and physical gelation. The approach is a version of Model C (see section 2.2.4) called the mean-field zeroth-order kinetic model [213]. Phase separation within the liquid mixture is described by the Ginzburg–Landau free energy, equation (1), while a free energy density of the form

$$f_c = -\frac{g}{2}c^2 + \frac{c^3}{3} \quad (24)$$

describes gelation (a sol–gel transition).  $c = c(T, \phi)$  is the gel concentration or fraction of molecules that are part of the system-spanning gel network, and the temperature-like coefficient  $g = g(T, \phi)$  sets the position of the sol–gel phase boundary in  $T$ – $\phi$  space. Model C-type dynamics are given by

$$\frac{\partial \phi}{\partial t} = \nabla \cdot M_\phi \nabla \frac{\delta F[\phi]}{\delta \phi} \quad \frac{\partial c}{\partial t} = -M_c \frac{\delta F_c}{\delta c} \quad (25)$$

where  $M_\phi$  and  $M_c$  are mobility coefficients. Coupling between phase separation and gelation enters the model in two ways. Since molecular mobility should decrease dramatically within the gel phase,  $M_\phi$  is made a fast-decaying function of  $c$ , e.g.  $M_\phi(c) = \exp(-c/c_0)$  where  $c_0 \ll 1$  is the characteristic gel concentration above which  $\phi$  rapidly becomes immobile. Second, the coefficient  $g = g(T, \phi)$  couples the preferred gel concentration to the local polymer/protein concentration. In [213],  $g$  is given by  $g(\phi) = (p\phi - \phi^*)/(1 - \phi^*)$  where  $p\phi$  is the concentration of cross-links and  $\phi^*$  is the polymer/protein concentration required to form a macroscopic gel at a given  $T$ . The relation  $p = \exp(\Delta F/k_B T)/[1 - \exp(\Delta F/k_B T)]$

is assumed, where  $\Delta F$  is an energy barrier associated with cross-linking. Thus the local preferred gel concentration  $c$  becomes  $>0$  when  $\phi > \phi^*/p$  locally, e.g. following the onset of phase separation after a sufficiently deep quench. The non-zero gel concentration couples back to  $\phi$  through  $M_\phi(c)$ , slowing the phase separation kinetics as gelation sets in. Elastic properties of the gel phase are neglected in this description. Such a model should nonetheless be capable of describing, e.g. the results reported in [140] on gel-arrested spinodal decomposition in lysozyme solutions (see section 3.1.1).

*A minimal kinetic model for coupled ternary phase separation, gelation, and chemical reactions.* Simultaneous phase separation, gelation, and chemical reaction kinetics in, e.g. *in vivo* optoDrop systems can be described using a modified form of the minimal kinetic model,

$$\begin{aligned} F_{\text{total}} &= \int_V (f_{\text{tRS}} + f_c) d\vec{r} \\ f_{\text{tRS}} &= \phi_A \ln \phi_A + \phi_B \ln \phi_B + \phi_C \ln \phi_C + \chi_{AB}\phi_A\phi_B + \chi_{AC}\phi_A\phi_C + \chi_{BC}\phi_B\phi_C + \sum_i (\lambda_i \nabla \phi_i)^2 \\ \frac{\partial \phi_A}{\partial t} &= \nabla \cdot M_A \nabla \frac{\delta F_{\text{tRS}}}{\delta \phi_A} - k_1(\vec{r}, t)\phi_A + k_2\phi_B & \frac{\partial \phi_B}{\partial t} &= \nabla \cdot M_B \nabla \frac{\delta F_{\text{tRS}}}{\delta \phi_B} + k_1(\vec{r}, t)\phi_A - k_2\phi_B \\ f_c &= -\frac{g}{2}c^2 + \frac{c^3}{3} & \frac{\partial c}{\partial t} &= -M_c \frac{\delta F_c}{\delta c}. \end{aligned} \quad (26)$$

$f_{\text{tRS}}$  is a ternary RS free energy density for  $\phi$  where  $\phi_A$ ,  $\phi_B$ , and  $\phi_C$  denote the concentrations of inactivated FUS, activated FUS, and other cytoplasmic molecules,  $\chi_{ij}$  are their coupling parameters, and  $\lambda_i$  are their interfacial energy coefficients. The light-induced chemical reactions are treated as a first order process  $A \xrightleftharpoons{k_2} B$ , with forward and backward rates  $k_1$  and  $k_2$ , respectively. Mobilities may be given by  $M_A(c) = M_B(c) = \exp(-c/c_0)$ , and the gel phase coefficient by  $g = g(\phi_A, \phi_B) = [\phi_B - \phi_B^* - p(\phi_A)]/(1 - \phi_B^*)$ , where  $p(\phi_A) = p_0\phi_A^m$  with  $p_0$  and  $m$  constants.

Figure 16(a) shows the phase diagram for one realization of this model. For given initial concentrations of  $A$ ,  $B$ , and  $C$  molecules, light-induced activation/chemical reactions can be used to quench the system along, e.g. the solid gold line, into the two-phase region delineated by the solid green line. The red arrows show two such example quenches; one shallow and one deep. Upon phase separation following the shallow quench, the equilibrium concentrations of  $\phi_A$  and  $\phi_B$  in the  $B$ -rich droplet phase (given by following the tie lines from the terminal red dot to the large  $\phi_B$  side of the binodal) lie outside of the sol-gel boundary (solid blue line). Gelation therefore does not occur, the droplets remain liquid-like and coarsen accordingly (figure 16(c)). Upon phase separation following the deep quench, formation of the droplet phase does require crossing the sol-gel boundary. Gelation therefore occurs some time after droplet formation, resulting in irregular, non-spherical morphologies such as that shown in figure 16(b). Droplet coarsening is slowed or arrested according to the strength/

degree of gelation (figure 16(c)). Under conditions of significant droplet Brownian motion, clustered aggregates of droplets then form.

## 5. Conclusion

The interior of living cells is an extremely complex but extremely well-organized environment. It is now well-established that one means by which cells organize this environment is by employing phase transitions to control the assembly and disassembly of condensates and related membrane-less bodies. Much less is quantitatively understood about the droplet formation processes and the role of nonequilibrium biological activity. In this review, we have critically assessed the current status of theoretical and key experimental developments

in the field of intracellular phase transitions, with particular focus on condensate assembly kinetics. Our primary aim has been to assess the degree to which classic models of nucleation, growth, and coarsening based on linear irreversible thermodynamics quantitatively describe phase separation processes within the inherently nonequilibrium intracellular environment.

To this end, we have categorized field-theoretic approaches employed to date in this area into four groups; passive, modulated passive, undriven chemically reactive, and driven chemically reactive. Various intracellular systems have been shown to be well-described by each of these approaches, reflecting the wide range of means by which cells can trigger assembly, mediate growth and coarsening kinetics, and modify material properties of condensates and related bodies. The findings that we have summarized therefore do not only support the now firmly established existence of phase-separated droplets within living cells, but also show that classic models of phase separation provide a quantitative foundation from which the assembly and aging kinetics of many of these droplets can be understood.

The first three categories outlined above are consistent with equilibrium thermodynamics which implies that detailed balance is satisfied. Condensates whose assembly via phase separation can be quantitatively described by models of these types therefore can be considered, from an effective thermodynamic viewpoint, to be passively demixing fluid droplets. Even though living cells actively consume energy, the

assembly of such bodies appears to be governed by relaxation towards an effective equilibrium. The kinetics and properties of condensates of this type can be significantly influenced by nonequilibrium activity, but the effects of this activity can be accounted for without altering the basic forms of the passive descriptions.

For example, nonequilibrium activity can drive increases in the concentrations of molecular species that phase separate above a threshold concentration. Here the cell itself acts as the experimenter by ‘externally’ navigating the cytoplasm and nucleoplasm globally through phase space, triggering various functional but effectively passive mixing and demixing transitions. In this way, relatively small global responses to stimuli, e.g. topping off the concentrations of a few key molecules, can be amplified into dramatic local changes in intracellular structure and subsequently function.

In addition to triggering passive demixing transitions, activity may also fine-tune these transitions by locally modulating effective interactions to, e.g. ensure the assembly of a particular condensates at a particular location. The effects of nonequilibrium activity on underlying molecular concentrations and pair-wise interactions can therefore play large roles in spatially and/or temporally modulating the nature of the effective equilibrium states of such condensates, but the nature of the assembly process remains well-described by passive or modulated passive models. Further application and extension of such approaches should continue to provide insight into the fundamental nature of many intracellular condensates.

Models in the fourth category outlined above, driven chemically reactive, do not satisfy detailed balance and are therefore not consistent with equilibrium thermodynamics. Our ability to understand condensates whose formation is strongly coupled to active processes relies on the efficacy of formulations of this type. One of the three emerging areas of focus that we have identified in the study of intracellular phase transitions is therefore further development of well-founded descriptions of driven chemically reactive systems. The ability of driven or active processes to alter the thermodynamic stability of phases [105] may have far-reaching consequences in terms of the cell’s ability to dynamically trigger condensate assembly/disassembly and mediate condensate size, composition, and functionality. We have also highlighted the development of models for systems with many components and the study of phase separation-induced formation of gels, solids, and irreversible aggregates as important emerging areas of study.

These topics all present formidable challenges, but we see much reason for excitement in the fact that these three areas bring current frontiers of development in classical condensed matter theory face-to-face with the frontiers now taking shape in the study of intracellular phase transitions. The present may therefore prove to be a formative moment in which it is becoming possible to address complex questions concerning cellular development, function, aging, and disease by isolating molecular driving forces for condensate assembly, quantitatively analyzing assembly and aging kinetics, controlling intracellular phase transitions in living cells, and developing new theories of phase transformations that merge foundational thermodynamic principles with highly nonequilibrium biological processes.

## ORCID iDs

Clifford P Brangwynne  <https://orcid.org/0000-0002-1350-9960>

## References

- [1] Sengers J L 2002 *How fluids unmix: Discoveries by the School of Van der Waals and Kamerlingh Onnes* vol 4 (The Netherlands: Edita Publishing House of the Royal)
- [2] Wilson E B 1899 The structure of protoplasm *Science* **33**–45
- [3] Heilbrunn L 1923 The colloid chemistry of protoplasm *Am. J. Physiol.-Legacy Content* **64** 481–98
- [4] Walter H and Brooks D E 1995 Phase separation in cytoplasm, due to macromolecular crowding, is the basis for microcompartmentation *FEBS Lett.* **361** 135–9
- [5] Simons K and Ikonen E 1997 Functional rafts in cell membranes *Nature* **387** 569
- [6] Brangwynne C P, Eckmann C R, Courson D S, Rybarska A, Hoege C, Gharakhani J, Jülicher F and Hyman A A 2009 Germline P granules are liquid droplets that localize by controlled dissolution/condensation *Science* **324** 1729–32
- [7] Brangwynne C P, Mitchison T J and Hyman A A 2011 Active liquid-like behavior of nucleoli determines their size and shape in *Xenopus laevis* oocytes *Proc. Natl Acad. Sci. USA* **108** 4334–9
- [8] Li P *et al* 2012 Phase transitions in the assembly of multivalent signalling proteins *Nature* **483** 336–40
- [9] Nott T J *et al* 2015 Phase transition of a disordered nuage protein generates environmentally responsive membraneless organelles *Mol. Cell* **57** 936–47
- [10] Jiang H, Wang S, Huang Y, He X, Cui H, Zhu X and Zheng Y 2015 Phase transition of spindle-associated protein regulate spindle apparatus assembly *Cell* **163** 108–22
- [11] Zeng M, Shang Y, Araki Y, Guo T, Huganir R L and Zhang M 2016 Phase transition in postsynaptic densities underlies formation of synaptic complexes and synaptic plasticity *Cell* **166** 1163–75
- [12] Su X, Ditlev J A, Hui E, Xing W, Banjade S, Okrut J, King D S, Taunton J, Rosen M K and Vale R D 2016 Phase separation of signaling molecules promotes t cell receptor signal transduction *Science* **352** 595–9
- [13] Wippich F, Bodenmiller B, Trajkovska M G, Wanka S, Aebersold R and Pelkmans L 2013 Dual specificity Kinase DYRK3 couples stress granule condensation/dissolution to mTORC1 signaling *Cell* **152** 791–805
- [14] Banani S F, Lee H O, Hyman A A and Rosen M K 2017 Biomolecular condensates: organizers of cellular biochemistry *Nat. Rev. Mol. Cell Biol.* **18** 285–98
- [15] Shin Y and Brangwynne C P 2017 Liquid phase condensation in cell physiology and disease *Science* **357** eaaf4382
- [16] Spector D L 2006 SnapShot: cellular bodies *Cell* **127** 1071.e1
- [17] Parker R and Sheth U 2007 P bodies and the control of mRNA translation and degradation *Mol. cell* **25** 635–46
- [18] Gall J G 2000 Cajal bodies: the first 100 years *Ann. Rev. Cell Dev. Biol.* **16** 273–300
- [19] Boisvert F-M, van Koningsbruggen S, Navascués J and Lamond A I 2007 The multifunctional nucleolus *Nat. Rev. Mol. Cell Biol.* **8** 574–85
- [20] An S, Kumar R, Sheets E D and Benkovic S J 2008 Reversible compartmentalization of de novo purine biosynthetic complexes in living cells *Science* **320** 103–6
- [21] Schwarz-Romond T, Merrifield C, Nichols B J and Bienz M 2005 The wnt signalling effector dishevelled forms dynamic protein assemblies rather than stable associations with cytoplasmic vesicles *J. Cell Sci.* **118** 5269–77

- [22] Schwarz-Romond T, Fiedler M, Shibata N, Butler P J G, Kikuchi A, Higuchi Y and Bienz M 2007 The dix domain of dishevelled confers wnt signaling by dynamic polymerization *Nat. Struct. Mol. Biol.* **14** 484–92
- [23] Schwarz-Romond T, Metcalfe C and Bienz M 2007 Dynamic recruitment of axin by dishevelled protein assemblies *J. Cell. Sci.* **120** 2402–12
- [24] Bilić J, Huang Y-L, Davidson G, Zimmermann T, Cruciat C-M, Bienz M and Niehrs C 2007 Wnt induces lrp6 signalosomes and promotes dishevelled-dependent lrp6 phosphorylation *Science* **316** 1619–22
- [25] Smalley M J, Signoret N, Robertson D, Tilley A, Hann A, Ewan K, Ding Y, Paterson H and Dale T C 2005 Dishevelled (dvl-2) activates canonical wnt signalling in the absence of cytoplasmic puncta *J. Cell. Sci.* **118** 5279–89
- [26] Sear R P 2007 Dishevelled: a protein that functions in living cells by phase separating *Soft Matter* **3** 680–4
- [27] Sear R P 2008 Phase separation of equilibrium polymers of proteins in living cells *Faraday Discussions* **139** 21–34
- [28] Berry J, Weber S C, Vaidya N, Haataja M and Brangwynne C P 2015 RNA transcription modulates phase transition-driven nuclear body assembly *Proc. Natl Acad. Sci.* **112** E5237–45
- [29] Hyman A A and Brangwynne C P 2011 Beyond stereospecificity: liquids and mesoscale organization of cytoplasm *Dev. Cell* **21** 14–6
- [30] Brangwynne C P 2011 Soft active aggregates: mechanics, dynamics and self-assembly of liquid-like intracellular protein bodies *Soft Matter* **7** 3052–9
- [31] Hyman A A and Simons K 2012 Beyond oil and water—phase transitions in cells *Science* **337** 1047–9
- [32] Brangwynne C P 2013 Phase transitions and size scaling of membrane-less organelles *J. Cell Biol.* **203** 875–81
- [33] Hyman A A, Weber C A and Jülicher F 2014 Liquid–liquid phase separation in biology *Ann. Rev. Cell Dev. Biol.* **30** 39–58
- [34] Zhu L and Brangwynne C P 2015 Nuclear bodies: the emerging biophysics of nucleoplasmic phases *Curr. Opin. Cell Biol.* **34** 23–30
- [35] Chong P A and Forman-Kay J D 2016 Liquid–liquid phase separation in cellular signaling systems *Curr. Opin. Struct. Biol.* **41** 180–6
- [36] Mitrea D M and Kriwacki R W 2016 Phase separation in biology; functional organization of a higher order *Cell Commun. Signaling* **14** 1
- [37] Shorter J 2016 Membraneless organelles: phasing in and out *Nat. Chem.* **8** 528–30
- [38] Bergeron-Sandoval L-P, Safaei N and Michnick S W 2016 Mechanisms and consequences of macromolecular phase separation *Cell* **165** 1067–79
- [39] Aumiller W M and Keating C D 2017 Experimental models for dynamic compartmentalization of biomolecules in liquid organelles: reversible formation and partitioning in aqueous biphasic systems *Adv. Colloid Interface Sci.* **239** 75–87
- [40] Nielsen F C, Hansen H T and Christiansen J 2016 RNA assemblages orchestrate complex cellular processes *Bioessays* **38** 674–81
- [41] Qin S and Zhou H-X 2017 Protein folding, binding and droplet formation in cell-like conditions *Curr. Opin. Struct. Biol.* **43** 28–37
- [42] Gunton J D, Shiriyev A and Pagan D L 2007 *Protein Condensation: Kinetic Pathways to Crystallization and Disease* (Cambridge: Cambridge University Press)
- [43] Weber S C and Brangwynne C P 2012 Getting RNA and protein in phase *Cell* **149** 1188–91
- [44] Eisenberg D and Jucker M 2012 The amyloid state of proteins in human diseases *Cell* **148** 1188–203
- [45] Ramaswami M, Taylor J P and Parker R 2013 Altered ribostasis: RNA–protein granules in degenerative disorders *Cell* **154** 727–36
- [46] Alberti S and Hyman A A 2016 Are aberrant phase transitions a driver of cellular aging? *BioEssays* **38** 959–68
- [47] Aguzzi A and Altmeyer M 2016 Phase separation: linking cellular compartmentalization to disease *Trends Cell Biol.* **26** 547–58
- [48] Wu H and Fuxreiter M 2016 The structure and dynamics of higher-order assemblies: amyloids, signalosomes and granules *Cell* **165** 1055–66
- [49] Taylor J P, Brown R H Jr and Cleveland D W 2016 Decoding als: from genes to mechanism *Nature* **539** 197–206
- [50] Brangwynne C P, Tompa P and Pappu R V 2015 Polymer physics of intracellular phase transitions *Nat. Phys.* **11** 899–904
- [51] Uversky V N 2017 Intrinsically disordered proteins in overcrowded milieu: membrane-less organelles, phase separation and intrinsic disorder *Curr. Opin. Struct. Biol.* **44** 18–30
- [52] Hill T L 1986 *An Introduction to Statistical Thermodynamics* (New York: Dover)
- [53] Lin Y-H, Forman-Kay J D and Chan H S 2016 Sequence-specific polyampholyte phase separation in membraneless organelles *Phys. Rev. Lett.* **117** 178101
- [54] Lin Y-H, Song J, Forman-Kay J D and Chan H S 2017 Random-phase-approximation theory for sequence-dependent, biologically functional liquid–liquid phase separation of intrinsically disordered proteins *J. Mol. Liq.* **228** 176–93
- [55] Feric M, Vaidya N, Harmon T S, Mitrea D M, Zhu L, Richardson T M, Kriwacki R W, Pappu R V and Brangwynne C P 2016 Coexisting liquid phases underlie nucleolar subcompartments *Cell* **165** 1686–97
- [56] Onuki A 2002 *Phase Transition Dynamics* (Cambridge: Cambridge University Press)
- [57] Goldenfeld N 1992 *Lectures on Phase Transitions and the Renormalization Group (Frontiers in Physics)* (Boulder, CO: Westview Press)
- [58] Stanley H 1971 *Introduction to Phase Transitions and Critical Phenomena (Int. Series of Monographs on Physics)* (Oxford: Oxford University Press)
- [59] Ratke L and Voorhees P 2002 *Growth and Coarsening: Ostwald Ripening in Material Processing (Engineering Materials and Processes)* (Berlin: Springer)
- [60] Bray A 2000 Coarsening dynamics of nonequilibrium phase transitions *Soft and Fragile Matter: Nonequilibrium Dynamics, Metastability and Flow (PBK) (Scottish Graduate Series)* ed M Cates and R Evans (London: Taylor and Francis) ch 8
- [61] Bray A J 2002 Theory of phase-ordering kinetics *Adv. Phys.* **51** 481–587
- [62] Tanaka H 2000 Viscoelastic phase separation *J. Phys.: Condens. Matter* **12** R207
- [63] Wang H and Davis R H 1993 Droplet growth due to brownian, gravitational, or thermocapillary motion and coalescence in dilute dispersions *J. Colloid Interface Sci.* **159** 108–18
- [64] Hohenberg P C and Halperin B I 1977 Theory of dynamic critical phenomena *Rev. Mod. Phys.* **49** 435–79
- [65] Lifshitz I M and Slyozov V V 1961 The kinetics of precipitation from supersaturated solid solutions *J. Phys. Chem. Solids* **19** 35–50
- [66] Wagner C 1961 Theorie der alterung von niederschlägen durch umlösen (ostwald-reifung) *Z. Elektrochem. Ber. Bunsenges. Phys. Chem.* **65** 581–91
- [67] Binder K 1977 Theory for the dynamics of ‘clusters’. II. Critical diffusion in binary systems and the kinetics of phase separation *Phys. Rev. B* **15** 4425–47
- [68] Siggia E D 1979 Late stages of spinodal decomposition in binary mixtures *Phys. Rev. A* **20** 595–605
- [69] Shimizu R and Tanaka H 2015 A novel coarsening mechanism of droplets in immiscible fluid mixtures *Nat. Commun.* **6** 7407

- [70] Furukawa H 1985 Effect of inertia on droplet growth in a fluid *Phys. Rev. A* **31** 1103–8
- [71] Weitz D, Huang J, Lin M and Sung J 1984 Dynamics of diffusion-limited kinetic aggregation *Phys. Rev. Lett.* **53** 1657
- [72] Kolmogorov A A N 1937 A statistical theory for the recrystallisation of metals *Izv. Akad. Nauk SSSR Neorg. Mater. (Inorg. Mater. (USSR))* **3** 355–9
- [73] Johnson W A and Mehl R F 1939 Reaction kinetics in processes of nucleation and growth *Trans. Am. Inst. Min. Metall. Eng.* **135** 416–42
- [74] Avrami M 1939 Kinetics of phase change. I. General theory *J. Chem. Phys.* **7** 1103–12
- [75] Avrami M 1940 Kinetics of phase change. II. Transformation time relations for random distribution of nuclei *J. Chem. Phys.* **8** 212–24
- [76] Avrami M 1941 Granulation, phase change and microstructure kinetics of phase change. III *J. Chem. Phys.* **9** 177–84
- [77] Cahn J W 1996 The time cone method for nucleation and growth kinetics on a finite domain *Proc. of an MRS Symp. on Thermodynamics and Kinetics of Phase Transformations (Boston, 1995)* vol 398 pp 425–38
- [78] Ham F S 1958 Theory of diffusion-limited precipitation *J. Phys. Chem. Solids* **6** 335–51
- [79] Shin Y, Berry J, Pannucci N, Haataja M P, Toettcher J E and Brangwynne C P 2017 Spatiotemporal control of intracellular phase transitions using light-activated optodroplets *Cell* **168** 1–13
- [80] Grant M and Elder K R 1999 Spinodal decomposition in fluids *Phys. Rev. Lett.* **82** 14–6
- [81] Sagui C and Grant M 1999 Theory of nucleation and growth during phase separation *Phys. Rev. E* **59** 4175
- [82] Yao J H, Elder K, Guo H and Grant M 1994 Late stage droplet growth *Phys. A: Stat. Mech. Appl.* **204** 770–88
- [83] Yao J H, Elder K, Guo H and Grant M 1993 Theory and simulation of ostwald ripening *Phys. Rev. B* **47** 14110
- [84] Ratke L 1990 Ostwald ripening in liquids *Low-Grav. Fluid Dyn. Transp. Phenom.* **130** 661–9
- [85] Lee K, Chen J and Gieseke J 1984 Log-normally preserving size distribution for brownian coagulation in the free-molecule regime *Aerosol Sci. Technol.* **3** 53–62
- [86] Meakin P 1990 Diffusion-limited droplet coalescence *Phys. A: Stat. Mech. Appl.* **165** 1–18
- [87] Onuki A 1997 Phase transitions of fluids in shear flow *J. Phys.: Condens. Matter* **9** 6119
- [88] Ginzburg V L and Landau L D 1950 On the theory of superconductivity *Zh. Eksp. Teor. Fiz.* **20** 35
- [89] van der Waals J 1893 *J. Stat. Phys.* **20** 197–244
- [90] Kondepudi D and Prigogine I 2014 *Modern Thermodynamics: from Heat Engines to Dissipative Structures* (New York: Wiley)
- [91] Onsager L 1931 Reciprocal relations in irreversible processes. I *Phys. Rev.* **37** 405
- [92] Onsager L 1931 Reciprocal relations in irreversible processes. II *Phys. Rev.* **38** 2265
- [93] Camley B A and Brown F L H 2010 Dynamic simulations of multicomponent lipid membranes over long length and time scales *Phys. Rev. Lett.* **105** 148102
- [94] Banjade S and Rosen M K 2014 Phase transitions of multivalent proteins can promote clustering of membrane receptors *Elife* **3** e04123
- [95] Banani S F, Rice A M, Peebles W B, Lin Y, Jain S, Parker R and Rosen M K 2016 Compositional control of phase-separated cellular bodies *Cell* **166** 651–63
- [96] Kato M *et al* 2012 Cell-free formation of RNA granules: low complexity sequence domains form dynamic fibers within hydrogels *Cell* **149** 753–67
- [97] Han T W *et al* 2012 Cell-free formation of RNA granules: bound RNAs identify features and components of cellular assemblies *Cell* **149** 768–79
- [98] Patel A *et al* 2015 A liquid-to-solid phase transition of the als protein fus accelerated by disease mutation *Cell* **162** 1066–77
- [99] Molliex A, Temirov J, Lee J, Coughlin M, Kanagaraj A P, Kim H J, Mittag T and Taylor J P 2015 Phase separation by low complexity domains promotes stress granule assembly and drives pathological fibrillization *Cell* **163** 123–33
- [100] Elbaum-Garfinkle S, Kim Y, Szczepaniak K, Chen C C-H, Eckmann C R, Myong S and Brangwynne C P 2015 The disordered p granule protein laf-1 drives phase separation into droplets with tunable viscosity and dynamics *Proc. Natl Acad. Sci.* **112** 7189–94
- [101] Wei M T, Elbaum-Garfinkle S, Holehouse A S, Chen C C-H, Feric M, Arnold C B, Priestley R D, Pappu R V and Brangwynne C P 2017 Phase behaviour of disordered proteins underlying low density and high permeability of liquid organelles *Nat. Chem.* **9** 1118
- [102] Saha S *et al* 2016 Polar positioning of phase-separated liquid compartments in cells regulated by an mrna competition mechanism *Cell* **166** 1572–84
- [103] Wang J T, Smith J, Chen B C, Schmidt H, Rasoloson D, Paix A, Lambrus B G, Calidas D, Betzig E and Seydoux G 2014 Regulation of RNA granule dynamics by phosphorylation of serine-rich, intrinsically disordered proteins in *C. elegans* *Elife* **3** e04591
- [104] Bazant M Z 2013 Theory of chemical kinetics and charge transfer based on nonequilibrium thermodynamics *Acc. Chem. Res.* **46** 1144–60
- [105] Bazant M Z 2017 Thermodynamic stability of driven open systems and control of phase separation by electro-autocatalysis *Faraday Discussions* **199** 423–63
- [106] Bungenberg de Jong H G 1949 Crystallisation—coacervation—flocculation *Colloid Science* vol 1, ed H R Kruyt (Amsterdam: Elsevier) pp 232–58
- [107] Dervichian D G 1954 A comparative study of the flocculation and coacervation of different systems *Discuss. Faraday Soc.* **18** 231–9
- [108] Overbeek J T G and Voorn M J 1957 Phase separation in polyelectrolyte solutions. Theory of complex coacervation *J. Cell. Comparative Physiol.* **49** 7–26
- [109] Giannoni E, Ramponi G, Zurdo J and Dobson C M 2002 Inherent toxicity of aggregates implies a common mechanism for protein misfolding diseases *Nature* **416** 507
- [110] Kim H J *et al* 2013 Mutations in prion-like domains in hnRNPA2B1 and hnRNPA1 cause multisystem proteinopathy and ALS *Nature* **495** 467–73
- [111] Lin Y, Proter D S, Rosen M K and Parker R 2015 Formation and maturation of phase-separated liquid droplets by rna-binding proteins *Mol. cell* **60** 208–19
- [112] Bolognesi B, Gotor N L, Dhar R, Cirillo D, Baldrihi M, Tartaglia G G and Lehner B 2016 A concentration-dependent liquid phase separation can cause toxicity upon increased protein expression *Cell Rep.* **16** 222–31
- [113] Ishimoto C and Tanaka T 1977 Critical behavior of a binary mixture of protein and salt water *Phys. Rev. Lett.* **39** 474–7
- [114] Tanaka T, Sun S-T and Nishio I 1981 Phase transition in gels *Scattering Techniques Applied to Supramolecular and Nonequilibrium Systems* ed S-H Chen *et al* (Boston, MA: Springer) pp 321–36
- [115] Thomson J A, Schurtenberger P, Thurston G M and Benedek G B 1987 Binary liquid phase separation and critical phenomena in a protein/water solution *Proc. Natl Acad. Sci.* **84** 7079–83
- [116] Taratuta V G, Holschbach A, Thurston G M, Blankschtein D and Benedek G B 1990 Liquid–liquid phase separation of aqueous lysozyme solutions: effects of pH and salt identity *J. Phys. Chem.* **94** 2140–4

- [117] Broide M L, Berland C R, Pande J, Ogun O O and Benedek G B 1991 Binary-liquid phase separation of lens protein solutions *Proc. Natl Acad. Sci. USA* **88** 5660–4
- [118] Berland C R, Thurston G M, Kondo M, Broide M L, Pande J, Ogun O and Benedek G B 1992 Solid-liquid phase boundaries of lens protein solutions *Proc. Natl Acad. Sci. USA* **89** 1214–8
- [119] Liu C, Lomakin A, Thurston G M, Hayden D, Pande A, Pande J, Ogun O, Asherie N and Benedek G B 1995 Phase separation in multicomponent aqueous-protein solutions *J. Phys. Chem.* **99** 454–61
- [120] Lomakin A, Asherie N and Benedek G B 1996 Monte carlo study of phase separation in aqueous protein solutions *J. Chem. Phys.* **104** 1646–56
- [121] Vlachy V, Blanch H and Prausnitz J 1993 Liquid–liquid phase separations in aqueous solutions of globular proteins *AIChE J.* **39** 215–23
- [122] Vekilov P G 2010 Phase transitions of folded proteins *Soft Matter* **6** 5254–72
- [123] Vekilov P G 2012 Phase diagrams and kinetics of phase transitions in protein solutions *J. Phys.: Condens. Matter* **24** 193101
- [124] Dumetz A C, Chockla A M, Kaler E W and Lenhoff A M 2008 Protein phase behavior in aqueous solutions: crystallization, liquid–liquid phase separation, gels and aggregates *Biophys. J.* **94** 570–83
- [125] Broide M L, Tominc T M and Saxowsky M D 1996 Using phase transitions to investigate the effect of salts on protein interactions *Phys. Rev. E* **53** 6325
- [126] Muschol M and Rosenberger F 1997 Liquid–liquid phase separation in supersaturated lysozyme solutions and associated precipitate formation/crystallization *J. Chem. Phys.* **107** 1953
- [127] Kulkarni A M, Dixit N M and Zukoski C F 2003 Ergodic and non-ergodic phase transitions in globular protein suspensions *Faraday Discussions* **123** 37–50
- [128] Filobelo L F, Galkin O and Vekilov P G 2005 Spinodal for the solution-to-crystal phase transformation *J. Chem. Phys.* **123** 014904
- [129] Stradner A, Sedgwick H, Cardinaux F, Poon W C, Egelhaaf S U and Schurtenberger P 2004 Equilibrium cluster formation in concentrated protein solutions and colloids *Nature* **432** 492–5
- [130] Shukla A, Mylonas E, Di Cola E, Finet S, Timmins P, Narayanan T and Svergun D I 2008 Absence of equilibrium cluster phase in concentrated lysozyme solutions *Proc. Natl Acad. Sci.* **105** 5075–80
- [131] Gibaud T, Cardinaux F, Bergenholtz J, Stradner A and Schurtenberger P 2011 Phase separation and dynamical arrest for particles interacting with mixed potentials—the case of globular proteins revisited *Soft Matter* **7** 857–60
- [132] Vekilov P G 2016 Nucleation of protein crystals *Prog. Cryst. Growth Charact. Mater.* **62** 136–54
- [133] Raccosta S, Manno M, Bulone D, Giacomazza D, Militello V, Martorana V and San Biagio P L 2010 Irreversible gelation of thermally unfolded proteins: structural and mechanical properties of lysozyme aggregates *Eur. Biophys. J.* **39** 1007–17
- [134] ten Wolde P R and Frenkel D 1997 Enhancement of protein crystal nucleation by critical density fluctuations *Science* **277** 1975–8
- [135] Illett S M, Orrock A, Poon W and Pusey P 1995 Phase behavior of a model colloid-polymer mixture *Phys. Rev. E* **51** 1344
- [136] Vekilov P G and Vorontsova M A 2014 Nucleation precursors in protein crystallization *Acta Crystal. Sect. F: Struct. Biol. Commun.* **70** 271–82
- [137] Li Y, Lubchenko V, Vorontsova M A, Filobelo L and Vekilov P G 2012 Ostwald-like ripening of the anomalous mesoscopic clusters in protein solutions *J. Phys. Chem. B* **116** 10657–64
- [138] Sear R P 2007 Nucleation: theory and applications to protein solutions and colloidal suspensions *J. Phys.: Condens. Matter* **19** 033101
- [139] Shah M, Galkin O and Vekilov P G 2004 Smooth transition from metastability to instability in phase separating protein solutions *J. Chem. Phys.* **121** 7505–12
- [140] Gibaud T and Schurtenberger P 2009 A closer look at arrested spinodal decomposition in protein solutions *J. Phys.: Condens. Matter* **21** 322201
- [141] Talanquer V and Oxtoby D W 1998 Crystal nucleation in the presence of a metastable critical point *J. Chem. Phys.* **109** 223–7
- [142] Zhang F, Roosen-Runge F, Sauter A, Roth R, Skoda M W, Jacobs R M, Sztucki M and Schreiber F 2012 The role of cluster formation and metastable liquid–liquid phase separation in protein crystallization *Faraday Discussions* **159** 313–25
- [143] Streets A M and Quake S R 2010 Ostwald ripening of clusters during protein crystallization *Phys. Rev. Lett.* **104** 178102
- [144] Sciotino F, Mossa S, Zaccarelli E and Tartaglia P 2004 Equilibrium cluster phases and low-density arrested disordered states: the role of short-range attraction and long-range repulsion *Phys. Rev. Lett.* **93** 055701
- [145] Pan W, Vekilov P G and Lubchenko V 2010 Origin of anomalous mesoscopic phases in protein solutions *J. Phys. Chem. B* **114** 7620–30
- [146] Vekilov P G, Pan W, Gliko O, Katsonis P and Galkin O 2009 Metastable mesoscopic phases in concentrated protein solutions *Aspects of Physical Biology* (Berlin: Springer) pp 65–95
- [147] Vorontsova M A, Maes D and Vekilov P G 2015 Recent advances in the understanding of two-step nucleation of protein crystals *Faraday Discussions* **179** 27–40
- [148] Lutsko J F and Nicolis G 2016 Mechanism for the stabilization of protein clusters above the solubility curve *Soft Matter* **12** 93–8
- [149] Lutsko J F 2016 Mechanism for the stabilization of protein clusters above the solubility curve: the role of non-ideal chemical reactions *J. Phys.: Condens. Matter* **28** 244020
- [150] Webster A and Cates M 1998 Stabilization of emulsions by trapped species *Langmuir* **14** 2068–79
- [151] Zhang H, Elbaum-Garfinkle S, Langdon E M, Taylor N, Occhipinti P, Bridges A A, Brangwynne C P and Gladfelter A S 2015 Rna controls polyq protein phase transitions *Mol. Cell* **60** 220–30
- [152] Taylor N, Elbaum-Garfinkle S, Vaidya N, Zhang H, Stone H A and Brangwynne C P 2016 Biophysical characterization of organelle-based rna/protein liquid phases using microfluidics *Soft Matter* **12** 9142–50
- [153] Kroschwitz S, Maharana S, Mateju D, Malinovska L, Nüske E, Poser I, Richter D and Alberti S 2015 Promiscuous interactions and protein disaggregases determine the material state of stress-inducible RNP granules *Elife* **4** e06807
- [154] Huber G 1991 Scheidegger's rivers, takayasu's aggregates and continued fractions *Phys. A: Stat. Mech. Appl.* **170** 463–70
- [155] Feric M and Brangwynne C P 2013 A nuclear F-actin scaffold stabilizes ribonucleoprotein droplets against gravity in large cells *Nat. Cell Biol.* **15** 1253–9
- [156] Feric M, Broedersz C P and Brangwynne C P 2015 Soft viscoelastic properties of nuclear actin age oocytes due to gravitational creep *Sci. Rep.* **5** 16607

- [157] Berry J, Shin Y, Brangwynne C P and Haataja M P 2018 *In vivo* nucleation, growth and coarsening kinetics of light-activated optogenetic RNP bodies to be submitted
- [158] Lee C F, Brangwynne C P, Gharakhani J, Hyman A A and Jülicher F 2013 Spatial organization of the cell cytoplasm by position-dependent phase separation *Phys. Rev. Lett.* **111** 088101
- [159] Weber S C and Brangwynne C P 2015 Inverse size scaling of the nucleolus by a concentration-dependent phase transition *Curr. Biol.* **25** 641–6
- [160] Corrales L R and Wheeler J C 1989 Chemical reaction driven phase transitions and critical points *J. Chem. Phys.* **91** 7097–112
- [161] Huberman B 1976 Striations in chemical reactions *J. Chem. Phys.* **65** 2013–9
- [162] Glotzer S C, Di Marzio E A and Muthukumar M 1995 Reaction-controlled morphology of phase-separating mixtures *Phys. Rev. Lett.* **74** 2034–7
- [163] Puri S and Frisch H 1994 Segregation dynamics of binary mixtures with simple chemical reactions *J. Phys. A: Math. Gen.* **27** 6027
- [164] Glotzer S C, Stauffer D and Jan N 1994 Monte carlo simulations of phase separation in chemically reactive binary mixtures *Phys. Rev. Lett.* **72** 4109
- [165] Qui T C, Nagaki T, Nakagawa T, Yano O and Soen T 1989 Immobilization of transient structures in polystyrene/poly(2-chlorostyrene) blends undergoing phase separation by using photocrosslinking *Macromolecules* **22** 2720–3
- [166] Lefever R, Carati D and Hassani N 1995 Comment on ‘Monte-Carlo simulations of phase separation in chemically reactive binary mixtures’ *Phys. Rev. Lett.* **75** 1674
- [167] Carati D and Lefever R 1997 Chemical freezing of phase separation in immiscible binary mixtures *Phys. Rev. E* **56** 3127
- [168] Griffin E E, Odde D J and Seydoux G 2011 Regulation of the MEX-5 gradient by a spatially segregated kinase/phosphatase cycle *Cell* **146** 955–68
- [169] Aumiller W M Jr and Keating C D 2016 Phosphorylation-mediated RNA/protein complex coacervation as a model for intracellular liquid organelles *Nat. Chem.* **8** 129–37
- [170] Pak C W, Kosno M, Holehouse A S, Padrick S B, Mittal A, Ali R, Yunus A A, Liu D R, Pappu R V and Rosen M K 2016 Sequence determinants of intracellular phase separation by complex coacervation of a disordered protein *Mol. Cell* **63** 72–85
- [171] Handwerger K E, Cordero J A and Gall J G 2005 Cajal bodies, nucleoli and speckles in the Xenopus oocyte nucleus have a low-density, sponge-like structure *Mol. Biol. Cell* **16** 202–11
- [172] Updike D L, Hachey S J, Kreher J and Strome S 2011 P granules extend the nuclear pore complex environment in the *C. elegans* germ line *J. Cell Biol.* **192** 939–48
- [173] King O D, Gitler A D and Shorter J 2012 The tip of the iceberg: RNA-binding proteins with prion-like domains in neurodegenerative disease *Brain Res.* **1462** 61–80
- [174] Sauter A, Roosen-Runge F, Zhang F, Lotze G, Jacobs R M and Schreiber F 2015 Real-time observation of nonclassical protein crystallization kinetics *J. Am. Chem. Soc.* **137** 1485–91
- [175] Shiriyayev A and Gunton J D 2004 Crystal nucleation for a model of globular proteins *J. Chem. Phys.* **120** 8318–26
- [176] Sear R P and Cuesta J A 2003 Instabilities in complex mixtures with a large number of components *Phys. Rev. Lett.* **91** 245701
- [177] Harmon T S, Holehouse A S and Pappu R V 2017 To mix, or to demix, that is the question *Biophys. J.* **112** 565–7
- [178] Jacobs W M and Frenkel D 2017 Phase transitions in biological systems with many components *Biophys. J.* **112** 683–91
- [179] Jacobs W M and Frenkel D 2013 Predicting phase behavior in multicomponent mixtures *J. Chem. Phys.* **139** 024108
- [180] Inoue T 1995 Reaction-induced phase decomposition in polymer blends *Prog. Polym. Sci.* **20** 119–53
- [181] Chan P K and Rey A D 1996 Polymerization-induced phase separation. 1. Droplet size selection mechanism *Macromolecules* **29** 8934–41
- [182] Zwicker D, Decker M, Jaensch S, Hyman A A and Jülicher F 2014 Centrosomes are autocatalytic droplets of pericentriolar material organized by centrioles *Proc. Natl Acad. Sci.* **111** E2636–45
- [183] Wueseke O, Zwicker D, Schwager A, Wong Y L, Oegema K, Jülicher F, Hyman A A and Woodruff J B 2016 Polo-like kinase phosphorylation determines *caenorhabditis elegans* centrosome size and density by biasing spd-5 toward an assembly-competent conformation *Biol. Open* **5** 1431–40
- [184] Zwicker D, Hyman A A and Jülicher F 2015 Suppression of oswald ripening in active emulsions *Phys. Rev. E* **92** 012317
- [185] Zwicker D, Seyboldt R, Weber C A, Hyman A A and Jülicher F 2017 Growth and division of active droplets provides a model for protocells *Nat. Phys.* **13** 408–13
- [186] Bugaj L J, Choksi A T, Mesuda C K, Kane R S and Schaffer D V 2013 Optogenetic protein clustering and signaling activation in mammalian cells *Nat. Methods* **10** 249–52
- [187] Lee S, Park H, Kyung T, Kim N Y, Kim S, Kim J and Do Heo W 2014 Reversible protein inactivation by optogenetic trapping in cells *Nat. Methods* **11** 633–6
- [188] Taslimi A, Vrana J D, Chen D, Borinskaya S, Mayer B J, Kennedy M J and Tucker C L 2014 An optimized optogenetic clustering tool for probing protein interaction and function *Nat. Commun.* **5** 4925
- [189] Weber C A, Lee C F and Jülicher F 2017 Droplet ripening in concentration gradients *New J. Phys.* **19** 053021
- [190] Patel A, Malinovska L, Saha S, Wang J, Alberti S, Krishnan Y and Hyman A A 2017 ATP as a biological hydrotrope *Science* **356** 753–6
- [191] Weber S N, Weber C A and Frey E 2016 Binary mixtures of particles with different diffusivities demix *Phys. Rev. Lett.* **116** 058301
- [192] Sear R P 2015 Liquids that form due to dynamics of the molecules that depend on the local density (arXiv:1503.06963)
- [193] Loschi M, Leishman C C, Berardone N and Boccaccio G L 2009 Dynein and kinesin regulate stress-granule and p-body dynamics *J. Cell Sci.* **122** 3973–82
- [194] Ganai N, Sengupta S and Menon G I 2014 Chromosome positioning from activity-based segregation *Nucl. Acids Res.* **42** 4145–59
- [195] Cates M E and Tailleur J 2015 Motility-induced phase separation *Annu. Rev. Condens. Matter Phys.* **6** 219–44
- [196] McCandlish S R, Baskaran A and Hagan M F 2012 Spontaneous segregation of self-propelled particles with different motilities *Soft Matter* **8** 2527–34
- [197] Stenhammar J, Wittkowski R, Marenduzzo D and Cates M E 2015 Activity-induced phase separation and self-assembly in mixtures of active and passive particles *Phys. Rev. Lett.* **114** 018301
- [198] Lee C F 2017 Interface stability, interface fluctuations and the Gibbs–Thomson relationship in motility-induced phase separations *Soft Matter* **13** 376–85
- [199] Redner G S, Baskaran A and Hagan M F 2013 Reentrant phase behavior in active colloids with attraction *Phys. Rev. E* **88** 012305
- [200] Mognetti B M, Šarić A, Angioletti-Uberti S, Cacciuto A, Valeriani C and Frenkel D 2013 Living clusters and crystals from low-density suspensions of active colloids *Phys. Rev. Lett.* **111** 245702

- [201] Liu F and Goldenfeld N 1989 Dynamics of phase separation in block copolymer melts *Phys. Rev. A* **39** 4805–10
- [202] Wittkowski R, Tiribocchi A, Stenhammar J, Allen R J, Marenduzzo D and Cates M E 2014 Scalar  $\phi^4$  field theory for active-particle phase separation *Nat. Commun.* **5** 4351
- [203] Prost J, Jülicher F and Joanny J 2015 Active gel physics *Nat. Phys.* **11** 111–7
- [204] Flory P J 1941 Molecular size distribution in three dimensional polymers. I. Gelation *J. Am. Chem. Soc.* **63** 3083–90
- [205] Stockmayer W H 1944 Theory of molecular size distribution and gel formation in branched polymers II. General cross linking *J. Chem. Phys.* **12** 125–31
- [206] Stauffer D, Coniglio A and Adam M 1982 Gelation and critical phenomena *Polymer Networks* ed K Dušek (Berlin: Springer) pp 103–58
- [207] von Smoluchowski M 1917 Versuch einer mathematischen theorie der koagulationskinetik kolloider lösungen *Z. Phys. Chem.* **92** 129–68
- [208] Witten T A and Sander L M 1981 Diffusion-limited aggregation, a kinetic critical phenomenon *Phys. Rev. Lett.* **47** 1400–3
- [209] Meakin P 1983 Formation of fractal clusters and networks by irreversible diffusion-limited aggregation *Phys. Rev. Lett.* **51** 1119–22
- [210] Mohan A, Elliot R and Fredrickson G H 2010 Field-theoretic model of inhomogeneous supramolecular polymer networks and gels *J. Chem. Phys.* **133** 174903
- [211] Trappe V, Prasad V, Cipelletti L, Segre P and Weitz D A 2001 Jamming phase diagram for attractive particles *Nature* **411** 772–5
- [212] Segre P, Prasad V, Schofield A and Weitz D 2001 Glasslike kinetic arrest at the colloidal-gelation transition *Phys. Rev. Lett.* **86** 6042
- [213] Sciortino F, Bansil R, Stanley H E and Alström P 1993 Interference of phase separation and gelation: a zeroth-order kinetic model *Phys. Rev. E* **47** 4615



**Joel Berry** is a theoretical / computational materials physicist currently appointed as a postdoctoral researcher at the University of Pennsylvania. He obtained his PhD in physics at McGill University and then held postdoctoral appointments at McMaster University / The University of British Columbia and Princeton University before moving to Penn. Joel's research interests center on multi-scale modeling of nonequilibrium phenomena associated with phase transitions and microstructure evolution in driven, transforming, and active materials. In addition to the principles of intracellular self-organization, he is also interested in the inter-relations between defect physics / kinetics, chemical thermodynamics / kinetics, and mechanics in inanimate 2D, layered, and 3D materials.



**Mikko P. Haataja** A native of Finland, Mikko P. Haataja obtained his MSc degree in engineering physics from Tampere University of Technology in 1995 and PhD in theoretical condensed matter physics from McGill University in 2001. After post-doctoral appointments at Princeton University (2001–2003) and McMaster University (2003–2004), he joined Princeton University as an Assistant Professor in 2004. Haataja is currently a Professor of Mechanical and Aerospace Engineering at Princeton, and his research interests range from biophysical systems (cells and membranes) to energy conversion/storage systems (solid oxide fuel cells and batteries), 2D layered materials (transition metal dichalcogenides), and organic thin films.



**Cliff Brangwynne** obtained a B.S. in Materials Science from Carnegie Mellon University in 2001, and his PhD in Applied Physics from Harvard University in 2007. He was a visiting fellow at the Max Planck Institute for the Physics of Complex Systems in Dresden, and was a Helen Hay Whitney Postdoctoral Fellow at the Max Planck Institute for Molecular Cell Biology and Genetics in Dresden. Since 2011 he has been a faculty member in the Department of Chemical and Biological Engineering at Princeton University. His work focuses on understanding the molecular biophysical mechanisms underling intracellular organization, particularly within the cell nucleus.